Non Linear Spectroscopy for Damage Detection on Aerospace materials

Polimeno, Umberto

Award date:
2010

Awarding institution:
University of Bath

Non Linear Spectroscopy for Damage Detection on Aerospace materials

Volume 1of 1

Umberto Polimeno

A thesis submitted for the degree of Doctorate of Philosophy

University of Bath

Department of Mechanical Engineering

November 2010

Dedication

Dedico questo lavoro a mia moglie Giusy che, con me, ha condiviso i sacrifici e le gioe di questi anni.

fatti non foste a viver come bruti
ma per seguir virtute e canoscenza

(Dante Alighieri, Divina Commedia, Inferno canto XXVI, 116-120)

Table of Contents

Table of Figures

Acknowledgments

During the time I spent, first at Cranfield University and afterwards at University of Bath, I had a chance to meet and collaborate with several people. Each of these people has in some way contributed to this work, whatever it was a brain-storming with some colleagues or university technician assistance. However some of them deserve special thanks. For constantly supporting and guiding me and for his patience and friendship I would particularly thank my supervisor Dr. Michele Meo.

My gratitude goes also to Dr. Giuseppe Zumpano, who has contributed to my personal and professional development during the first period of my PhD and to Giovanni Orlando for his friendship and for making me seeing things from a different perspective.

Thanks also to the technicians and staff of the Mechanical Engineering Department of University of Bath whose contribution made this work possible.

Finally, I would like to thank my father and my brother for believing in me.

Abstract

The research activities of this work concentrated on nonlinear material properties in presence of damages or defects. In particular the attention is focused on the low velocity impact damages on laminated composite materials and on the development of new methodology for non destructive damage detection.

Low velocity impact damage morphology is characterized by contact surfaces and open cracks, thus the scope of this work is to study the nonlinear wave propagation and acoustic contacts nonlinearity in damaged medium.

The work has been inspired by recent studies about nonlinear behaviour of contact surfaces in geomaterials, which contain a large number of discontinuities, and the non linear spectroscopy methodologies able to measure nonlinear properties induced by this class of defects.

Hysteretic model called PM-space has been proposed to characterize nonlinear behaviour of damage in homogeneous medium and used in FE in house code to simulate wave propagation effects. Numerical results shows nonlinearities such as harmonics generation and wave's modulation strictly connected with damaged material model, which acts as the only nonlinear source in the medium.

Based on the numerical results an experimental campaign has investigated the nonlinear spectroscopy methodology: Nonlinear Resonance Ultrasound Spectroscopy (NRUS) and Nonlinear Wave Modulation Spectroscopy (NWMS) and their ability to measure phenomena such as harmonics generation, wave modulation and dependency of resonance frequency in damaged laminated composite. The results proposed are very promising as the nonlinear properties are well correlated to the damage presence and severity.

Same techniques have been also applied to study clamping condition on intact samples. Results presented show that weak bond can also generate nonlinearities such as sidebands in agreement evidence provided in literature.

In addition a damage localization technique has been established and results compare against thermal base methodology (Active Pulse Thermography and Thermosonics) are in good agreement.

List of abbreviation

- AE: Acoustic Emission
- BVID: Barely Visible Impact Damage
- CAN: Contact Acoustic Nonlinearity
- CLT: Classical Lamination Theory
- HMEU: Hysteretic Mesoscopic Elastic Unit
- LT: Lock In Thermography
- NDE: Non Destructive Evaluation
- NDT: Non Destructive Technique
- NEWS: Nonlinear Elastic Wave Spectroscopy
- NRUS: Nonlinear Resonance Ultrasonic Spectroscopy
- NWMS: Nonlinear Wave Modulation Spectroscopy
- PM-space: Preisach-Mayergoyz space
- PT: Pulse Thermography

CHAPTER 1 INTRODUCTION

1.1 The importance of research in the non destructive inspection methodologies

Nowadays many structural and new material applications require more and more the use of non destructive techniques (NDT). Many benefits can be achieved from a wide and a proper application of NDT, starting from the control of manufacturing process to guarantee high quality production, ending to the maintenance program of those structural components for which the integrity is one of the fundamental requirements. Moreover the most important aspect of NDT technologies is the possibility to increase the safety of human life in all application. Is not a just coincidence if the first regulation about safety inspection has been amended by the State of Connecticut after the explosion in 1854 of a boiler that killed 21 people and injured 50 [1].

In the recent past the coming of the digital technology and the fast improvement of computer performance have drastically modified many aspects of our life, indeed a great contribution has been brought to the NDT too [3]. Hardware improvements have allowed the possibility to process and store a constantly increasing amount of data. Computer science has also contributed in the development of user friendly tools to limit as much as possible the human factor. Applications, such as pattern recognition program for an automatic interpretation of inspection results and digital image enhancement to increase signal to noise ratio and help the human eye, have been some of most valuable contribution of computer technologies to NDT applications.

A large number of companies are deeply involved in NDT technologies; aerospace, automotive, oil, energy production and manufacturing are just an example of non destructive inspection field of application where safety and production quality might benefit of any improvement in the inspection methodologies.

However if NDT has affected design, manufacturing and maintenance giving an outstanding contribution in terms of safety and extension of component life, on the other end the sustained economic effort has become significant. For instance an average airline spends 12% for maintenance program of its annual operating costs; regional airlines can easily reach 20% [2].

Taking into account also the economic point of view, innovations in the inspection methodology can represent an important reduction of maintenance costs and an improving of safety.

In this work the attention is focused on the aerospace field and on those material that are becoming more and more important in this sector such as composite laminate. In the Table 1-1 is displayed and overview of the typical maintenance program adopted by airlines; all of these stages are characterized by the use of different techniques that guarantee the reliability and cost effectiveness.

When Service is Performed	Type of Service Performed	Impact on Airline Service
Prior to each flight	"Walk-around" – visual check of aircraft exterior and engines for damage, and leakage	None
Every 2-7 days	Service check (line maintenance opportunity) - service consumables (engine oils, hydraulic fluids, oxygen) and tire and brake wear	Overnight layover
Every 25-40 days	A-checks (line maintenance check) - detailed check of aircraft and engine interior, service and lubrication of systems (e.g., ignition, generators, cabin, air conditioning, hydraulics, structures, and landing gear)	Overnight layover
Every 45-75 days	B-checks (packaged A-checks) – torque tests, internal checks, and flight controls	Overnight layover
Every 12-15 months	C-checks (base maintenance visit) - detailed inspection and repair of engines and systems	Out of service 3-5 days
Every 2-5 years (depending on usage or mandatory inspection/modification requirements)	Heavy maintenance visit (or maintenance program visit) – corrosion protection and control program and structural inspections/modifications	Out of service up to 30 days

Source: Based on New Materials for Next-Generation Commercial Transports, NMAB-476, National Research Council, Washington, DC: National Academy Press (1996).

Table 1-1. Maintenance program for airline companies [4]

Each of these services is strictly connected with the part to be inspected and the choice of methodology has to take into account many factors as: time consuming, part accessibility, type of damages, sensitivity, etc. An overview of the most common methodologies with their advantages and limitations is presented in the Table 1-2.

	Damage Type	Advantages	Limitations
Visual Inspection	• Fatigue cracks • Delamination	• Does not require sophisticated equipment • Relatively inexpensive	• Time consuming • Limited accuracy
Ultrasonics	• Fatigue cracks • BVID • Delamination • Corrosion	• Well established and understood • Sensitive to small damage • Possible damage location • Good depth ranging • Relatively inexpensive • Possible in-flight monitoring	• Point monitoring (requires scanning) • Requires coupling • Often does not detect closed crack • Sensitive to geometry
Eddy Current	• Fatigue cracks	• Detection of small crack • Possible noncontact testing • Does not require coupling • Possible data storage • Relatively inexpensive	• Used mostly for crack Detection • Point monitoring (requires scanning) • Requires specific skills • Requires calibration • Poor penetration (max. monitored thickness -6 mm)
Acoustic Emission	• Fatigue cracks • BVID • Delamination • corrosion	• Well established and understood • Large structures can be monitored • Not sensitive to geometry • Possible in-flight monitoring	• Requires load (passive technique) • Not reproducible • Not sensitive to small damage
X-Ray Radiography	• Fatigue cracks • BVID • Delamination • Corrosion	• Fast monitoring • Good penetration • Relatively inexpensive	• Not sensitive to small damage • Not possible for large structures
Thermography	• Fatigue cracks • BVID • Delamination	• Fast monitoring • Large structures can be monitored	• Expensive • Not sensitive to small damage • Poor penetration
Shearography	• Fatigue cracks • BVID • Delamination • Corrosion	• Fast monitoring • Large structures can be monitored	• Very Expensive • Not well developed • Requires load (passive technique)

Table 1-2. Summary of NDT techniques used for aircraft damage monitoring and inspection [5].

From business point of view, what is really critical for airline companies is the time that an aircraft spent out of service where the cost of maintenance is summed to the lack of returns. Usually, see Table 1-1, heavy structural inspections require the airplane to be out of service, thus an improvement of structural integrity test, able to reduce the inspection time, can significantly alleviate the economic effort dedicated to safety, without affecting the structural reliability.

The ideal solution, which at the moment represents the long term view of many research activities around the world, is to have a system embedded in the structure able to provide a continuous monitoring of structural health condition. This approach will allow identifying damaged parts during the service and the scheduling of aimed maintenance, reducing time and cost to keep the aircraft safe.

However, this type of technology requires first a research effort to improve the ability of detecting defects in early stage, before critical failure affects the structural safety.

Previous studies reported in the next paragraph, have demonstrated the aptitude of nonlinear properties in highlighting the presence of damages before significant variation of linear properties becomes measurable.

At this scope, the work here presented, investigates the non linear properties induced by defects and their capabilities for damage detection and localisation.

1.2 Objectives

The purpose of this work is not to investigate in detail all of the methodologies currently applied in the industry.

A brief describition of the most important and diffused techniques will be given in the next chapters. However this thesis is focused on the non linear effects of elastic wave propagation induced by material defects as fatique cracks, flaws or impact damage.

The modern ultrasonic techinques concern the observation of linear phenomena about wave propagate in continiuous medium such as attenuation, velocity variation and time of flight, but in 1998 [6] a comparison has been made about sensitivity at early damage stage between linear and non linear properties of elastic wave. Starting from some previous works [7]-[8] where harmonics generation have been detected when fatigue damage occurs in aluminium, P. Nagy [6] has investigated the behaviour of 2090 aluminium alloy specimen under fatigue load, and measured the attenuation and velocity change during fatigue cycle. Attenuation and speed wave are functions of external deformation and can be expressed in a series expansion:

$$c(\varepsilon_{ext}) = c_0 + c_1\varepsilon_{ext} + c_2\varepsilon_{ext}^2 \quad (1.1)$$

$$\alpha(\varepsilon_{ext}) = c_0 + \alpha_1\varepsilon_{ext} + \alpha_2\varepsilon_{ext}^2 \quad (1.2)$$

In the equation (1.1) ε_{ext} is the external deformation, *c* is the speed of sound in the medium calculated as a function of c_0, sound velocity without external stress, and c_n is *n*th-order acoustic elastic coefficients. Similarly in the equation (1.2) α is the attenuation, α_0 is the attenuation without external stress, and α_n is the *n*th-order acoustic elastic coefficients. The red line in Figure 1.1 shows the linear static modulus, the blue line is linear velocity (0th-order) and the black line non linear (2nd-order) attenuation and velocity coefficients monitored during fatigue test, normalized to their initial values. The experiment [6] was stopped approximately after 15000 cycles, when the first detectable crack was observed at the site of maximum strain, and the results presented (Figure 1.1) show the nonlinear parameters increase monotonically during the test and become ten times bigger than the initial value at the end of experiment. Instead the linear attenuation has a slight increase of 9% and linear velocity reduced by a factor of 0.7 only.

Similar experiments have been carried out on different type of materials as ABS and PVC polymer or FM300 adhesive layer [6] and same conclusions have

been reached: nonlinear parameters are much more sensitive to the early stage of damages.

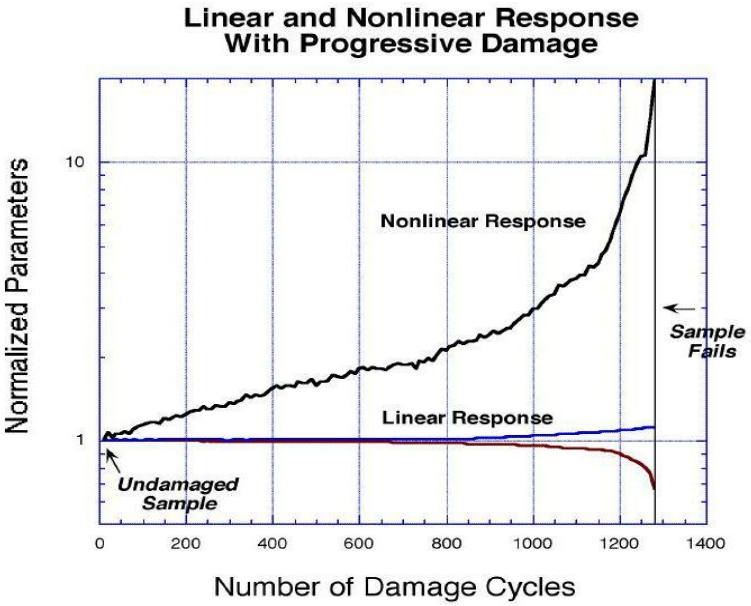

Figure 1.1. The variation of linear (static modulus in red and velocity in blue) and nonlinear parameters (black line) with fatigue in 2090 aluminium alloy.

Inspections able to detect damages in their early stage with a better understanding of nonlinear material behaviour could reduce maintanance operation and increase the general safety of the components.

On the light of these experimental evidences this work investigates the nonlinear phenomena induced by defects in materials from both numerical and experimental point of view.

1.3 Thesis outline and research approach description

The second and the third chapter of this thesis are dedicated, respectively, to an overview of non destructive techniques for damage detection (NDT) currently in use and to a brief introduction on elasticity and wave propagation in solid media.

Chapter 4 is dedicated to an overview of some of the critical aspects and problems that might occur during the operative life of composite parts. In particular a description of damages induced by low velocity impact will be provided, followed by a description of observable effects due to weak and loose bonding. Those laminates having impact damage or weak bonds are characterized by nonlinear behaviour that will be under investigation in the following chapters.

A brief description of the current methodologies in use to inspect composite part has been also presented.

Chapter 5 is dedicated to nonlinear material properties and wave propagation as these aspects represents the starting point to investigate nonlinear effects in faulty composite parts. Experimental evidence has demonstrated how defects and loose bonds show some hysteretic properties.

Similar behaviour has been noticed also on a different material kind: geomaterials, for which the heterogeneous composition and the high number of voids justify the hysteretic behaviour. Some of the experimental evidences and hysteretic material model is also presented. Taking inspiration from these approaches, a similar material model has been developed to simulate composite damaged area based on the assumption that defects in homogeneous materials presents voids and flaw just as geomaterials.

Then nonlinear material model has been implemented in the finite element software developed in house in order to perform non linear time dependent analysis and to study the effects on the wave propagation induced by material portion modelled as hysteretic (chapter 6). The results shown in this work have provided a qualitative understanding on the observable features in structural response. Nevertheless due by the complexity and lack of information about damages morphology it was not possible carrying out a numerical quantitative analysis of the phenomena that would have allowed an exact prediction of nonlinear properties. Anyhow the data collected from the numerical tests has driven the experimental campaign providing an understanding on the wave

distortion and nonlinear behaviours. Indeed all these information have helped in preparing and analysing laboratory test which are reported.

The experimental test (chapter 7) carried out on some pre-damaged laminate composite samples have been focused on the estimation of nonlinear properties, predicted by numerical analysis, and on the correlation with the magnitude of nonlinear source as defects or weak boundary conditions.

Chapter 8 is dedicated to a low velocity impact test performed at the University of Bath on composite laminate specimens. The damaged samples have been used to estimate the damage position based on the magnitude measurement of non linear features. The outcome of this test is an image able to highlight the damage position. This result has been also compared with other methodologies available at the University of Bath for damage localization (such as the pulse thermography) and the comparison shows a good agreement between the methods.

Finally the last section is dedicated to summarizing the research outcome and to highlight the potential benefit introduced by the proposed methodology.

CHAPTER 2 OVERVIEW OF NON DESTRUCTIVE INSPECTION METHODS

2.1 Acoustic Emission

During deformation solid can spontaneously release locally stored energy as sound burst when a sufficiently high stress occurs and these waves are emitted in discrete pulses. This phenomenon is called acoustic emission (AE) or stress wave emission (SWE) and it is due to the presence of: grain boundaries sliding, plastic deformation, inclusion, corrosion, cracking, etc... [3]. Acoustic bursts propagate through the media and they can be detected by sensors on the solid surface and processed in two ways: direct and indirect. The first approach consists in measuring the arrivals time of AE and its energy [9]. The indirect method

involves the demodulation or convolution algorithm to identify the damage location [10].

AE inspection belongs to the passive class of NDT because no external excitation is needed and the operative loads cause the stress that induces the release of the stored energy by the defects. The vibration level induced by operative load could be very complex and bigger than the vibration induced by AE and eventually the presence of noise can make difficult the processing of data. However this technique presents some advantages [3]:

1) Large area covered by a relatively small number of sensors.
2) Defects in inaccessible areas can be detected.
3) Usable for on-line test.

AE technology has many industrial applications in NDT and manufacturing such as [3]:

- Crack propagation
- Corrosion detection
- Leak detection
- Reactor vessels monitoring
- Deforming process: rolling, forging and extruding
- Welding

2.2 Ultrasonic method

Currently ultrasonic methods are one of the most widely NDT used in many fields: aerospace, medical screening, pipeline, railway, nuclear power. The basic idea of this methodology consists in using high-frequency elastic waves to investigate structures [11]. Different applications involve the use of wave at

specific frequency range, the spectrum of phenomena range of interest is presented in the Figure 2.1.

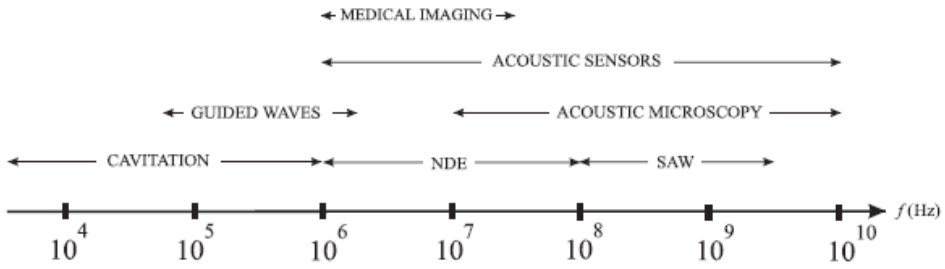

Figure 2.1. Frequency range for ultrasonic application [12].

Common applications involve signal processing to estimate those phenomena strictly connected with damage presence like: signal attenuation, scattering, time of flight diffraction (TODF) and so on.

One of the most popular applications is based on the use of bulk wave measuring their attenuation and echo time of flight. Piezoelectric transducers are used to generate an ultrasonic pulse that travels typically in water where the specimen under investigation is immersed. Interface areas, such water-sample or sample-air (typically in internal damages), generate reflection wave that can be detected by the same probe or some other sensors. To obtain single point measurement (A-scan), multiple scan along one line (B-scan) or a surface image of specimen (C-scan) the inspection is carried out moving the probe over the surface of specimens.

Another common application of UT in NDE is the use of surface acoustic wave (SAW) in semi-infinite solid like Rayleigh Wave [12]. This kind of wave are really useful when the main goal of inspection is check the presence of damage on the surface or near surface region because Rayleigh waves are really sensitive to surface damage and the depth of wave penetration is linked to the frequency [11].

Lamb wave are also widely used in thin plates where these type of waves are sensitive to the change in boundary condition which are affected by the presence

of defects, moreover they can propagate for a long distance [11] reducing drastically the time needed to inspect large thin structures.

2.3 Electromagnetic methods

Materials such as metals or carbon fibres have good electro-magnetic conductivity properties and the magnetic field can be used for NDE. Inducing a magnetic field on the specimens the lines of forces can be observable and surface breaking or subsurface flaw causes the distortion of magnetic field producing flux leakage field [3]. One of the most common methods is called magnetic particle flaw detection technique; in order to highlight defect presence finely divided ferromagnetic particles are applied to the specimen, these particles are attracted in the high line force density area, namely where flux leakage are generated by surface or subsurface defect.

Common application for this method is the detection of surface or sub-surface flaw in the following fields:

- Welds inspection
- Railroad wheels
- Aircraft engine parts such as turbine blades

2.4 Radiography

Radiography methods are the based on the interaction between X-ray electromagnetic waves and materials. Major advantages of X-ray come from their wavelengths and energy, typically wavelength is between 10 and 0.01 nanometers and energy between 120 eV and 120 keV. Like visible waves X-ray can be absorbed or scattered by material, but since the energy is much higher than light

these waves tend to pass trough medium offering the chance to observe inside the specimens once the wave has got through it. Along the path through the test pieces density variation affects the wave attenuation and the image resulting can highlight the presence of defects or flaw like voids, inclusion or open crack [16]. Moreover the progress in computing and electronic capabilities nowadays allow the use of computer tomography that represents the evolution of standard X-ray adding the possibility to have three dimension information of samples.

Despite their advantages there are some issues using X-ray. First of all there is same safety problems for humans related to the danger of X-rays and high energy required, so the use of heavy shield system is mandatory.

In addition close cracks are not detectable, and even if the crack is open the ability to detect flaws is related to defect orientation, ideally its long dimension should be parallel to the wave propagation direction; in this case the interaction is maximized. Finally the equipments are really expensive, especially for computer tomography.

X-ray, today, is well established technology in medical diagnosis and aerospace industry thanks to its ability to inspect through the thickness and the possibility to retrieve detailed information deeply in to the media.

2.5 Eddy-Current methods

Coils generate electromagnetic field when they are excited by alternating current. If conductive materials are immersed in electromagnetic field there are current induced on the materials itself, these currents are called: Eddy-current that in turn induced a secondary magnetic field in opposite direction on the coil. This double induction process causes a variation of coil impedance that can be monitored and used for damage detection [3], indeed, defects affect the secondary magnetic field and so the coil impedance.

Usually NDE using Eddy-current is carried out moving the coil over the surface specimen, no coupling, contact or material preparation are required for this methodology. Furthermore equipment has become increasingly portable and lightweight allowing fast test response [17].

However some limitations are represented by the difficulty to inspect subsurface sample condition in ferromagnetic materials and by the complexity of results that requires high trained inspectors.

Surface inspection using eddy current is today a common application in aircraft metallic component and engine parts such as the root of turbine blades.

2.6 Thermography

Thermographic methods have quite wide use in many non destructive disciplines; infrared images are used to inspect thermal insulation of building or to check operating condition of electronic devices, these methodologies have been called passive thermography. There is another infrared (IR) methodology to perform non destructive inspection and it is called: active thermography. This last group is really interesting for aerospace NDT; it consists in exciting the test piece and observing its thermal behaviour. Mainly samples can be stimulated by pulse flash (PT - Pulse thermography), periodic heat wave (LT- Lock-in thermography) or ultrasonic excitation (Vibrothermography or Thermosonics) [18]. In the first two cases, where the samples is stimulated by heat as a pulse or periodic wave, defects in the specimens affect local thermal material behaviour, so recording the infrared emission is possible to localize damage. In the last method defects act as a heat source, indeed, during mechanical excitation discontinuity surfaces can rub together and heat up [19].

The recent innovations on IR camera and on the digital infrared imaging have solved most of the problems related to the use of these methodologies; moreover LT and PT techniques are contactless.

IR methods are suitable to detect subsurface defects; nevertheless the thickness of inspected layer depends of material properties and inspection time.

Vibrothermograpy is a really promising contact method but it is still under investigation by the research community.

Thermography application can be found in civil engineering to monitor the thermal insulation or temperature behaviour of large area. In the aerospace world PT and LT are commonly used to detect delamination in thin composite panel and to verify bonding condition between parts.

CHAPTER 3 FOUNDATIONS OF ELASTICITY AND WAVE PROPAGATION

3.1 Introduction

Wave propagation phenomena are of great interest for the capabilities in structure characterization. Waves travelling through a medium bring with them a lot of information such as material properties, boundary condition and how structures react to external excitation. The purpose of this chapter is to introduce some basic concept of elasticity and wave propagation in order to increase readability of next chapters even for not expert readers and to introduce notation that will be used in the remaining chapters.

3.2 Elasticity, brief introduction to concept and notation

Elasticity is a physical property of such materials that are able to return in their original shape after a deformation induced by an external stress field. This ability depends also on the intensity of stress field and common experience suggests that materials keep elastic behaviour in a certain range of external stress and temperature. The purpose of this work is to study materials in the elastic range.

To introduce stress notation let us think of an infinitesimal cubic element of the body [20]. The body in equilibrium under external force field reacts with a field of internal forces; the intensity of the internal forces per unit area is the stress. Stresses acting on the infinitesimal element can be represented as in Figure 3.1, where σ and τ denote normal and shear stress respectively. First stresses subscripts indicates the normal to the plane where the stress is acting, the second subscript indicates the direction of the stress.

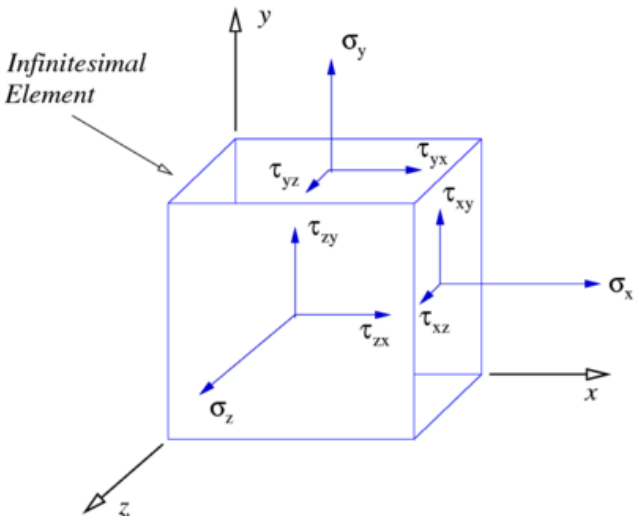

Figure 3.1. Stresses components on an infinitesimal element.

Assuming that the body under investigation has enough constrains to prevent any rigid motion; particles displacement is possible only if body deformation occurs. If *u*, *v* and *w* are the particles displacement respectively in x, y and z

direction then the deformation of infinitesimal element can be represented in terms of strain:

$$\varepsilon_x = \frac{\partial u}{\partial x}; \qquad \epsilon_y = \frac{\partial v}{\partial y}; \qquad \epsilon_z = \frac{\partial w}{\partial z}; \tag{3.1}$$

$$\gamma_{xy} = \frac{\partial u}{\partial y} + \frac{\partial v}{\partial x}; \quad \gamma_{xz} = \frac{\partial u}{\partial z} + \frac{\partial w}{\partial x}; \quad \gamma_{yz} = \frac{\partial v}{\partial z} + \frac{\partial w}{\partial y} \tag{3.2}$$

The equation (3.1) shows the relation between the displacement and the strain in normal direction of infinitesimal element, instead the equation (3.2) represents the relation between displacement and shear strain.

The relation between stress and strain has been established experimentally and it is known as Hooke's Law [21]-[22], which the generalised form is represented in (3.3):

$$\begin{Bmatrix} \sigma_1 \\ \sigma_2 \\ \sigma_3 \\ \sigma_4 \\ \sigma_5 \\ \sigma_6 \end{Bmatrix} = \begin{bmatrix} C_{11} & C_{12} & C_{13} & C_{14} & C_{15} & C_{16} \\ C_{21} & C_{22} & C_{23} & C_{24} & C_{25} & C_{26} \\ C_{31} & C_{32} & C_{33} & C_{34} & C_{35} & C_{36} \\ C_{41} & C_{42} & C_{43} & C_{44} & C_{45} & C_{46} \\ C_{51} & C_{52} & C_{53} & C_{54} & C_{55} & C_{56} \\ C_{61} & C_{62} & C_{63} & C_{64} & C_{65} & C_{66} \end{bmatrix} \begin{Bmatrix} \varepsilon_1 \\ \varepsilon_2 \\ \varepsilon_3 \\ \varepsilon_4 \\ \varepsilon_5 \\ \varepsilon_6 \end{Bmatrix} \tag{3.3}$$

The stiffness matrix [C] showed in the above equation is symmetric therefore elastic materials have 21 independent constants that allow full description of material behaviour. The inverse of stiffness matrix: $[S]=[C]^{-1}$ is called compliance matrix and it allows to express the strain field as a function of stress as showed in equation (3.4):

$$\{\epsilon\} = [C]^{-1}\{\sigma\} = [S]\{\sigma\} \tag{3.4}$$

Introducing some symmetry in material behaviour the number of independent constant can be further reduced. This is the case for isotropic materials where materials properties are equal in all directions thus all body planes are symmetry plane. Under isotropic assumption there only 2 independent elastic constant and the resulting stiffness matrix is:

$$C = \begin{bmatrix} C_{11} & C_{12} & C_{12} & 0 & 0 & 0 \\ C_{12} & C_{11} & C_{12} & 0 & 0 & 0 \\ C_{12} & C_{12} & C_{11} & 0 & 0 & 0 \\ 0 & 0 & 0 & C_{44} & 0 & 0 \\ 0 & 0 & 0 & 0 & C_{44} & 0 \\ 0 & 0 & 0 & 0 & 0 & C_{44} \end{bmatrix}; \quad C_{44} = \frac{C_{11} - C_{22}}{2} \tag{3.5}$$

A wide variety of engineering materials belong to isotropic category such as: aluminium, steel and the majority of metals alloy.

However another class of materials has become of great interest in engineer since the last decades of the past century; those materials are called orthotropic. This class of materials has the three mutually orthogonal planes of symmetry and it is characterized by nine independent elastic constants.

Composites made with different kind of material such as: carbon or glass fibre and epoxy matrix belong to orthotropic class and their main advantages are the low density, and the possibility to tailor mechanical performances specifically for each applications varying the fibres quantity and direction.

Without enter in the details of composite mechanics, for which references [21] and [23]are suggested, the stiffness matrix for this class of material can expressed as followed:

$$[C] = \begin{bmatrix} C_{11} & C_{12} & C_{13} & 0 & 0 & 0 \\ C_{12} & C_{22} & C_{13} & 0 & 0 & 0 \\ C_{13} & C_{13} & C_{33} & 0 & 0 & 0 \\ 0 & 0 & 0 & C_{44} & 0 & 0 \\ 0 & 0 & 0 & 0 & C_{55} & 0 \\ 0 & 0 & 0 & 0 & 0 & C_{66} \end{bmatrix} \tag{3.6}$$

Moreover for some composite such as laminated there is an axis of material symmetry, this condition reduces further the number of independent constant to five. These materials are called transversely isotropic material and assuming that z axis is of symmetry the stiffness matrix has the following form:

$$[C] = \begin{bmatrix} C_{11} & C_{12} & C_{13} & 0 & 0 & 0 \\ C_{12} & C_{22} & C_{13} & 0 & 0 & 0 \\ C_{13} & C_{13} & C_{22} & 0 & 0 & 0 \\ 0 & 0 & 0 & C_{44} & 0 & 0 \\ 0 & 0 & 0 & 0 & C_{44} & 0 \\ 0 & 0 & 0 & 0 & 0 & C_{66} \end{bmatrix}; \quad C_{66} = \frac{C_{11} - C_{12}}{2} \tag{3.7}$$

Generally material properties are determined experimentally in laboratory in terms of engineering constant: Young' modulus, Poisson's ratio and so on. Engineering constants generally are measured experimentally using material specimens through simple tests as uniaxial tension or shear test. The use of engineering constant in place of stiffness coefficients is usually preferred as their intrinsic physical meaning.

In order to understand the relationship between engineering constant and strain-stress relationship the equation (3.4) is taken into account as the lab testing usually assume a known stress field, so through the measurement of strain field is possible the evaluation of engineering constant and built directly the compliance matrix, which in the case of orthotropic material can be expressed as follow:

$$\begin{Bmatrix}\varepsilon_1\\ \varepsilon_2\\ \varepsilon_3\\ \varepsilon_4\\ \varepsilon_5\\ \varepsilon_6\end{Bmatrix} = \begin{bmatrix} 1/E_1 & -\nu_{21}/E_2 & -\nu_{31}/E_3 & 0 & 0 & 0\\ -\nu_{21}/E_2 & 1/E_2 & -\nu_{32}/E_3 & 0 & 0 & 0\\ -\nu_{13}/E_1 & -\nu_{23}/E_2 & 1/E_3 & 0 & 0 & 0\\ 0 & 0 & 0 & 1/G_{23} & 0 & 0\\ 0 & 0 & 0 & 0 & 1/G_{13} & 0\\ 0 & 0 & 0 & 0 & 0 & 1/G_{12}\end{bmatrix} \begin{Bmatrix}\sigma_1\\ \sigma_2\\ \sigma_3\\ \sigma_4\\ \sigma_5\\ \sigma_6\end{Bmatrix} \tag{3.8}$$

where: E_i is the Young's modulus, which represents the relation between the amount of strain measure in direction 1 with unaxial stress applied in the same direction. The Poisson's ratio ν_{ij} characterizes the strain in direction j when a stress is applied in direction i. G is the shear modulus and it represents the shear strain to the shear stress.

Similar relation can be obtained for isotropic material:

$$\begin{Bmatrix}\varepsilon_1\\ \varepsilon_2\\ \varepsilon_3\\ \varepsilon_4\\ \varepsilon_5\\ \varepsilon_6\end{Bmatrix} = \frac{1}{E}\begin{bmatrix} 1 & -\nu & -\nu & 0 & 0 & 0\\ -\nu & 1 & -\nu & 0 & 0 & 0\\ -\nu & -\nu & 1 & 0 & 0 & 0\\ 0 & 0 & 0 & 1+\nu & 0 & 0\\ 0 & 0 & 0 & 0 & 1+\nu & 0\\ 0 & 0 & 0 & 0 & 0 & 1+\nu\end{bmatrix} \begin{Bmatrix}\sigma_1\\ \sigma_2\\ \sigma_3\\ \sigma_4\\ \sigma_5\\ \sigma_6\end{Bmatrix} \tag{3.9}$$

$$G = \frac{E}{2(1+\nu)}$$

where engineering constant are the same in all direction and to describe material behaviour the 2 independent elastic constant can be chosen between E,G and ν.

Lame's constant , λ and μ, can also be used to characterise isotropic material:

$$\lambda = G\frac{E-2G}{3G-E}; \qquad \mu = G \tag{3.10}$$

3.3 Plane stress assumption for laminated composites

Laminated composited panels are made by adding many layers together. Each of these layers is characterized by a composition of two materials: fibres and matrix, where the fibre component increases the stiffness tensile properties in only one specific direction and the matrix in the others. Singularly the two components are not extremely suitable for structural application, however, the combination of both makes laminated composites really appealing in terms of stiffness and weight.

A single layer of composites, with the fibre at zero angles respect to reference system x-y, is characterized by orthotropic stress strain relationship as shown in the equation (3.6). If no forces are applied in out of plane direction, plane stress assumption can be invoked; it consists in assuming the following stress component equal to zero:

$$\sigma_3 = 0; \qquad \sigma_4 = 0 \quad and \quad \sigma_5 = 0 \tag{3.11}$$

The equation (3.11) reduces the stress-strain relationship to:

$$\begin{Bmatrix} \sigma_x \\ \sigma_y \\ \tau_{xy} \end{Bmatrix} = [Q]\{\varepsilon\} = \begin{bmatrix} Q_{11} & Q_{12} & 0 \\ Q_{12} & Q_{22} & 0 \\ 0 & 0 & Q_{66} \end{bmatrix} \begin{Bmatrix} \varepsilon_x \\ \varepsilon_y \\ \gamma_{xy} \end{Bmatrix} \tag{3.12}$$

where

$$Q_{11} = \frac{E_1}{1-\nu_{12}\nu_{21}};\ Q_{22} = \frac{E_2}{1-\nu_{12}\nu_{21}}\ ;\ Q_{12} = \frac{\nu_{21}E_1}{1-\nu_{12}\nu_{21}};$$
$$Q_{66} = G_{12}; \qquad \upsilon_{12} = \frac{E_2}{E_1}\upsilon_{12} \tag{3.13}$$

If the fibres are not aliened to the reference system forming an angle θ≠0, then a rotation must be applied using the following rotation matrix:

$$T = \begin{bmatrix} m^2 & n^2 & 2mn \\ n^2 & m^2 & -2mn \\ -mn & mn & m^2-n^2 \end{bmatrix}; m = \cos\theta; n = \sin\theta \tag{3.14}$$

Thus the equation (3.12) becomes:

$$\begin{Bmatrix} \sigma_x \\ \sigma_y \\ \tau_{xy} \end{Bmatrix} = [T^{-1}QRTR^{-1}]\{\varepsilon\} = \left[\overline{Q}\right]\{\varepsilon\} \tag{3.15}$$

where

$$R = \begin{bmatrix} 1 & 0 & 0 \\ 0 & 1 & 0 \\ 0 & 0 & 2 \end{bmatrix} \tag{3.16}$$

In order to compute the stiffness properties of laminated panel, the classical lamination theory (CLT) [23] assumes that:

- Laminated panel of thickness *t* is made by *n* orthotropic layers perfectly bonded together
- For in plane loading the strain distribution ε^0 is constant through the thickness and
- Linear variation of strain through thickness in case of bending load

Thus for a single layer *k* is possible to superimpose the two effect of in plane and bending load as follow:

$$\begin{Bmatrix}\sigma_x\\ \sigma_y\\ \tau_{xy}\end{Bmatrix}_k = \begin{bmatrix}\overline{Q_{11}} & \overline{Q_{12}} & \overline{Q_{16}}\\ \overline{Q_{12}} & \overline{Q_{22}} & \overline{Q_{26}}\\ \overline{Q_{16}} & \overline{Q_{26}} & \overline{Q_{66}}\end{bmatrix}_k \left(\begin{Bmatrix}\epsilon_x^0\\ \epsilon_y^0\\ \gamma_{xy}^0\end{Bmatrix} + z \begin{Bmatrix}\kappa_x\\ \kappa_y\\ \kappa_{xy}\end{Bmatrix} \right) \tag{3.17}$$

$$k = 1..n$$

where *k* is the generic layer. The superscript *"0"* indicate the strain at the middle plain, κ is the curvature and z is the distance from panel middle plane.

Integrating through the thickness of laminated panel the resultant stress *N* and momentum *M* per unit width can be computed as follow:

$$\begin{Bmatrix}N_x\\ N_y\\ N_{xy}\end{Bmatrix} = \int_{-\frac{t}{2}}^{\frac{t}{2}} \begin{Bmatrix}\sigma_x\\ \sigma_y\\ \tau_{xy}\end{Bmatrix}_k dz = \sum_{k=1}^{n} \int_{z_{k-1}}^{z_k} \begin{Bmatrix}\sigma_x\\ \sigma_y\\ \tau_{xy}\end{Bmatrix} dz$$
$$\begin{Bmatrix}M_x\\ M_y\\ M_{xy}\end{Bmatrix} = \int_{-\frac{t}{2}}^{\frac{t}{2}} \begin{Bmatrix}\sigma_x\\ \sigma_y\\ \tau_{xy}\end{Bmatrix}_k z dz = \sum_{k=1}^{n} \int_{z_{k-1}}^{z_k} \begin{Bmatrix}\sigma_x\\ \sigma_y\\ \tau_{xy}\end{Bmatrix} z\, dz \tag{3.18}$$

where z is the distance of layer surface (top or bottom) from the panel middle plain.

Substituting the equation (3.17) in the (3.18) it is possible to obtain the following constitutive equation:

$$\begin{Bmatrix}N_x\\ N_y\\ N_{xy}\end{Bmatrix} = \begin{bmatrix}A_{11} & A_{12} & A_{16}\\ A_{12} & A_{22} & A_{26}\\ A_{16} & A_{26} & A_{66}\end{bmatrix} \begin{Bmatrix}\epsilon_x^0\\ \epsilon_y^0\\ \gamma_{xy}^0\end{Bmatrix} + \begin{bmatrix}B_{11} & B_{12} & B_{16}\\ B_{12} & B_{22} & B_{26}\\ B_{16} & B_{26} & B_{66}\end{bmatrix} \begin{Bmatrix}\kappa_x\\ \kappa_y\\ \kappa_{xy}\end{Bmatrix}$$
$$\begin{Bmatrix}M_x\\ M_y\\ M_{xy}\end{Bmatrix} = \begin{bmatrix}B_{11} & B_{12} & B_{16}\\ B_{12} & B_{22} & B_{26}\\ B_{16} & B_{26} & B_{66}\end{bmatrix} \begin{Bmatrix}\epsilon_x^0\\ \epsilon_y^0\\ \gamma_{xy}^0\end{Bmatrix} + \begin{bmatrix}D_{11} & D_{12} & D_{16}\\ D_{12} & D_{22} & D_{26}\\ D_{16} & D_{26} & D_{66}\end{bmatrix} \begin{Bmatrix}\kappa_x\\ \kappa_y\\ \kappa_{xy}\end{Bmatrix} \tag{3.19}$$

where:

$$A_{ij} = \sum_{k=1}^{n} \left(\overline{Q}_{ij}\right)_k (z_k - z_{k-1})$$

$$B_{ij} = \frac{1}{2}\sum_{k=1}^{n} \left(\overline{Q}_{ij}\right)_k (z_k^2 - z_{k-1}^2) \tag{3.20}$$

$$D_{ij} = \frac{1}{3}\sum_{k=1}^{n} \left(\overline{Q}_{ij}\right)_k (z_k^3 - z_{k-1}^3)$$

The expressions in equation (3.24) are also known as in plane stiffness matrix (*A*), bending stiffness matrix (*D*) and coupling matrix (*B*).

3.4 Wave propagation in infinite medium, a brief introduction.

Navier's differential equation [24] and [25], shown in the equation (3.21) is the starting point to describe wave propagation in infinite media:

$$(\lambda + \mu)\left(\frac{\partial^2 u}{\partial^2 x^2} + \frac{\partial^2 v}{\partial x \partial y} + \frac{\partial^2 w}{\partial x \partial y}\right) + \mu\nabla^2 u + \rho f_x = \rho\frac{\partial^2 u}{\partial t^2}$$

$$(\lambda + \mu)\left(\frac{\partial^2 u}{\partial x \partial y} + \frac{\partial^2 v}{\partial^2 y^2} + \frac{\partial^2 w}{\partial x \partial y}\right) + \mu\nabla^2 v + \rho f_y = \rho\frac{\partial^2 v}{\partial t^2} \tag{3.21}$$

$$(\lambda + \mu)\left(\frac{\partial^2 u}{\partial x \partial y} + \frac{\partial^2 v}{\partial x \partial y} + \frac{\partial^2 w}{\partial^2 z^2}\right) + \mu\nabla^2 w + \rho f_z = \rho\frac{\partial^2 w}{\partial t^2}$$

where: u, v and z are particle displacements in x; y and z reference system, f_x, f_y and f_z are the body forces. λ and μ are the first and second Lame's constants, ρ is material density.

Expressing the equation in (3.22) in vector format the following equation is obtained:

$$(\lambda + \mu)\nabla\nabla \cdot u + \mu\nabla^2 u + \rho f = \rho\ddot{u} \tag{3.22}$$

A different formulation of displacement equation is available by introducing scalar and vector potential: Φ and H such that:

$$u = \nabla\Phi + rot\ \Psi; \qquad \nabla\Psi = 0 \tag{3.23}$$

Using the same approach for mass forces:

$$f = \nabla\varphi + rot\ \psi; \qquad \nabla\psi = 0 \tag{3.24}$$

The formulation of displacement and body forces field in terms of gradient of a scalar (Φ and φ) and curl of a vector (Ψ and ψ) in the equations (3.23) and (3.24) is due to Helmholtz. Moreover the condition of zero divergence vector guarantees the uniqueness of solution, thus this condition applied to (3.23) provide the following relation:

$$\nabla u = \nabla^2\Phi \tag{3.25}$$

and substituting the equations (3.23) and (3.24) in the (3.22) the following expression has been obtained:

$$\nabla\left[c_1^2\nabla^2\varphi - \frac{\partial^2\varphi}{\partial t^2} + \Phi\right] + rot\left[c_2^2\nabla^2\psi - \frac{\partial^2\psi}{\partial t^2} + \Psi\right] = 0 \tag{3.26}$$

where:

$$c_1^2 = \frac{\lambda + 2\mu}{\rho}; \quad c_2^2 = \frac{\mu}{\rho} \tag{3.27}$$

Equation (3.27) shows wave speed formulations and their dependencies on material properties. The two wave speeds are associated with two different kinds of waves; for a better understanding of wave typology correlated with speed wave in equation (3.27) it is possible to start from equation (3.26) that is satisfied by the (3.28) and (3.29):

$$c_1^2\nabla^2\varphi - \frac{\partial^2\varphi}{\partial t^2} = -\Phi \tag{3.28}$$

$$c_2^2\nabla^2\psi - \frac{\partial^2\psi}{\partial t^2} = -\Psi \tag{3.29}$$

If φ and ψ satisfy equations (3.28) and (3.29) then displacement field *u*, defined in (3.23) is a solution for the problem described in equation (3.22). The function φ is called longitudinal potential and ψ is called transverse potential.

Let assume now Ψ=0 with ψ=0 as initial condition for $t=t_0$; the equation (3.28) becomes the homogeneous equation with zero initial condition; this means that ψ is always zero. Thus from equation (3.23) follows that:

$$u = \nabla\Phi \quad and\ rot\ u = 0 \tag{3.30}$$

The solution of above equation does not involve any particles rotation, but only particle translation is present, for these kinds of waves are called longitudinal. The

velocity of longitudinal wave (also called P-wave) is c_1 as show in equation (3.27).

Similarly assuming Φ=0 and as initial condition φ=0 the solution of (3.24) is a displacement field with no longitudinal components. These waves are called transverse or shear waves and their propagation speed is c_2 as it has been described in equation (3.27).

Longitudinal and transverse waves travel independently in a homogeneous medium until the wave front meets the boundary, than reflected waves are generated [24].

3.5 Non linear wave propagation

The approached used in the previous paragraphs to describe wave propagation phenomena is based on linear elasticity theory.

However, a more general formulation of stress - strain relation involve terms up to and including the second order. Linear effect for a single frequency wave will produce a simple periodic solution, whereas the introduction of higher order terms in the wave's formulation includes non linear phenomena such as non periodic solution of a monochromatic wave propagating through a non linear medium.

Introducing the third order terms into the elastic strain energy E the following expression has been obtained [25]:

$$E = \mu\varepsilon_{ik}^2 + \frac{\lambda}{2}\varepsilon_{jj}^2 + \frac{A}{3}\varepsilon_{ik}\varepsilon_{ij}\varepsilon_{kj} + B\varepsilon_{ik}^2\varepsilon_{jj} + \frac{C}{3}\varepsilon_{jj}^3 \tag{3.31}$$

where A,B and C are the third order elastic constant the Lagrangian strain is given by:

$$\varepsilon_{ik} = \frac{1}{2}\left(\frac{\partial u_i}{\partial x_k} + \frac{\partial u_k}{\partial x_i} + \frac{\partial u_j}{\partial x_i}\frac{\partial u_j}{\partial x_k}\right) \tag{3.32}$$

Taking into account equation (3.31) and (3.32) Goldber [27]-[28]has derived a general formulation of the wave equations, where the simplified expression for a wave propagating along x direction is reported in equation (3.33).

$$\begin{aligned}
&\rho\frac{\partial^2 u_x}{\partial t^2} - \alpha\frac{\partial^2 u_x}{\partial x^2} = \beta\frac{\partial^2 u_x}{\partial x^2}\frac{\partial^2 u_x}{\partial x^2} + \gamma\left(\frac{\partial^2 u_y}{\partial x^2}\frac{\partial^2 u_y}{\partial x} + \frac{\partial^2 u_z}{\partial x^2}\frac{\partial^2 u_z}{\partial x}\right)\\
&\rho\frac{\partial^2 u_y}{\partial t^2} - \mu\frac{\partial^2 u_y}{\partial x^2} = \gamma\left(\frac{\partial^2 u_y}{\partial x^2}\frac{\partial^2 u_x}{\partial x} + \frac{\partial^2 u_x}{\partial x^2}\frac{\partial^2 u_y}{\partial x}\right)\\
&\rho\frac{\partial^2 u_z}{\partial t^2} - \mu\frac{\partial^2 u_z}{\partial x^2} = \gamma\left(\frac{\partial^2 u_z}{\partial x^2}\frac{\partial^2 u_x}{\partial x} + \frac{\partial^2 u_x}{\partial x^2}\frac{\partial^2 u_z}{\partial x}\right)
\end{aligned} \tag{3.33}$$

where:

$$\begin{aligned}
&\alpha = \lambda + 2\mu\\
&\beta = 3\alpha + 2A + 6B + 2C\\
&\gamma = \alpha + \frac{A}{2} + B
\end{aligned} \tag{3.34}$$

Solution of non linear wave equation might be extremely complex, however, Landau [26] suggested the use a successive approximation method in order to isolate linear and non linear contribution and understand the effects of those high order terms. Thus the first step consist in the linear solution of monochromatic waves, at frequency ω_i, travelling simultaneously in to a linear medium leads to linear solution where the displacement field is governed by a superposition of different contributes, each of them depending from a frequency content of a single wave. For example in the case of two waves the displacement field can be fully described by the (ω_1, k1) and (ω_2, k2) where the wave number k_i is given by:

$$k = \frac{\omega}{c} \tag{3.35}$$

Solving the problem for the high order terms implies the resolution of inhomogeneous equation has components that depend on ω_1, ω_2 and the sum of the two frequencies.

This implies the generation of a third wave with:

$$\omega_3 = \omega_1 \pm \omega_3 \tag{3.36}$$

Anharmonic effects might occur also when only a single wave is travelling; in this case the non linear solution includes the generation of a second wave with twice the frequency and wave number.

In conclusion Landau solution describes the generation of non linear effects such as harmonics generation (2ω) and sidebands ($\omega_2 + \omega_1$) when wave propagation in non linear medium is under investigation.

CHAPTER 4 NON LINEAR SOURCES IN A HOMOGENEOUS MEDIUM: DEFECTS AND CONTACT SURFACES

4.1 Introduction

This chapter is dedicated to an introduction of nonlinear phenomena that can occur in solids as resulting of the interaction of mechanical waves with contact boundaries. Experimental evidences will be presented about a class of nonlinear effects that are associated to a nonlinear dynamics of contact interfaces or imperfect bonds.

In addition, damages from low velocity impact on composite laminate will be described. Of particular interest is the morphology of this type of damages which is mainly represented by delamination, matrix cracks and broken fibres. All of

these defects, induced by low velocity impact can be represented by contact surfaces.

Therefore understanding the basic principles of the dynamic behaviour of contact interfaces is a crucial aspect in the process of researching a new approach that is able to detect damages in early stages through the analysis of nonlinear properties.

4.2 Low velocity impact damages in composite laminate

In the recent years the use of composite material in many primary structure has drastically increased thanks to the advantages that this class of new materials has introduced in the design and manufacturing process. Lightness and the possibility to tailor stiffness based on specific application are some of most appealing properties for many industrial sectors as aerospace, automotive, power generation etc. . . .

However, one of the main concerns in the application of composite materials is the behaviour to impact damages. Only in the recent past the research community has made a big effort to better understand material and defect properties induced by impact damages.

Impact behaviour is usually quite a complex problem and a common accepted approach is to indentify three main categories: low velocity impacts, high velocity impacts and ballistic impacts [29].

High velocity impacts are characterized by a ratio between impact velocity and the speed of compressive wave propagating through the thickness, when this ratio is greater than the maximum strain to failure. In this case since the first contact, between impactor and plate, the compressive wave generated by the contact itself is able to damage the sample.

Ballistic impacts usually referred to an initial projectile speed high enough to fully penetrate the specimen with zero residual velocity.

During a low velocity impact the contact between the projectile and the target last longer than the time needed by the waves to propagate all over the plate and the damages usually occur for a severe bending of the plate itself or, in the case of stiffer laminate high localize contact stress . Events such as tools dropping or debris hitting aircraft during the take off can be included in the low velocity impact category and currently they represent a big concern in composite application as the damage induced might be not detectable by a visible inspection.

4.2.1 Low velocity impact damage morphology

Impacts under low velocity condition induce three types of defects in composite laminate: delamination, matrix cracking and fibres failures [30].

Delamination usually occurs between adjacent plies with different orientation due to the stiffness mismatching and can propagate through the thickness. Moreover the cracks so generated might also split and propagate at the ply interfaces because of shear stress concentrations in the matrix close to the crack tips.

Impact load also generates a high tensile stress which can cause a stress concentration at fibre matrix interfaces and then two type of matrix failures as showed in Figure 4.1.

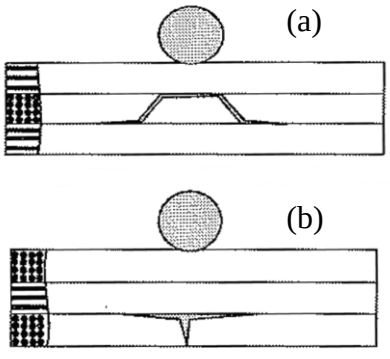

Figure 4.1 Matrix crack: (a) tensile crack, (b) shear crack (see ref. [29]).

The first kind of matrix failure represented in Figure 4.1 (a) is called a tensile crack, and it occurs when the in plane normal stress is greater than ply tensile strength. The second type is called shear crack (see Figure 4.1) and it depends on the transverse shear stress.

Crack propagation path, across matrix, during the impact depends on the laminate stiffness. For rigid laminated plate the impact produces a high stress concentration on the top ply causing the failure on the first ply and the consequently propagation through the thickness as shown in Figure 4.2 (a). Instead in flexible laminate the bending stress is the reason of the first failure (see Figure 4.2 (b)).

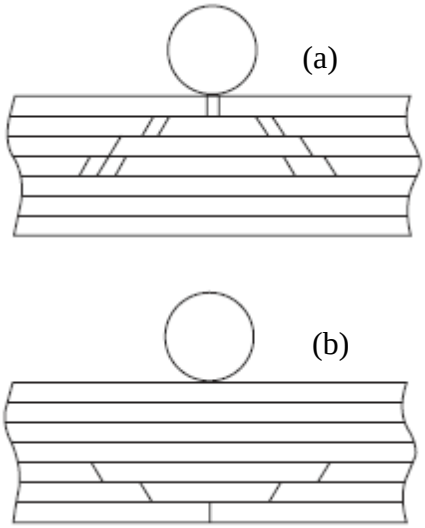

Figure 4.2. Crack propagation path in rigid (a) and flexible (b) laminated plate.

Although fibres in laminated composited significantly contributes to material strength, fibres usually are brittle and limited capability in energy absorption. As a consequence impact might cause a fibre breakage and the consequently crack propagation is perpendicular with respect to the fibres direction.

The Figure 4.3 show the destructive inspection results on a composite laminated specimen after a low velocity impact [31]. The test sample consist of a carbon fibre reinforced plastic (CFRP) laminate [04/904/04] impacted at 1 Joule

using a drop tower. After the impact test the specimen has been inspected using C-scan methodology in order to estimate the delamination area occurred after the impact. Then the sample has been cut along three different directions Q, P and R to allow a microscope observation of the three surfaces.

The micrographs reported in Figure 4.3 highlight the presence of bending crack and delamination in correspondence of impact location and even along the three observable directions.

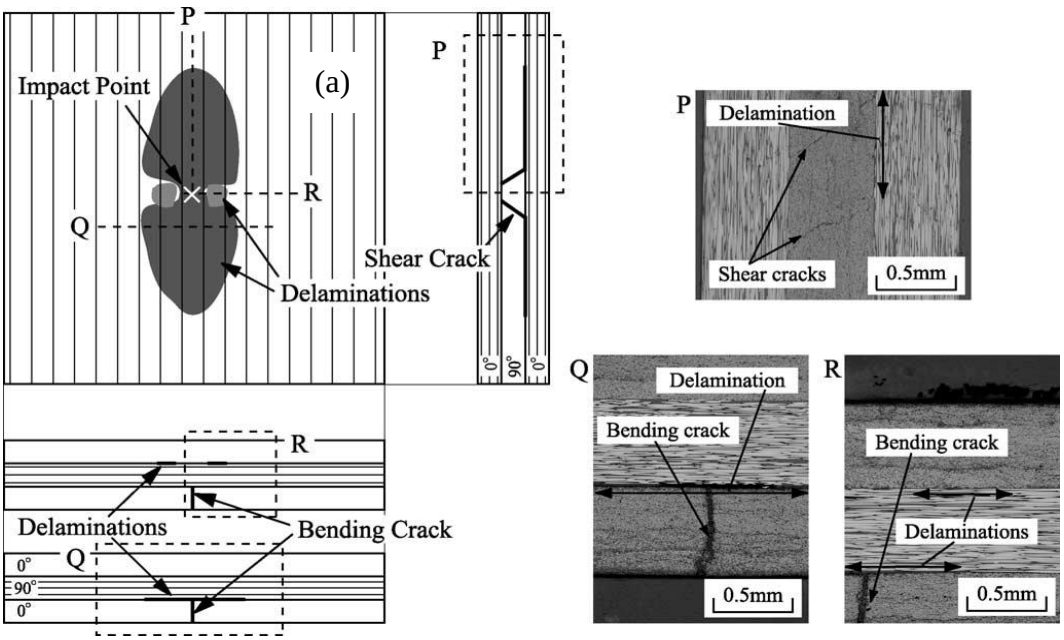

Figure 4.3. Illustration of delamination area evaluated by C-scan (a) and cross-sectional micrographs of the laminate subjected to low-velocity impact [31].

4.2.1 Experimental analysis and characteristic parameters of low velocity impact on laminated composite.

Several interesting studies have been carried out on the behaviour of laminated and honeycomb composite behaviour during the impact [32] to [38]. Observations of contact force between the impactor and the target have highlighted some important information about the capability of composites to absorb and dissipate

energy during impact and the consequently generation of damages such as delamination and matrix cracking. In Figure 4.4 an example of contact force time versus time and displacement is reported [32].

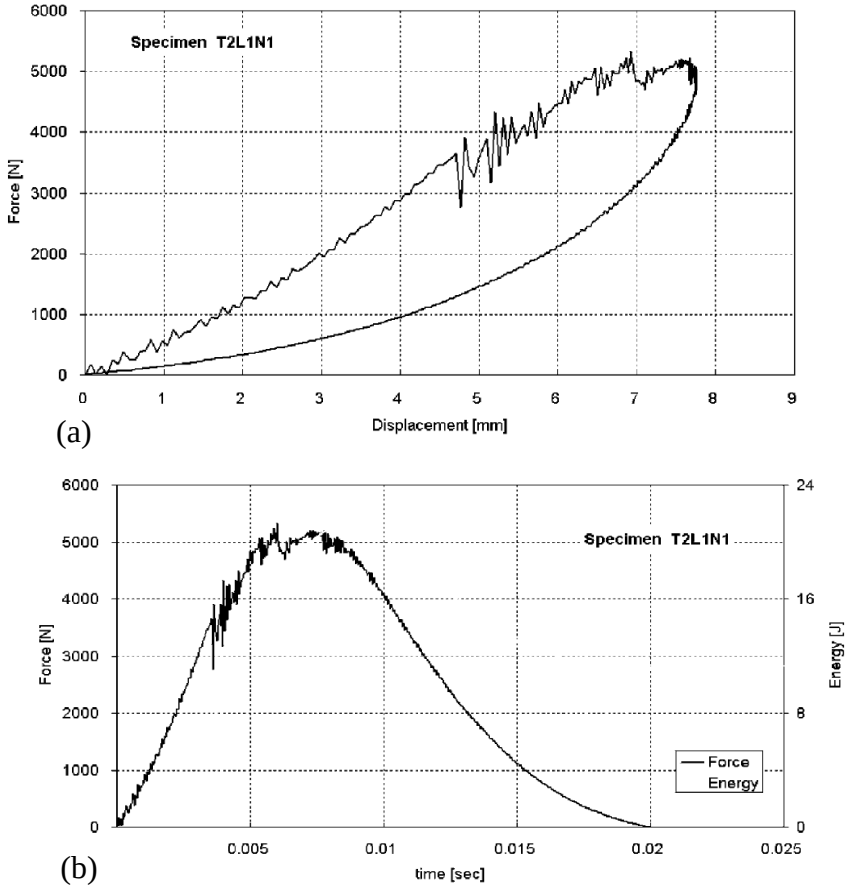

Figure 4.4. Contact Force versus displacement (a) and time (b) during an impact on glass fibre reinforced plastic (GFRP) specimen [32] for rebounded impact.

Observing the the force history in Figure 4.4 is possible to identify the first composite failure which happens when the force history suddenly passes from a smooth rise to a large oscillation behaviour. Consequently the contact force continues to rise and other failure occurs until the impactor reaches the maximum indentation (the full kinetic energy has been converted into mechanical energy)

and the plate rebounds releasing the mechanical energy. During the rebound the contact force follows a different path in Figure 4.4(a) and the area described is the energy loss due manly by the energy dissipated by the failure mechanism.

In APPENDIX - A are also reported the force history for the case where the impactor stops on the sample (the specimen dissipeted all the kinectic energy) and when the impactor perforates the surface.

In conclusion observing the force history is possible to identify four important parameters that allow the characterization of materials under low velocity impact:

- Force threshold for the first material failure
- Maximum force
- Impact energy: the energy needed to stop the impactor.
- The dissipated energy which is equal to the impact energy in the case of no rebound.

4.3 Non linear contact acoustic

Imperfections and defects seen in the morphology of composite following a low velocity impact (see Figure 4.3) are discontinuities at interfaces. Mechanical waves interact with those surfaces generating non linear structural response. In order to understand the behaviour surfaces at discontinuities there is an interesting approach based on the acoustic interaction of surfaces in close proximity which create an open or closed contact. The contact acoustic non-linearity (CAN) from both mathematical [39] and experimental [40] point of view has been investigated by Solodov to clarify the contact effect of close interfaces under a periodic load [41].

4.3.1 Clapping mechanism for non bonded surfaces

The first mechanism analyzed is related to the effect of normal loads applied to the interfaces. Normal stiffness of such non bonded contact has the compression

component higher than the tensile one. This kind of bi-modular contact can be described by the piece-wise stress-strain relation [43]:

$$\sigma = C^{II}\left[1 - H(\varepsilon(t) - \varepsilon^0)\,\frac{\Delta C}{C^{II}}\right]\epsilon \tag{4.1}$$

where H(ε) is the Heaviside unit step function [42], the ε^0 is the static initial compression strain able to guarantee the contact between the surfaces and it restore the intact linear properties (as shown in Figure 4.5) which have C^{II} as the second order linear elasticity term. ΔC is given by the following expression:

$$\Delta C = C^{II} - \left(\frac{d\sigma}{d\varepsilon}\right)_{\varepsilon>0} \tag{4.2}$$

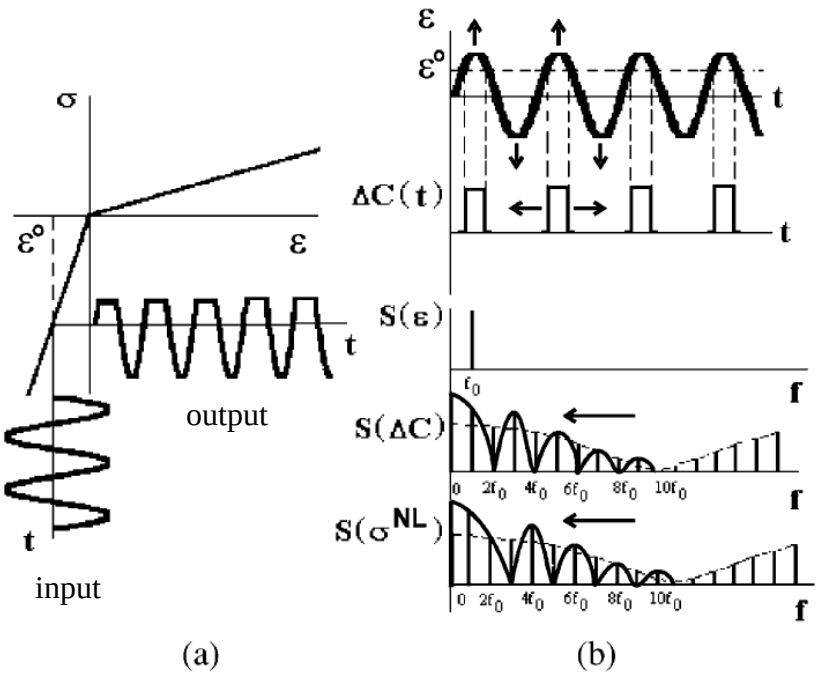

Figure 4.5. CAN model. (a) piece-wise stress-strain relation. (b) CAN spectrum characteristic, arrows indicate direction of growing amplitude [43].

Under periodic excitation the input strain expression is given by:

$$\varepsilon(t) = \varepsilon_0 \cos(\omega_0 t) \tag{4.3}$$

The stiffness variation can be computed substituting the equation (4.3) into equation (4.1) :

$$\Delta C(t) = H(\varepsilon_0 \cos(\omega_o t) - \varepsilon^0)\frac{\Delta C}{C^{II}} \tag{4.4}$$

The equation (4.4) represents a pulse modulation function showed in Figure 4.5 of period T

$$T = \frac{2\pi}{\omega} \tag{4.5}$$

Nonlinear stress component is given by:

$$\sigma^{NL}(t) \sim \Delta C(t)[\varepsilon(t) - \varepsilon^0] \tag{4.6}$$

Spectrum component of expression (4.6) are also shown in Figure 4.5 and both odd and even harmonics are presents as the result of the modulation effect introduced by acoustic contact.

The clapping mechanism described above take into account only the acoustic effect on smooth interfaces, in other words the model does not include effects introduced by friction.

Rough surfaces introduce also tangential traction due by friction, which affects elastic properties. Stress-strain relationship became nonlinear hysteretic as above a certain strain threshold ε_1 where the kinetic friction force is too small to ensure

the coupling between the surfaces as shoed in Figure 4.6. Even the contact stiffness C(t) changes to a pulse mode twice over the stain input period C_S.

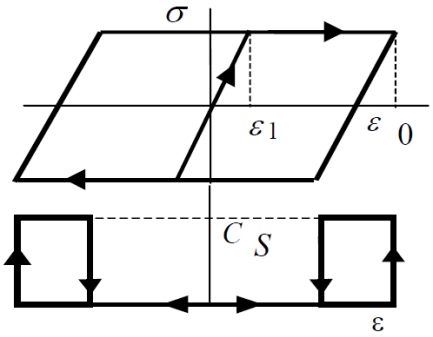

Figure 4.6 Stress-strain curve and stiffness variation due to friction [41]

Thus the contact stiffness assumes the following expression to take into account roughness:

$$C(t) = \frac{C_S}{2}\{1 - sign(\dot{\varepsilon})sign[\varepsilon + sign(\dot{\varepsilon})\varepsilon_1]\} \tag{4.7}$$

Nonlinear stress component even in this case is given by the equation (4.6). However, the output spectrum in this condition contains only odd harmonics [41].

4.3.2 Clapping mechanism for bonded surfaces

Another possible application for the CAN methodology is the analysis of bonded interfaces where the contact between two surfaces is guaranteed by a static normal force that can be an adhesive or a pressure due to a clamping condition. This case is of particular interest not only to study geomaterials (class of material extremely rich in this type of discontinuity) but also to study the bonding condition of in service structures.

Bonding forces also introduce hysteresis into dynamic behaviour of bonded surfaces [41], hysteresis that can take into account introducing a bi-stable interface model [44] (see Figure 4.7). Assuming F_{eff} as the bonding force, F_o bonding force for open interfaces and F_c for close interfaces, the equilibrium position are y_o and y_c are the width of the open and close interfaces width, respectively. Under clapping effect of surfaces the equilibrium position jumps from y_o to y_c as the contact width has been attracted by a strong equilibrium condition ($F_c >> F_o$). This discontinuity in the distance between the interfaces is the reason of hysteresis.

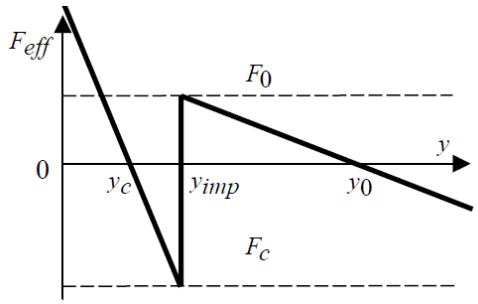

Figure 4.7 Schematic model of bonding force for a bi-stable interface [44] .

4.3.3 Experimental evidence of nonlinear modulation due by clapping interfaces.

In order to support the theoretical approach described in the previous paragraph some of the experimental evidence, found in literature [40]-[41]-43], are reported in this section.

The experimental campaign has been focused on the vibration measurement of a metal or glass samples with an inner interface with both smooth and rough surface to simulate normal traction and friction coupling clapping condition. The samples have been excited with a periodic load and structural responses have been acquired by an accelerometer or laser vibrometer.

The Figure 4.9 shows the results of a test carried out on smooth interfaces and the predicted higher harmonics are clearly visible in the frequency domain.

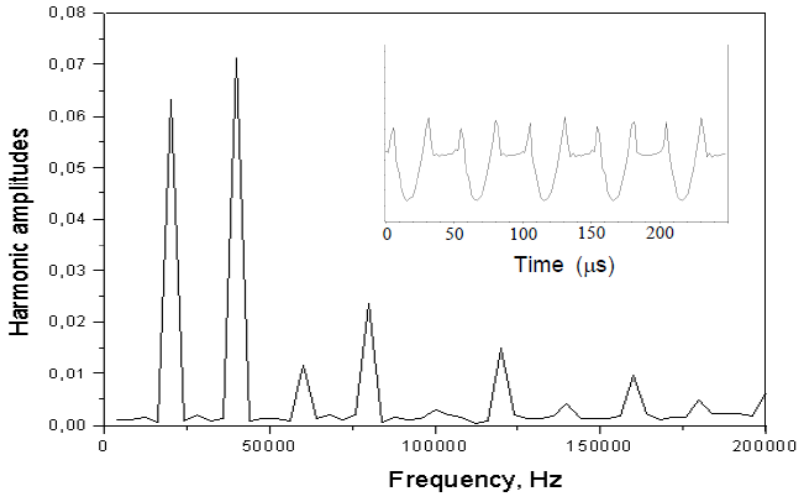

Figure 4.8 FFT and time history of vibration response due by clapping interfaces subjected to an excitation at 20 kHz [41].

The second test has been carried out on rough surfaces to estimate the effect of friction coupling. Even in this case the spectrum component displayed in Figure **4.9** highlights the presence of harmonics and sub-harmonics with odd components prevailing on the evens.

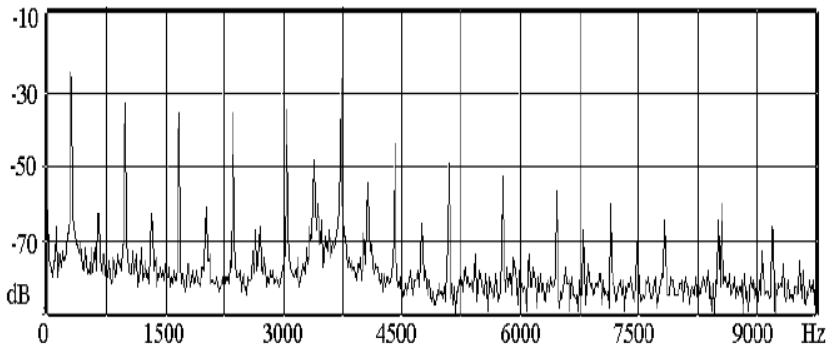

Figure 4.9 FFT vibration response due by friction coupled interfaces subjected to an excitation at 350Hz [41].

4.4 Conclusions

The description of low velocity impact damages morphology in laminated composite has highlighted the presence of many discontinuity interfaces subsequent to the impact, such as delamination or matrix crack.

In order to asses a methodology able to detect these kinds of defects it is extremely important to understand properties, behaviour and nonlinear properties of these discontinuities in a homogeneous material.

The methodology found in literature, and here described, investigates the non linear acoustic contact behaviour in geomaterials or between surfaces expressly created in laboratory. The proposed approach is able to predict nonlinearities and the experimental evidence reported validate the model.

In the next chapters, taking inspiration from these results, a similar approach will be presented in order to develop a nonlinear material model for numerical analysis and to perform an experimental campaign on carbon fibre reinforced plastic samples.

CHAPTER 5 NON LINEAR MODEL FOR MATERIAL CHARACTERIZATION

5.1 Introduction

As discussed in the previous chapters this work intends to explore new solution to improve damage detection methodologies. Today, much attention is devoted to the implementation of linear acoustic for structural health monitoring within a predictive maintenance program. Linear methods in acoustical non-destructive testing analyze the wave speed changes, the reflection of waves due to damage presence, and/or amplitude changes to assess the presence and location of structural anomalies. However, a new class of promising non destructive evaluation techniques (NDE) is being developed based on the monitoring of material nonlinear elastic wave behaviour [41] to [50].

Several researchers [6] have shown that the monitoring of nonlinear elastic wave properties is more effective than linear acoustic methods since they are able to show early signs of material degradation long before changes of linear acoustic properties.

In the previous chapter morphology of low velocity impact on laminated composite has been described and acoustic response of defects have been analysed. Non linear properties are a key aspect to properly describe such discontinuity and hysteresis effects which are clearly visible in the structural responses.

In the next paragraphs a novel approach is described in order to take into account the non linear hysteretic effect introduced by defects in material.

5.2 Non linear classical theory

The Landau and Lifshitz approach for nonlinear wave propagation is based on the perturbation of wave speed in terms of strain [25], thus for a P-wave propagating along a bar the speed of the wave can also be expressed as follow:

$$c^2 = c_0^2 \left[1 + \beta \left(\frac{\partial u}{\partial x} \right) + \delta \left(\frac{\partial u}{\partial x} \right)^2 + \cdots \right] \tag{5.1}$$

where c is the perturbed velocity, c_o is the unperturbed velocity (term able to describe linear wave propagation as seen in paragraph 3.4). The terms β and δ are coefficients introduced to characterize quadratic and cubic non linear effects.

Assuming that P-wave modulus M is:

$$M = \lambda + 2\mu \tag{5.2}$$

The wave speed can be also expressed as:

$$c^2 = \frac{M}{\rho} \tag{5.3}$$

The wave speed expansion can be included in the wave equation to take into account also nonlinear effect such as the generation of harmonics. As the modulus M is the derivative of stress respect to the strain in the static case, even the stress-strain relation (also known as equation of state EOS) became non linear:

$$\sigma = M(\varepsilon + \beta\varepsilon^2 + \delta\varepsilon^3 + \cdots) \tag{5.4}$$

The equation (5.4) describes classical nonlinear effect induced by small defects [50]-[51]. However researches in geophysics have showed how the mechanics of cracks and interstices inside materials introduce also a sort of memory effect on the load history [48]-[50]-[51]-[52] that can be described as hysteretic behaviour. Crack, voids, discontinuity surface and interstices are extremely diffuse in geo-materials, a lot of efforts have been made to understand the behaviour of such materials and find a reasonable model to simulate non linear effects induced by these features. Metallic alloy and composite material have different micro structure; however damaged materials present internal voids, flaws, cracks and interstices just as in geomaterials.

In the next paragraphs a non classical material model will be described as a way to represents those features of behaviour and following the model will be used to simulate numerically damaged materials.

5.3 Non linear non classical approach: hysteretic model

Experimental evidence [41]-[46]-[47] showed that classical nonlinear models cannot explain the nonlinear behaviour generated by local nonlinear forces due to damage presence (such as cracks, voids and contacts). A theoretical description of this behaviour can be given by the nonlinear mesoscopic elastic material model, which contains terms that describe classical nonlinearity, as well as hysteresis, and discrete [41]-[46]-[47] .This is possible by adding to the nonlinear classical stress strain relationship, a stress dependence on strain time derivative (see equation (5.5)), which allows the reproduction of phenomena like hysteresis and material memory introduced by damage in material used in aerospace structures:

$$\sigma = \int K(\varepsilon, \dot{\varepsilon}) d\varepsilon \tag{5.5}$$

where K is the nonlinear and hysteretic modulus given by:

$$K(\varepsilon, \dot{\varepsilon}) = K_0\{1 - \beta\varepsilon - \delta\varepsilon^2 - \alpha[\Delta\varepsilon + \varepsilon(t)sign(\dot{\varepsilon}) \dots]\} \tag{5.6}$$

where K_0 is the linear modulus, $\Delta\varepsilon$ is the strain amplitude change over the last period, β and δ classical nonlinear coefficients, and α material hysteresis measure. The full spectrum of options given by equation (5.6) (see ref [41]) is summarized in Table 5-1.where the pure nonlinear hysteretic behaviour is displayed alongside with the classical nonlinear and linear materials.

Experimental and numerical evidences [41]-[46]-[47] showed that:

- the 3rd harmonic is quadratic with the fundamental amplitude for a purely hysteretic material and cubic according to classical nonlinear theory.
- A second-order sideband $f_2 \pm 2\ f_1$, generated by a bi-tone excitation (f_1 and f_2) has amplitude proportional to $\alpha A_1 A_2$ for a purely hysteretic material, in

contrast with an amplitude dependence proportional to $C(\beta, \delta)A_1^2A_2$ for a classical nonlinear material.

For a classical nonlinear material, the first order sideband ($f_2 \pm f_1$) amplitude is linear with the excitation amplitudes β.

	Linear	Nonlinear Classic 1st order (β)	Nonlinear Classic 2nd order (δ)	Nonlinear Hysteretic (α)
Modulus(ε)	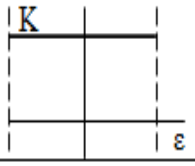	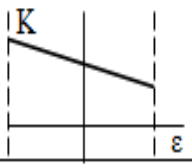	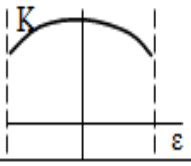	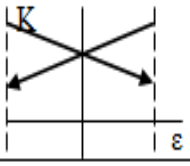
Stress(ε)	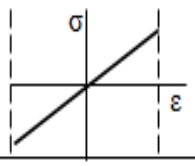	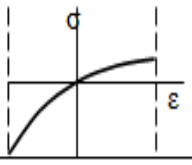	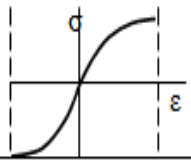	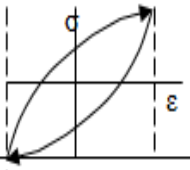
Modulus(t)	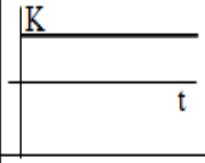	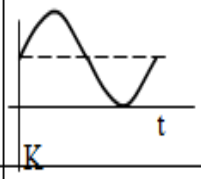	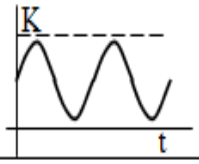	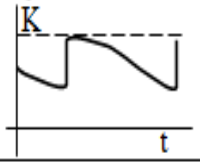
Strain(t)	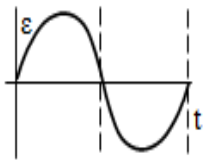	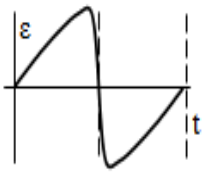	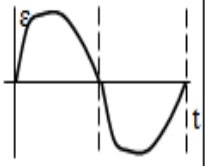	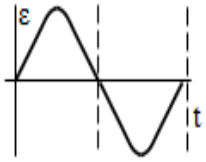
Strain Spectrum	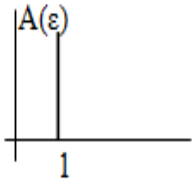	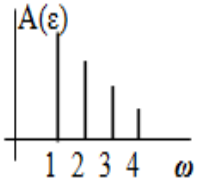	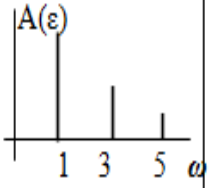	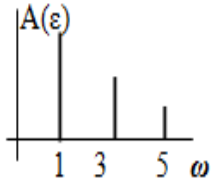
Harmonic Amplitude Dependence	No Dependence	2nd Harm.: slope 2 3rd Harm.: slope 3 4th Harm.: slope 4 Etc.	No even Harm. 3rd Harm.: slope 3 5th Harm.: slope 5 Etc.	No even Harm. 3rd Harm.: slope 2 5th Harm.: slope 2 Etc.

Table 5-1 Acoustic contribution of the material model coefficients [45].

5.3.1 Mesoscopic approach: PM-Space

As mentioned before, the complex compliance and local nonlinear forces due to damage presence may entirely dominate the relatively small atomic nonlinearity leading to a nonlinear behavior that cannot be explained with classical nonlinear models. In order to solve the classical nonlinear model inadequacy, a model was introduced by McCall and Guyer [53], in analogy with the hysteretic electromagnetic behaviour of ferromagnetic materials described by Preisach and Mayergoyz [56]-[58] as the PM space. The main model assumption was that the macroscopic behaviour of highly heterogeneous material (e.g. rocks) is the resultant of the behaviour of a large number of mesoscopic structural particles incorporating nonlinear features such as micro cracks, voids joints and contact surfaces.

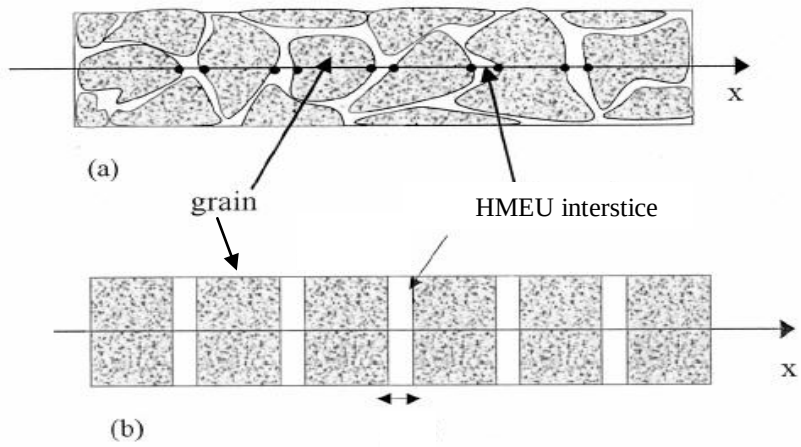

Figure 5.1: (a) Configuration of heterogeneous material. The grain represents linear elastic material and the interstices are the soft bonds between the grains due at the presence of cracks and plasticity zone around, contact surface and joints. (b) One dimensional representation of rock material [49].

The mesoscopic structural particles or Hysteretic Mesoscopic Elastic Unit (HMEU) is thought to be constituted by a grain and a HMEU interstice (Figure 5.1).

The HMEU grain behaves classically with its nonlinear elastic module K described by equation (5.6), with $\alpha=0$. In contrast the HMEU interstice is characterised by a step behaviour defined by two couples of parameters: the two equilibrium lengths (l_o, l_c) and a pair of pressures (P_c, P_o) with $P_c \geq P_o$. In particular, the strain component of Hysteretic Mesoscopic Elastic Unit HMEU can be represented as the strain of a micro-crack induced by an external pressure that opens and closes the crack itself.

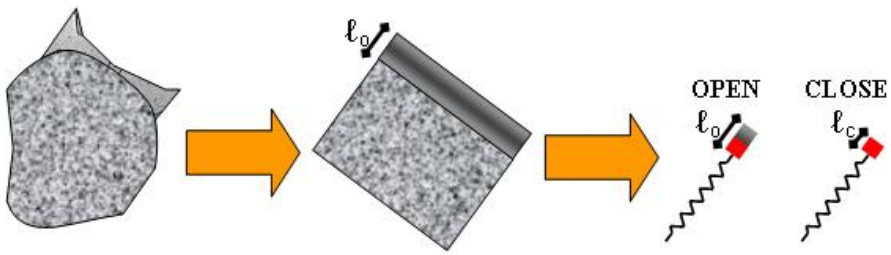

Figure 5.2 Hysteretic mesoscopic elastic unit

From Figure 5.3, it is clear that when the applied pressure increases from zero up to P the equilibrium length of the mesoscopic unit interstice (see Figure 5.1) is l_o, but when the pressure equalizes at P_c the equilibrium length changes and the new state of HMEU interstice is determined by the new equilibrium length l_c. In this new status the equilibrium length remains l_c until the pressure is reduced to below P_o, where the equilibrium length is l_o. In this work, by convention, the stress generated by a compression load is considered positive.

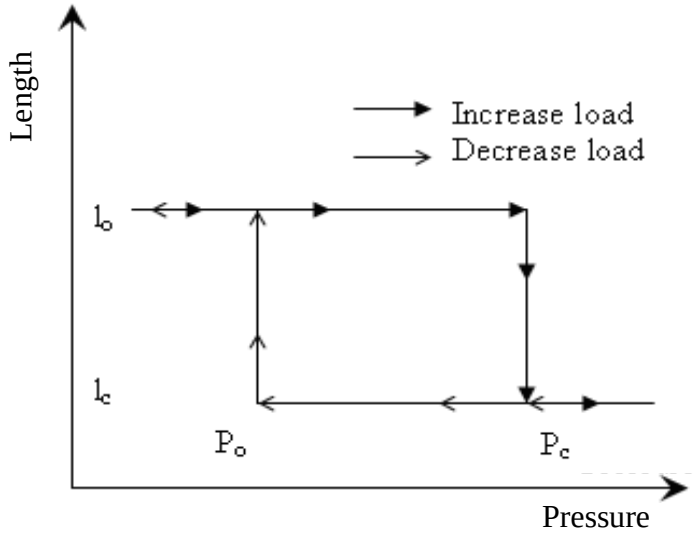

Figure 5.3: Behaviour of hysteretic mesoscopic elastic unity (HMEU). A HMEU is characterized by a couple of pressures (P_c,P_o) and equilibrium lengths (l_o, lc).

Therefore, the material nonlinear macroscopic behaviour can be imaged as an entity made up by a large number of HMEU characterised by different couples of (P_c, P_o). The distribution of HMEU in the plane (P_c, P_o) of the macroscopic entity is localised below a 45 degree line, since P_c must be larger than P_o. An example of PM space is shown in Figure 5.4 where P_c and P_o were defined by the following equation:

$$P_c = 100 r_c^2$$
$$P_o = P_o \sqrt{r_o} \qquad (5.7)$$

where r_c is a random number between 0 and 1.

The elements on the diagonal of Figure 5.4 correspond to mechanical elements that close and open at the same pressure P_c=P_o, so these elements do not have

hysteretic behaviour, therefore behaves as HMEU grains. The other elements showed in Figure 5.4 introduce the hysteretic behaviour.

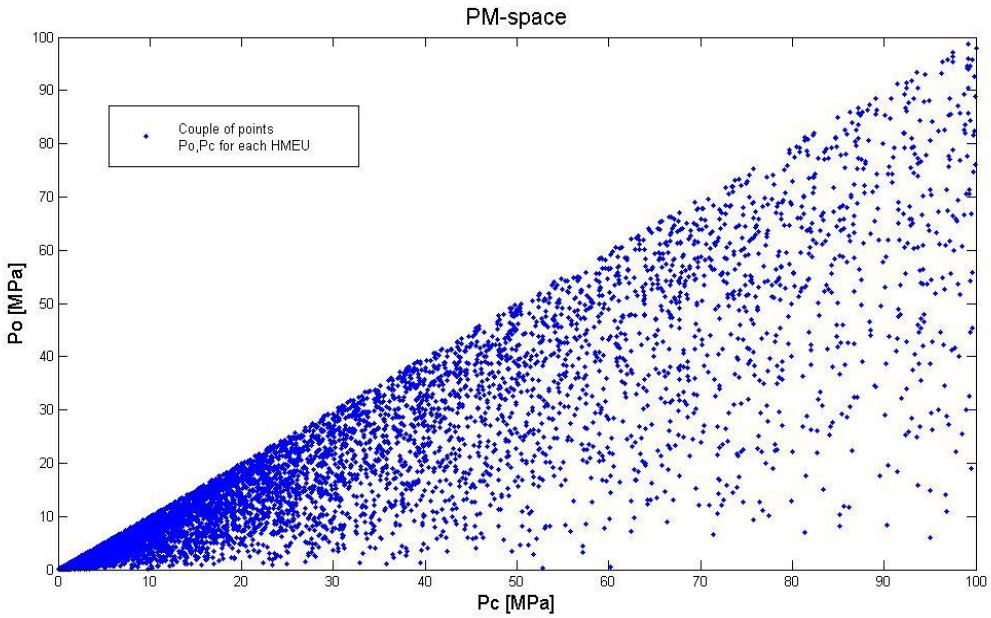

Figure 5.4: Preisaich – Mayergoyz space (PM-space), each mechanicals element has hysteretic property characterized by open pressure (P_o) and close pressure (P_c).

The distribution of the HMEU on the (Pc, Po) plane can be derived using quasistatic measurements of the material strain according to specifically designed protocol loads.

The macroscopic material stress-strain curve can be derived by the PM space distribution as described in the following paragraph.

5.3.2 Material Stress-Strain curve evaluation

The evaluation of the material stress-strain curve using the PM space nonlinear elastic material model can be easily understood if described with a simple

example. Assuming that a beam under axial load is made of a material defined by the PM space described in Figure 5.4.

Then, according to the load protocol, described in Figure 5.5-b, each time a step change of the applied pressure ΔP occurs a certain number of HMEUs close or open consistently with their characteristic pressures (Pc, Po).

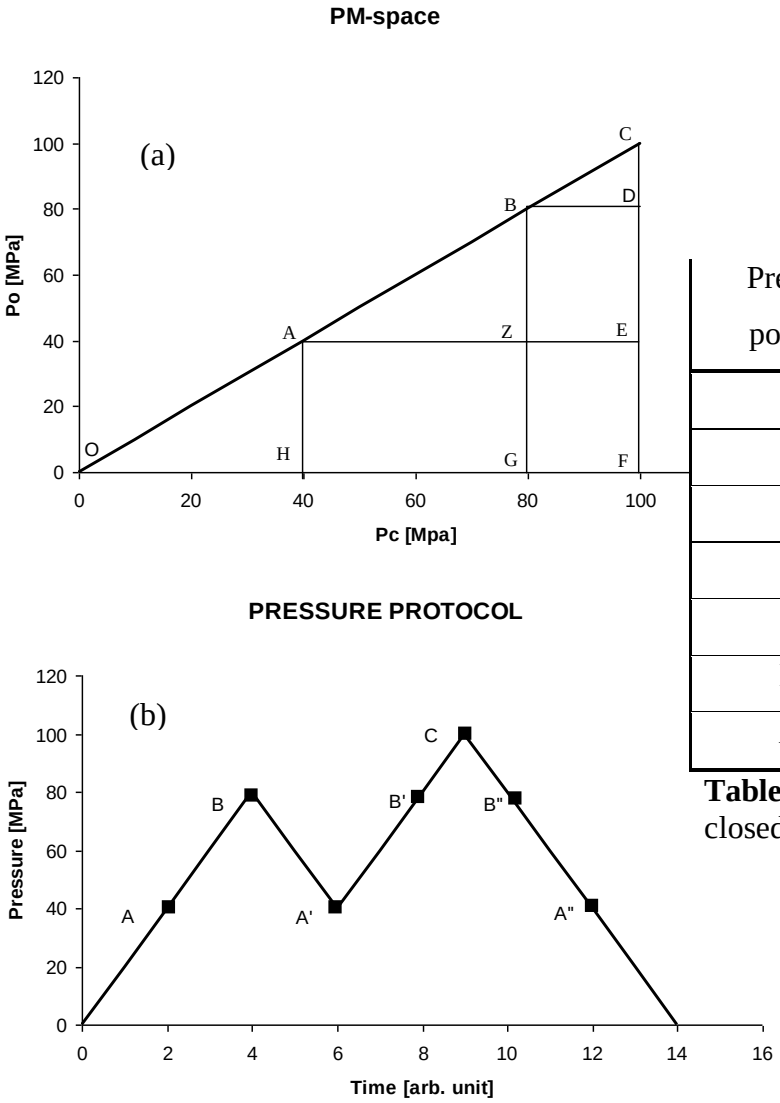

Pressure point	Closed area
A	OAHO
B	OBGO
A’	OAZGO
B’	OBGO
C	OCFO
B’’	OBDFO
A’’	OAEFO

Table 5-2: Pressure vs. closed area in PM-space

Figure 5.5: PM-space with key points (a) to evaluation the strain when the specimen is under the pressure protocol showed (b).

Hence, supposing that all HME units have the same equilibrium length (l_c, l_o), the number of units closed at the instant t is function of the number of HME units

that closes or opens due to ΔP. More specifically, increasing the pressure Po from zero to P_A (pressure in point A, see Figure 4-b, the HMEUs that have the pressure $P_c \leq P_A$ are closed (see Figure 5.6-A). If the pressure is further increased to P_B, all the HMEU with $P_c \leq P_B$ are closed, as described in Figure 5.6-B. Then, decreasing the pressure from P_B to $P_{A'}$, the HMEU enclosed in the triangle ABZ (Figure 5.6-a) open (there is $P_c \geq P_{A'}$), see Figure 5.6-C, to close once again the pressure is increased again to P_B (Figure 5.6-B and Figure 5.6-D). The remaining steps of the load protocol (Figure 5.5-b) were described in Figure 5.5-a, and in Table 5-2.

Since, the previous history of the material is recorded by the HME closed units defined by the minima and maxima of the pressure protocols drawing in the (Po, Pc) plane a staircase line [56].

Once the number of the HMEU interstices closed is known, the non-classical correction K_1 of the classical nonlinear elastic module K (α=0) can be evaluated as follows:

$$\begin{aligned} \frac{1}{K_1} &= -\frac{1}{L(P)} \frac{L(P+\Delta P) - L(P)}{\Delta P}; \quad P \to P + \Delta P \\ \frac{1}{K_1} &= -\frac{1}{L(P)} \frac{L(P) - L(P-\Delta P)}{-\Delta P}; \quad P \to P - \Delta P \end{aligned} \tag{5.8}$$

where the term L(P) is the length of the specimen, when the pressure is P.

$$\begin{aligned} L(P) &= n_c(P) \cdot l_c + \left(N - n_c(P)\right) \cdot l_o \\ L(P+\Delta P) &= n_c(P+\Delta P) \cdot l_c + \left(N - n_c(P+\Delta P)\right) \cdot l_o \\ L(P-\Delta P) &= n_c(P-\Delta P) \cdot l_c + \left(N - n_c(P-\Delta P)\right) \cdot l_o \end{aligned} \tag{5.9}$$

where N is the total number of HMEU, $n_c(P)$ is the number of HMEU closed when the pressure is P;

l_c and l_o are the equilibrium lengths of HMEU.

Therefore, considering only the contribution of the HMEU interstice to the material deformation, the strain generated by a stress P is given by the following expression:

$$\varepsilon = \frac{L_0 - L(P)}{L_0} \tag{5.10}$$

where L_0 is the initial length of specimen.

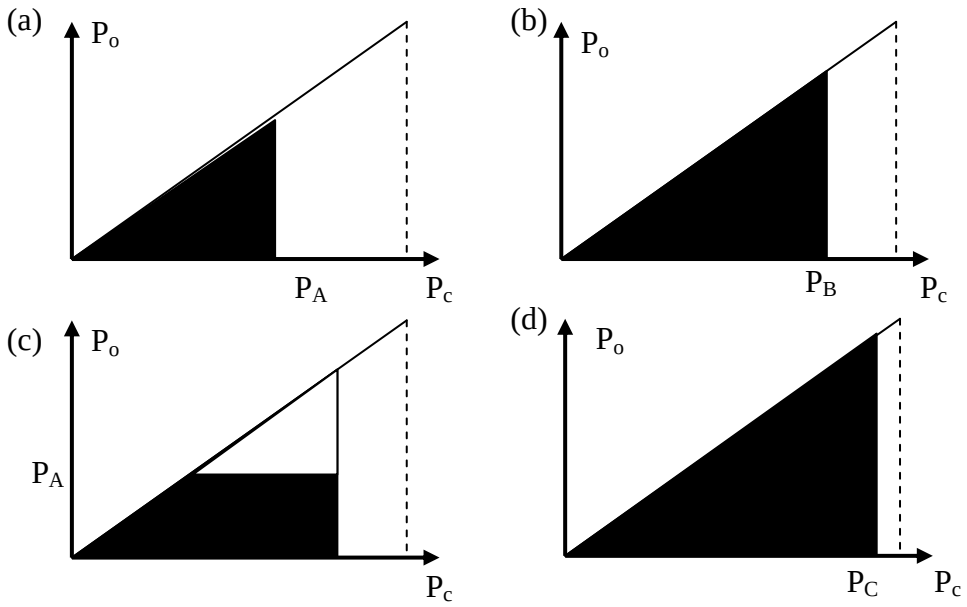

Figure 5.6. PM-space under the pressure P_A and P_B. In section A the triangle is the area with HMEU closed by the pressure P_A. In section B In the black area, there are the units closed when the pressure starts from P_A up to P_B. The total numbers of closed units when the pressure is PB are in the black area plus triangle. In the section C in the white triangle there are the units opened by the protocol load when it is in $P_{A'}$. In the section D the pressure returns at P_B and the PM-space is the same of section II.

An example of strain-stress curve for a non classical nonlinear material is reported in Figure 5.7 . This strain-stress curve was computed using the PM-Space displayed in Figure 5.4 and the pressure protocol described in Figure 5.8.

As expected a hysteretic behaviour was observed in Figure 5.4 as well as material memory effect, as described in literature [49]-[56]-[57]-[58]. Moreover, this behaviour was in agreement with experimental and numerical tests [51]-[54] carried out on rocks.

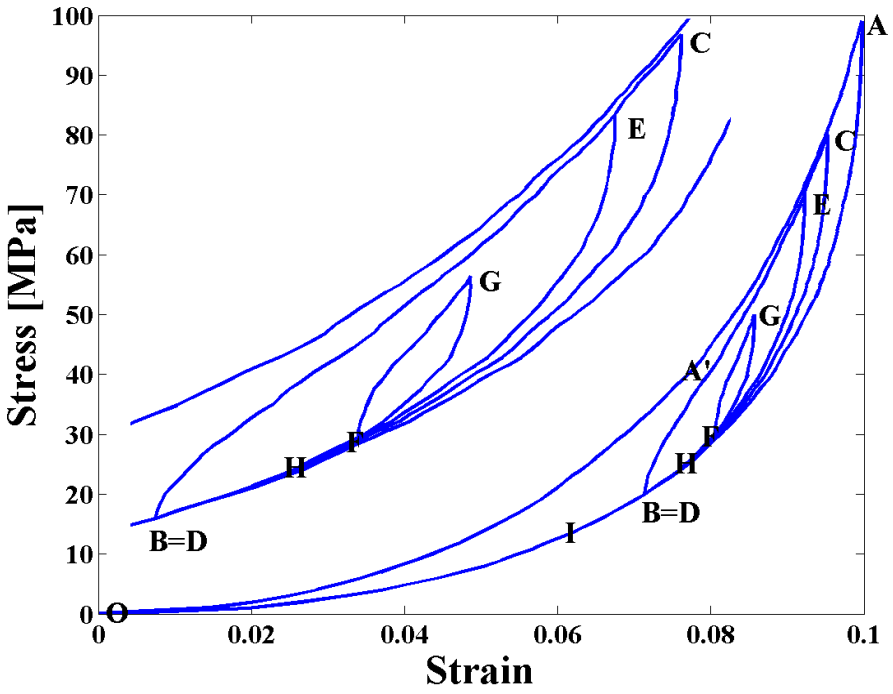

Figure 5.7 Stress-Strain relation evaluated with PM-space

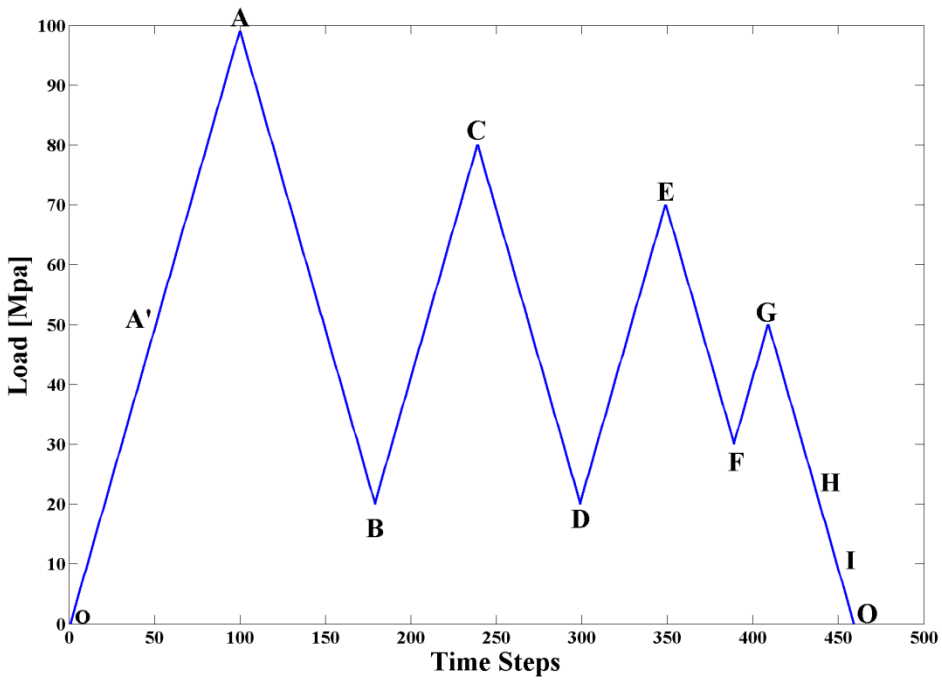

Figure 5.8: Pressure protocol used in the numerical test

5.4 Conclusion

The work presented in this chapter describes the approach (PM-space) followed in previous studies and its ability to reproduce the elastic hysteretic behaviour of geomaterials.

Hysteretic contribution in such class of materials is mainly due to presence of void and discontinuities. These features introduce nonlinear behaviour of stress-strain relationship making the material equation of state non unique and dependent on the stress history.

Similar features are also present in damaged homogeneous material such as laminated composites, where low velocity impact can generate discontinuity surfaces and flaws.

The PM-space has been introduced to numerically simulate the material hysteresis effects of damaged parts and in the following chapter it will play a key role for a numerical investigation of nonlinear properties induced by defects.

CHAPTER 6 NUMERICAL SIMULATION OF NON LINEAR MODEL BASED ON FINITE ELEMENT METHOD

6.1 Introduction

This chapter is focused on numerical simulation as a way to predict nonlinear effect induced by defects in materials. Nowadays many commercial FE (Finite Element) codes provide reliable method to solve nonlinear problem, both from geometrical and material point of view. At the beginning of this work long discussion has been done on the opportunity to use one of the commercial codes or developed an in house FE code. After an investigation on the commercial available codes at the department (ANSYS, NASTRAN) the decision was made to produce an in house code in Fortran 90. The reasons of this choice are mainly due by the absence of hysteretic models able to reproduce behaviour as shown in the previous chapter, but most important, because writing in house Finite Element

code is a great opportunity to improve knowledge on numerical method and it gives the chance to tailor the code to specific needs giving at the same times the flexibility in terms of new enhancement that only 100% visibility on the code can be guaranteed.

The priority of the project was to define an algorithm for nonlinear hysteretic simulation to be implemented by the FE solver. However one of the first steps that should be under the attention of developers is the Mesh generation that can be easily solved for one dimension geometry (as a beam) or as a simple 2D problem. Although this is an interesting numerical problem that can really affect not only the performance of the code but also the accuracy, it has been decided that it was not a priority. The solution identified for mesh generation was to let ANSYS build the mesh. Taking advantage of the potentiality of APDL ANSYS language it is possible to easily built parameterized model and export nodes position, element properties etc... . Thus the approach followed in this work is to use ANSYS as pre-processor, export mesh properties and provide it as an input for in house code.

In this chapter a short introduction to Linear Finite Element Method is provided and a paragraph is dedicated to numerical method for linear equation system solution.

For further details on numerical methods and FE theory some books are highly recommendable over the wide literature presents on this particular topic, those books were a guidelines for this work and they are reported in the reference as: [59]-[60]-[61].

Then the attention will be focused on the numerical implementation of the Presayrch-Mayergoyz model for material hysteretic behaviour in FE code. Some examples of numerical simulation will be provided and they will be of great help for a quantitative analysis of nonlinear phenomena that following in this work will be investigated in laboratory tests.

6.2 Linear dynamic FE theory

Formulation of finite element problem begins with the approximation of continuum problem, where a continuous body is reduced to a finite discrete distribution of elements. Each element is interconnected with a number of nodal points, called nodes, distributed at the boundary of the elements (for some application nodes can be present even in the interior of the element). The displacements of nodal points are the problem unknown and to find them the principle of virtual work (or virtual displacement) has to be invoked. This principle state that the equilibrium of a body requires that for any compatibles small displacements the total internal work is equal to external virtual work [59].

Assuming that the external forces acting on the body could be: body forces, surface forces and concentrated force in the nodes; the total external virtual work, L_e, can be expressed as shown in equation (6.1):

$$\int_{V_e} \{\delta u\}^T \{F\} dV + \int_{S_e} \{\delta u\}^T \Phi \, dS + \sum_{i=1}^{N} \{\delta u\}_i^T \{P\}_i = L_e \qquad (6.1)$$

where {δu} is the small virtual displacement, {F} is the body force, Φ indicates surface force, and P_i is the concentrated forces in the nodal position.

Total virtual internal work, L_i can be written as follow:

$$\int_{V_e} \{\delta \varepsilon\}^T \{\sigma\} dV + \int_{V_e} \{\delta u\}^T \rho \{\ddot{u}\} \, dV + \int_{V_e} \{\delta u\}^T k_d \{\dot{u}\} \, dV = L_i \qquad (6.2)$$

where {δε} is virtual strain corresponding to the virtual displacement, σ is the internal stress, ρ is the mass density, {ü} is the nodes accelerations and k_d is material damping parameters.

The relation coming from the equality of (6.1) and (6.2) is not yet in the right formulation and in order to make explicit the dependency of the L_i and L_e from nodal degree of freedom (which in the most general case can be six: three translational and three rotational) another assumption is required: displacement of generic point of an element can be computed interpolating the degree of freedom of elements nodes, {d} using some special function, [N], called shape functions. Shape function can be of different type and order depending of the problems under investigation. The shape functions [N] are function only of space, rather than {u} displacement are function of space and time [59]-[60]-[61].

For the purpose of this work linear shape function has been used in the FE code. The equations (6.3) describe the relation between a generic element point and nodal displacements *U*.

$$\begin{aligned} \{u\} &= [N]\{U\} \\ \{\dot{u}\} &= [N]\{\dot{U}\} \\ \{\ddot{u}\} &= [N]\{\ddot{U}\} \end{aligned} \tag{6.3}$$

A new differential operator $[\partial]$ can be obtained writing equations (3.1) and (3.2) in matrix notation as in equation (6.4).

$$\begin{Bmatrix} \varepsilon_x \\ \varepsilon_y \\ \varepsilon_z \\ \gamma_{xy} \\ \gamma_{yz} \\ \gamma_{zx} \end{Bmatrix} = [\partial]\{u\} = \begin{bmatrix} \frac{\partial}{\partial x} & 0 & 0 \\ 0 & \frac{\partial}{\partial y} & 0 \\ 0 & 0 & \frac{\partial}{\partial z} \\ \frac{\partial}{\partial y} & \frac{\partial}{\partial x} & 0 \\ 0 & \frac{\partial}{\partial z} & \frac{\partial}{\partial y} \\ \frac{\partial}{\partial z} & 0 & \frac{\partial}{\partial x} \end{bmatrix} \begin{Bmatrix} u \\ v \\ w \end{Bmatrix} \tag{6.4}$$

In analogy with the (6.4) the matrix [B] can be defined as follow:

$$[B] = [\partial][N] \tag{6.5}$$

Substituting the equations (6.3), (6.4) and (6.5) in the equation (3.3) the relation between the stress and nodal displacements can be written as shown in equation (6.6):

$$\{\sigma\} = [C]\{\varepsilon\} = [C][B]\{U\} \tag{6.6}$$

Replacing displacement, stress and strain in the equation (6.1) and (6.2) with the corresponding formulation in terms of degree of freedom {d} (d.o.f) in (6.3), (6.5) and (6.6) the principle of virtual work can be expressed as follow:

$$\begin{aligned}\{\delta d\}^T \Bigg[\int_{V_e} [B]^T[C][B]dV\{U\} + \int_{V_e} \rho[\mathrm{N}]^{\mathrm{T}}[\mathrm{N}]\, dV\{\ddot{U}\} \\ + + \int_{V_e} \mathrm{k_d}[\mathrm{N}]^{\mathrm{T}}[\mathrm{N}]\, dV\{U\} \\ - \int_{V_e} [N]^T\{F\}dV - \int_{S_e} [N]^T \Phi\, dS - \sum_{i=1}^{N} \{P\}_i \Bigg] = 0\end{aligned} \tag{6.7}$$

Grouping the elements in equation (6.7) as described in equations (6.8)

$$
\begin{aligned}
[M] &= \int_V \rho[N]^T[N]dV \\
[D] &= \int_V k_d[N]^T[N]dV \\
[K] &= \int_V [B]^T[C][B]dV \\
\{R\} &= \int_{V_e} [N]^T\{F\}dV + \int_{S_e} [N]^T\Phi\, dS + \sum_{i=1}^{N}\{P\}_i
\end{aligned}
\tag{6.8}
$$

the principle of virtual work, excluding the solution {d}=0 is equivalent to the system of differential equation written in (6.9) where {d} is the unknown.

$$[M]\{\ddot{U}\} + [D]\{\dot{U}\} + [K]\{U\} = \{R\} \tag{6.9}$$

The equation above, as imposed by principle of virtual work, satisfies the equilibrium between external forces and internal forces (inertia, damping and internal reaction terms).

To solve the equation (6.9) there are mainly two categories of solution: implicit and explicit methods and they have the following general form:

$$\{U\}^{t+\Delta t} = f\left(\{U\}^t, \{\dot{U}\}^t, \{\ddot{U}\}^t, \{U\}^{t-\Delta t}, ...\right) \quad \textit{Explicit form} \tag{6.10}$$

$$\{U\}^{t+\Delta t} = f\left(\{U\}^{t+\Delta t}, \{\dot{U}\}^{t+\Delta t}, \{\ddot{U}\}^{t+\Delta t}, \{U\}^t, ...\right) \quad \textit{Implicit form} \tag{6.11}$$

The first solution, explicit formulation, is very fast because, the system equations are uncoupled, so for each time step each node has one equation in one unknown, the displacement U at time t+Δt. On the other hand, explicit methods

are prone to stability problems that force the selection of very small time step integration (Δt), resulting in long computational times.

The second solution, the implicit method, generates a system of coupled equations, the solution of which requires particular inversion algorithms.

6.3 Explicit formulation: central difference method

The discrete form of equation (6.9) in the time can be obtained with a central difference scheme. The displacements are derived by expanding the displacements {U} in Taylor series [60]:

$$\begin{aligned}\{U\}^{t+\Delta t} &= \{U\}^t + \Delta t\{\dot{U}\}^t + \frac{\Delta t^2}{2}\{\ddot{U}\}^t + \frac{\Delta t^3}{3!}\{\dddot{U}\}^t + o(\Delta t)^4 \\ \{U\}^{t-\Delta t} &= \{U\}^t - \Delta t\{\dot{U}\}^t + \frac{\Delta t^2}{2}\{\ddot{U}\}^t - \frac{\Delta t^3}{3!}\{\dddot{U}\}^t + o(\Delta t)^4\end{aligned} \tag{6.12}$$

and approximating the velocity and acceleration as follow:

$$\begin{aligned}\{\dot{U}\}^t &= \frac{1}{2\Delta t}\left(\{U\}^{t+\Delta t} - \{U\}^{t-\Delta t}\right) \\ \{\ddot{U}\}^t &= \frac{1}{\Delta t^2}\left(\{U\}^{t+\Delta t} - 2\{U\}^t + \{U\}^{t-\Delta t}\right)\end{aligned} \tag{6.13}$$

Substituting the equations (6.12) and (6.13) in equation (6.9) and rearranging, the time discrete equation of motion is given by:

$$\left[\frac{1}{\Delta t^2}[M]+\frac{1}{2\Delta t}\right]\{U\}^{t+\Delta t}=\{R\}^t-[K]\{U\}^t + \frac{1}{\Delta t^2}[M](2\{U\}^t-\{U\}^{t-\Delta t})+\frac{1}{2\Delta t}[D]\{U\}^{t-\Delta t} \tag{6.14}$$

In this form, the problem is made by uncoupled linear equation if and only the matrices $[M]$ and $[C]$ are diagonal.

Alternatively, for non diagonal $[C]$ an uncoupled linear equation system can be obtained using the following approximation of the structural acceleration and velocity:

$$\begin{aligned}\{\dot{U}\}^{t-\frac{\Delta t}{2}}&=\frac{1}{\Delta t}\left(\{U\}^t-\{U\}^{t-\Delta t}\right)\\ \{\ddot{U}\}^t&=\frac{1}{\Delta t}\left(\{\dot{U}\}^{t+\frac{1}{2}\Delta t}-\{\dot{U}\}^{t-\Delta t}\right)=\frac{1}{\Delta t^2}\left(\{U\}^{t+\Delta t}-2\{U\}^t+\{U\}^{t-\Delta t}\right)\end{aligned} \tag{6.15}$$

Then, rewriting the equation (6.9) as:

$$[M]\{\ddot{U}\}^t+[C]\{\dot{U}\}^{t-\frac{\Delta t}{2}}+[K]\{U\}^t=\{R\}^t \tag{6.16}$$

and substituting (6.15) and (6.16) in (6.16) yields:

$$\frac{1}{\Delta t^2}[M]\{U\}^{t+\Delta t}=\{R\}^t-[K]\{U\}^t + \frac{1}{\Delta t^2}[M]\left(\{U\}^t+\Delta t\{\dot{U}\}^{t-\Delta t}\right)-[D]\{U\}^{t-\frac{\Delta t}{2}} \tag{6.17}$$

Both equation (6.14) and (6.17) are conditionally stable, therefore the time step has to be accurately chosen. Equation (6.14) is conditionally stable if and only if:

$$\Delta t \leq \frac{2}{\omega_{\max}} \tag{6.18}$$

where $\omega_{\max}$ is the highest natural frequency of interest for the investigation

For the equation (6.17), the stability condition is as follows:

$$\Delta t \leq \frac{2}{\omega_{\max}}\left(\sqrt{1+\varepsilon^2}-\varepsilon\right) \tag{6.19}$$

where the $\omega_{\max}$ is the highest undamped natural frequency and ε is the ratio between the modal damping at $\omega_{\max}$ and the critical damping [60]

6.4 Implicit approach: Newmark scheme

One of the most used implicit methods is the Newmark scheme [59]. This is based on the Crank-Nicholson scheme, where displacements are calculated as follows:

$$\begin{aligned} \dot{U}^{t+\Delta t} &= \dot{U}^{t} + \left[\left(\frac{1}{2}-\alpha\right)\cdot\ddot{U}^{t} + \delta\cdot\ddot{U}^{t}\right]\cdot\Delta t \\ U^{t+\Delta t} &= U^{t} + \ddot{U}^{t}\cdot\Delta t + \left[\left(\frac{1}{2}-\alpha\right)\cdot\ddot{U} + \alpha\cdot\ddot{U}^{t+\Delta t}\right]\cdot\Delta t^2 \end{aligned} \tag{6.20}$$

where $U^{t+\Delta t}$ is the displacement vector (or rotation) of all degree of freedom at time step $t+\Delta t$ and U^{t} is the known displacement vector at time step t, $\dot{U}$ and $\ddot{U}$ indicate, respectively, the velocity and acceleration, α and δ are parameters that can be evaluated using equation (6.21) in order to guarantee stability (see Figure 6.1).

$$\delta \geq \frac{1}{2} + \gamma; \quad \alpha \geq \frac{1}{4}(1+\gamma)^2 \qquad \gamma \geq 0 \tag{6.21}$$

where γ is the amplitude decay [62].

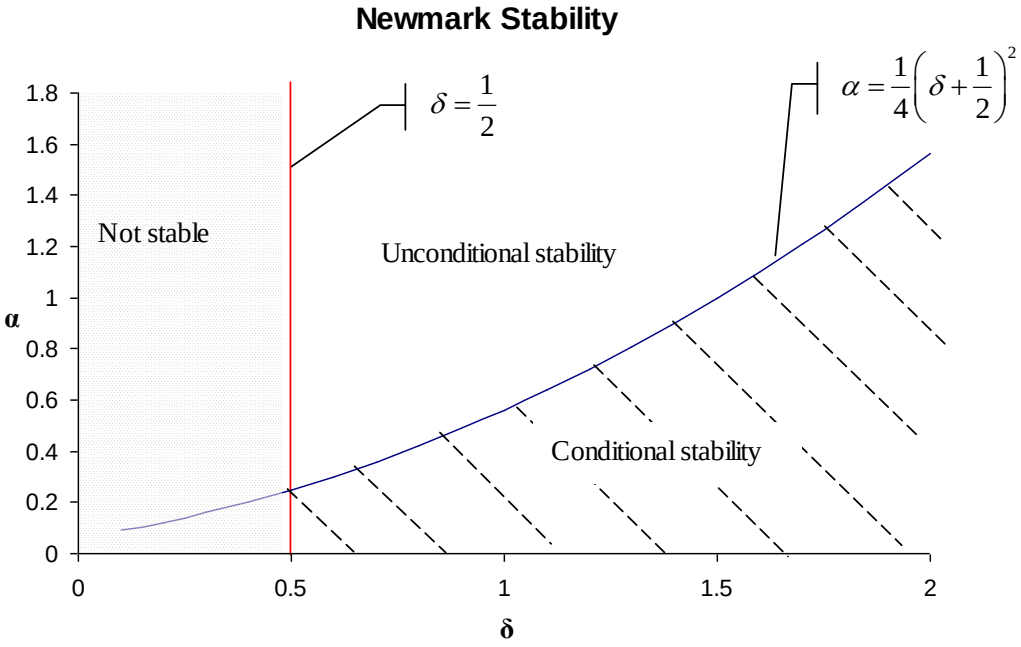

Figure 6.1. Numerical stability diagram for Newmark scheme depending on the parameters α and δ

.

Rearranging the equation (6.9) in terms of the equations (6.20) and then regrouping, the following form of the equation of motion is obtained:

$$\left[\hat{K}\right]\{U\}^{t+\Delta t} = \left\{\hat{R}\right\}^{t+\Delta t} \tag{6.22}$$

where $\left[\hat{K}\right]$ is the dynamic stiffness matrix (6.23) and $\left\{\hat{R}\right\}^{t+\Delta t}$ the dynamic force resultant (6.24)

$$\left[\widehat{K}\right] = [K] + a_0[M] + a_1[C] \tag{6.23}$$

$$\begin{aligned}\left\{\widehat{R}\right\}^{t+\Delta t} = \{R\}^{t+\Delta t} + [M]\left(a_0\{U\}^t + a_2\left\{\dot{U}\right\}^t + a_3\left\{\ddot{U}\right\}^t\right) \\ + [D]\left(a_1\{U\}^t + a_4\left\{\dot{U}\right\}^t + a_5\{\ddot{U}\}^t\right)\end{aligned} \tag{6.24}$$

with the parameters integration defined as follows:

$$\begin{aligned} a_0 &= \frac{1}{\alpha\Delta t^2} & a_1 &= \frac{\delta}{\alpha\Delta t} \\ a_2 &= \frac{1}{\alpha\Delta t} & a_3 &= \frac{1}{2\alpha} - 1 \\ a_4 &= \frac{\delta}{\alpha} - 1 & a_5 &= \frac{\Delta t}{2}\left(\frac{\delta}{\alpha} - 2\right) \\ a_6 &= \Delta t\left(1-\delta\right) & a_7 &= \delta\Delta t \end{aligned} \tag{6.25}$$

During the computation, at each time integration step the displacements are known from system equation (6.23) and, after, the accelerations and velocities can be updated using the following expressions:

$$\begin{aligned}\ddot{U}^{t+\Delta t} &= a_0\left(U^{t+\Delta dt} - U^t\right) - a_2\dot{U}^t - a_3\ddot{U}^t \\ \dot{U}^{t+\Delta t} &= \dot{U}^t + a_6\ddot{U}^t + a_7\ddot{U}^{t+\Delta t}\end{aligned} \tag{6.26}$$

The Newmark integration procedure is schematised in APPENDIX - B. The linear equations system of (6.22) remains to be solved by numerical methods which are the topic of the next chapter.

6.5 Numerical resolution of linear equation system

In literature, a number of solvers for linear system of equations are available. These can be divided in two categories: direct methods and iterative methods (see Figure 6.2).

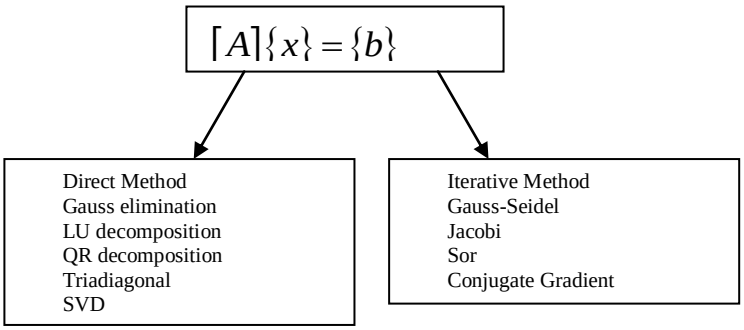

Figure 6.2. Some possible methods to solve linear system equation that can be divided into two classes.

The first class of methods are based on the decomposition of matrix A, and they provide an exact solution. For the second class, the solution is obtained through an iterative procedure aimed at minimizing the residue vector (see equation (6.27)). In this case the accuracy of the solution depends on the tolerance convergence parameter chosen to stop the iteration procedure when a norm of the residue vector is smaller than this parameter.

$$\{R\} = \{b\} - [A]\{\bar{x}\} \tag{6.27}$$

where the $\{\bar{x}\}$ is the attempted solution of the system.

Among the solver analysed only three were implemented in the FE code: the LU-decomposition, the Tridiagonal algorithm (direct methods) and the Conjugate Gradient method (CG) (iteration method).

6.5.1 LU decomposition

The LU decomposition is a direct solver based on the decomposition of the coefficient matrix A of the linear system (equation (6.28)) in two matrices L and U (eq. (6.29)), called respectively the upper and lower matrix [63].

$$[A]\{x\} = \{b\} \tag{6.28}$$

$$[A] = [L][U]$$

$$\begin{pmatrix} a_{11} & \cdots & a_{1n} \\ \vdots & \ddots & \vdots \\ a_{n1} & \cdots & a_{nn} \end{pmatrix} = \begin{pmatrix} \alpha_{11} & 0 & \cdots & 0 \\ \alpha_{21} & \alpha_{22} & \cdots & 0 \\ \vdots & \vdots & \ddots & \vdots \\ \alpha_{n1} & \alpha_{n2} & \cdots & \alpha_{nn} \end{pmatrix} \begin{pmatrix} \beta_{11} & \beta_{12} & \cdots & \beta_{1n} \\ 0 & \beta_{22} & \cdots & \beta_{2n} \\ \vdots & \vdots & \ddots & \vdots \\ 0 & 0 & \cdots & \beta_{nn} \end{pmatrix} \tag{6.29}$$

Substituting the equation (6.29) in equation (6.28) and rearranging the following expression is obtained:

$$[A]\{x\} = \left([L]\cdot[U]\right)\{x\} = [L]\cdot\left([U]\{x\}\right) = \{b\} \tag{6.30}$$

Therefore the solution of (6.28) can be split in two steps:

$$[L]\{y\} = \{b\} \tag{6.31}$$

$$[U]\{x\} = \{y\} \tag{6.32}$$

The particular form of matrices L and U allows using the following technique to solve the linear system:

Forward substitution

$$y_1 = \frac{b_1}{\alpha_{11}}$$
$$y_i = \frac{1}{\alpha_{ii}}\left(b_i - \sum_{j=1}^{i-1} \alpha_{ij} y_j \right) \quad i = 2,3,.....,N \tag{6.33}$$

Backward substitution

$$x_N = \frac{y_N}{\beta_{NN}}$$
$$x_i = \frac{1}{\beta_{ii}}\left(y_i - \sum_{j=i+1}^{N} \beta_{ij} x_j \right) \quad i = N-1, N-2,.....,1 \tag{6.34}$$

where N is the dimension of the square matrices *A*, *L* and *U*.

In order to decompose the matrix A into the upper and lower matrices, U and L, the Crout`s algorithm was used. This provides the coefficients of the matrices, L and U, by exploiting the matrix product properties (eq.(6.35)).

$$\begin{aligned} i < j \quad &\Rightarrow \quad \alpha_{i1}\beta_{1j} + \alpha_{i2}\beta_{2j} + ... + \alpha_{ii}\beta_{ij} = a_{ij} \\ i = j \quad &\Rightarrow \quad \alpha_{i1}\beta_{1j} + \alpha_{i2}\beta_{2j} + ... + \alpha_{ii}\beta_{jj} = a_{ij} \\ i > j \quad &\Rightarrow \quad \alpha_{i1}\beta_{1j} + \alpha_{i2}\beta_{2j} + ... + \alpha_{ij}\beta_{jj} = a_{ij} \end{aligned} \tag{6.35}$$

where α_{ij} and β_{ij} are, respectively, the coefficients of the matrix U and B.

The number of equations in (6.35) is N^2 (total number of coefficient in matrix NxN) but the number of unknown is N^2+N, so there are N arbitrarily unknown to specify. Therefore, the upper matrix diagonal coefficients were assumed to be unitary:

$$\alpha_{ii} = 1 \quad i = 1,...., N \tag{6.36}$$

Afterwards, the Crout`s algorithm evaluates the lower matrix coefficients (6.37) and finally the remaining upper matrix coefficients (6.38)

$$i = 1,..., j \Rightarrow \quad \beta_{ij} = a_{ij} - \sum_{k=1}^{i-1} \alpha_{ik} \beta_{kj} \tag{6.37}$$

$$i = j+1,..., N \Rightarrow \quad \alpha_{ij} = \frac{1}{\beta_{jj}} \left(a_{ij} - \sum_{k=1}^{i-1} \alpha_{ik} \beta_{kj} \right) \tag{6.38}$$

Eventually, it has to be mentioned that the LU decomposition is quite expensive from a computational point of view, since it requires $\frac{N^3}{6}$ operation.

6.5.2 Tridiagonal method

The tridiagonal method is the quickest methods investigated and it can be applied only if the coefficient matrix A of the linear system of equation (6.28) is tridiagonal, and it satisfies the condition of diagonal dominance.

$$\begin{bmatrix} b_1 & c_1 & 0 & 0 & \cdots & 0 \\ a_2 & b_2 & c_2 & 0 & \cdots & 0 \\ 0 & a_3 & b_3 & c_3 & \cdots & 0 \\ \vdots & \vdots & \vdots & \ddots & \vdots & \vdots \\ \vdots & \vdots & \vdots & \vdots & \ddots & \vdots \\ 0 & 0 & 0 & 0 & a_n & b_n \end{bmatrix} \begin{Bmatrix} u_1 \\ u_2 \\ u_3 \\ \vdots \\ \vdots \\ u_n \end{Bmatrix} = \begin{Bmatrix} r_1 \\ r_2 \\ r_3 \\ \vdots \\ \vdots \\ r_n \end{Bmatrix} \tag{6.39}$$

$$|b_j| > |a_j| + |c_j|$$

The linear system solution is computed using the same approach followed in the LU decomposition in the equations (6.33) and (6.34). In this way, the number of operations necessary for the computation of the solution is $O(N)$.

6.5.3 Conjugate Gradient method

The Conjugate Gradient (CG) method is an iterative procedure that minimises the residue vector R:

$$\{R\} = \{b\} - [A]\{\bar{x}\} \tag{6.40}$$

where the $\{\bar{x}\}$ is an approximated solution updated at each iteration. At the first iteration the solution vector can be chosen arbitrarily, however, a correct choice can considerably reduce the number of iterations.

The CG [64] method can be used only for symmetric and positive definite matrices which is always the case for structural matrices. The CG procedure is aimed at finding the ideal solution $\{x_{id}\}$ that satisfies the following equation:

$$\{r\} = \{b\} - [A]\{x_{id}\} = 0 \tag{6.41}$$

In this case for symmetric and definite positive matrices, equation (6.41) can be written as follows [63]:

$$F(x) = \frac{1}{2}\{r\}^T [A]^{-1} \{r\} = \frac{1}{2}(\{b\} - [A]\{x_{id}\})^T [A]^{-1} (\{b\} - [A]\{x_{id}\}) = 0 \tag{6.42}$$

where *F(x)* is equal zero only when $\{x\} = \{x_{id}\}$ and for $\{x\} \neq \{x_{id}\}$ *F(x)>0*. So finding the solution of the linear algebraic system in equation (6.28) is equivalent to finding the minimum of *F*(x). Hence, the problem is to find a series of $\{x^k\}$ that has decreasing $F(x^k)$ values where k is the iteration number. Therefore, starting from an arbitrary vector (as initial solution) and, then, at each step the new

solution is computed as a correction of the previous according to the fastest decreasing direction P_k of F [64]. The velocity of convergence of this method depends on tolerance parameter and especially from the good conditioning of matrix A. To accelerate the convergence process a conjugate direction of p_k can be evaluated as follows:

$$\{p\}_{k+1}^{T}[A]\{p\}_{k} = 0 \tag{6.43}$$

where $\{p\}_{k+1}$ is the conjugate direction.

6.6 Non linear finite element analysis: PM-space implementation and numerical test cases

In this section the transient numerical analysis of beams and plates is investigated through non linear finite element model. The purpose of this section is to understand what the effects of a damage insertion are in a homogeneous medium, in particular the phenomena related to a non linear hysteretic model will be investigated and how the material characterized with PM-space approach can influence waves travelling in the medium.

The results of these numerical simulations provided important indication on how nonlinear features behave and this information has been used later to perform experimental tests.

6.7 Implementation of PM-space in FE code.

In chapter 5 the hysteretic elastic modulus was computed using the PM-space using a statistical distribution of mesoscopic units. For the simulation of damaged homogeneous material some assumptions have been made:

- Material is everywhere linear elastic, excepting where the damage is localised.
- Damaged areas are characterized by elastic model plus hysteretic contribution computed using PM-space
- Distribution of mesoscopic units is constant in PM-space and compression stress equivalent to 5MPa is able to saturate the PM-space (see Figure 6.3)
- When all mesoscopic units are closed there is a total contribution to compression strain of 0.1%

The above assumptions have allowed the evaluation of the hysteretic contribution to the elastic properties in a more efficient way using the following formulation:

$$E = \frac{\sigma}{\varepsilon} = \frac{\sigma}{\max\_strain \frac{A_c}{A_{total}}} \tag{6.44}$$

The above equation computes the contribution to elastic modulus estimating the area of PM-space corresponding to closed units. Assuming constant distribution of mesoscopic unit the strain ε due to the hysteretic behaviour for the stress σ is proportional to the ratio of closed unit area, *Ac*, and PM-space total area, A_{total}, multiplied by the strain corresponding to the all PM-space area. As shown chapter 5 the hysteretic contribution depends not only from an

instantaneous stress but also on its history, which in terms of FE implementation means that stresses at the current and previous iterations must to take into account in the computation of closed area A_C, whereas A_{total} and *max_strain* are constant parameters depending from the problem properties.

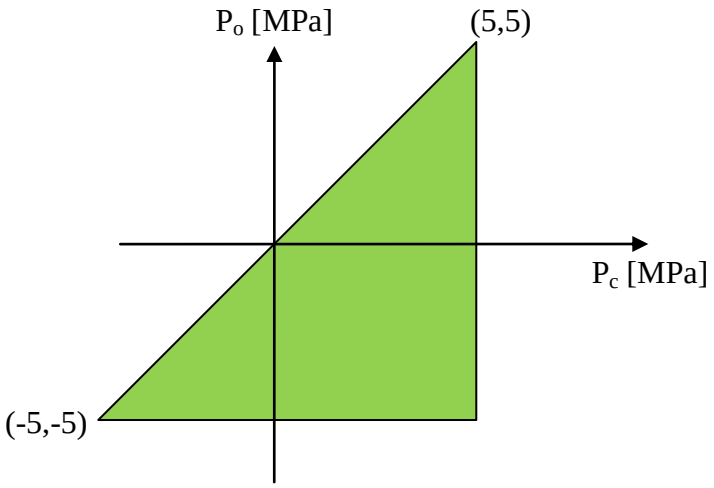

Figure 6.3. PM-space configuration with uniform mesoscopic distribution

Under these assumptions the implementation of PM-space involves the evaluation of nonlinear elastic properties for every iteration, as a consequence for every numerical iteration the stiffness matrix should be reassembled increasing dramatically the computational cost. However the hysteretic part is just a part of resultant elastic properties which have the following expression:

$$[K] = [K_L] + [\Delta K_{NL}] \tag{6.45}$$

Where $[K_L]$ is the linear stiffness matrix and $[\Delta K_{NL}]$ is the hysteretic contribution. Using this formulation it is possible to rewrite the equation (6.9) as follow:

$$[M]\{\ddot{U}\} + [D]\{\dot{U}\} + [K]\{U\} = \{R\} - [\Delta K_{NL}]\{U\} \tag{6.46}$$

In other words the nonlinear contribution is computed as the equivalent perturbation forces introduced by the hysteretic effect and then applied to the linear model to take into account material nonlinearities. Therefore there is no need to assemble the stiffness matrix every iteration as it is not time dependent. Moreover nonlinear part is a function of stress from current and previous iterations, thus once the linear problem is solved at the current iteration the evaluation of hysteretic contribution involves only the solution of one equation, (6.44) in one unknown A_c.

6.8 Numerical analysis 1D model

For this numerical test case, a twenty cm long beam (

Figure **6.4**) was selected, with the following material properties:

- Elastic Modulus: E=10 GPa
- Density: ρ =2600 kg/m^3
- Cross section area= 1cm^2

The damping term c in the equation of motion was assumed to be:

$$c = -\frac{\pi f}{Q} v \tag{6.47}$$

where v is the p-wave speed (see equation (3.27)), f excitation frequency and Q = 80 over a large frequency range (1kHz to 1MHz). The beam was modelled by using 5000 rod elements (one degree of freedom for each node). An axial excitation force was located at the left end of the bar, applied at a nodal location.

Figure 6.4. Geometrical model of beam for FE analysis.

The damage was simulated by a hysteretic nonlinear material represented by a uniform density PM space elements in the triangle (-5 MPa, 5 MPa), see Figure 6.3.

The generic element has been considered linear, therefore axial displacement *u* is to be linear in axial coordinate *s*, moreover the displacement *u* must satisfy the nodal displacement (dof): $u=U_i$ and on the other hand $u=U_j$. Thus the generic displacement *u* can be expressed as followed [60]:

$$u = \frac{L-s}{L}U_i + \frac{s}{L}U_j \xrightarrow{yields} u = \begin{bmatrix} \frac{L-s}{L} & \frac{s}{L} \end{bmatrix} \begin{Bmatrix} U_i \\ U_j \end{Bmatrix} \tag{6.48}$$

where L is the element length. Substituting the (6.48) in (6.3) and in (6.5) the shape function and strain displacement matrix chosen for the beam analysis are:

$$N = \begin{bmatrix} \frac{L-s}{L} & \frac{s}{L} \end{bmatrix}; \quad [B] = \frac{d}{ds}[N] = \begin{bmatrix} -\frac{1}{L} & \frac{1}{L} \end{bmatrix} \tag{6.49}$$

Assuming the beam cross section area A is constant the integral (6.8) becomes:

$$[K] = \int_o^L [B]^T AE\,[B] ds = \frac{AE}{L}\begin{bmatrix} 1 & -1 \\ -1 & 1 \end{bmatrix} \tag{6.50}$$

The equation (6.50) represent the linear elastic stiffness matrix, similarly the nonlinear contribution can be compute as shown in equation (6.51) once elastic properties ΔE are evaluated through PM-space.

$$[\Delta K_{NL}] = \frac{\Delta E\, A}{L}\begin{bmatrix} 1 & -1 \\ -1 & 1 \end{bmatrix} \tag{6.51}$$

The above local stiffness matrix has to be assembled in global stiffness matrix generating a global tridiagonal stiffness matrix

The mass matrix is assumed to be diagonal where each element corresponds to the half of element mass concentrated at the nodal position. Global damping matrix is tridiagonal as the local matrix for each element is:

$$D = \begin{bmatrix} c & -c \\ -c & c \end{bmatrix} \tag{6.52}$$

Following this formulation it is possible to fully determine all the elements in equation (6.9), thus non linear analysis can be performed using Newmark algorithm and allowing PM-space to compute hysteretic contribution at each iteration.

The integration time step has been chosen according to equation (6.53):

$$\Delta t_1 = \frac{1}{2}\frac{l}{V} \tag{6.53}$$

where V is the P wave speed and l is the element length.

6.8.1 Numerical results

The numerical analysis has been carried out on the same beam described in the previous paragraph, with a continuous external load with a frequency of 1 KHz and with two different configurations of damage. In the first configuration the length of damage zone is of 5 cm and starts at 2 cm from the right end, in the second case the length of damage zone is of 3 cm and starts at 3 cm from the right end. Furthermore to compare the PM-space effect with another kind of linear approach the damage zone was simulated by imposing an elastic modulus equal to 9.6GPa. This elastic modulus is the average modulus evaluated with PM-space in damaged elements.

The strain amplitude of fundamental, second, third and fifth harmonic of the element at 10 cm from the source was investigated for different load amplitude: 500, 1000, 2000, 4000, 8000, 16000, 32000, 64000, 128000, and 256000 Pa.

To obtain the fundamental and harmonics of the strain signal, only the last 10 of the 100 periods of the excitation signal were considered. Then a Fast Fourier Transform of this signal was performed. With this approach only the stationary effect were considered while transient effect were neglected.

In the Figure 6.5 the behaviour of a damaged beam shows an increment of amplitude relative to the damage position. This effect is more evident observing the odd harmonic as showed in Figure 6.6 and Figure 6.7, where the amplitudes of intact and damage beam with constant elastic modulus can be neglected.

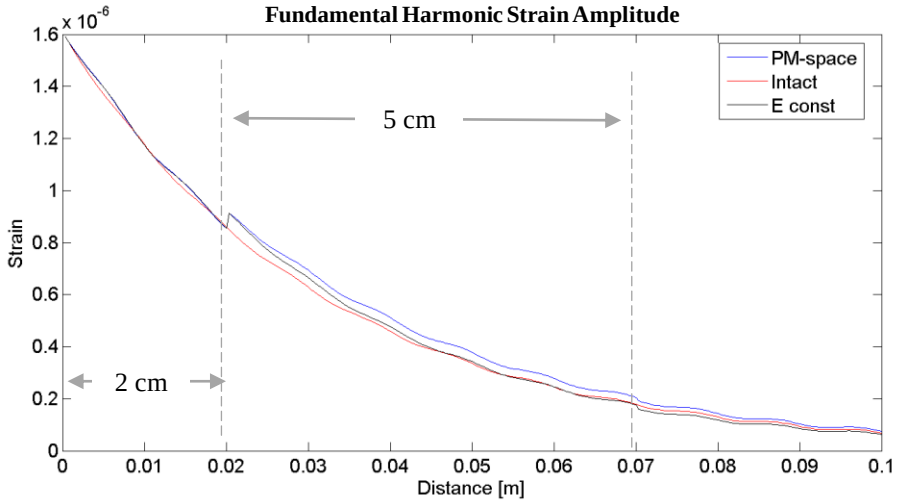

Figure 6.5: Fundamental Strain Amplitude against the distance. The damage is located at 2 cm from the right end and its extension is of 5 cm. The blue line is related at PM-space behaviour, the red to the intact beam and the black to the damaged zone modelled with a constant value of elastic modulus.

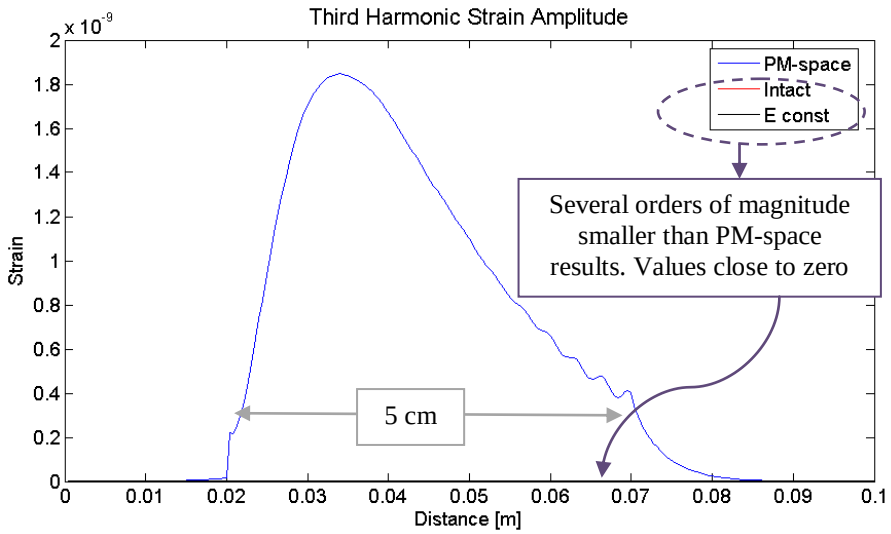

Figure 6.6: Third Harmonic Strain Amplitude against the distance. The damage is located at 2 cm from the right end, and the dimension of damage is of 5 cm. The amplitude of intact (red) and damaged beam, modelled with constant value of E=9.6GPA (black), are several orders of magnitude smaller than beam modelled with PM-space.

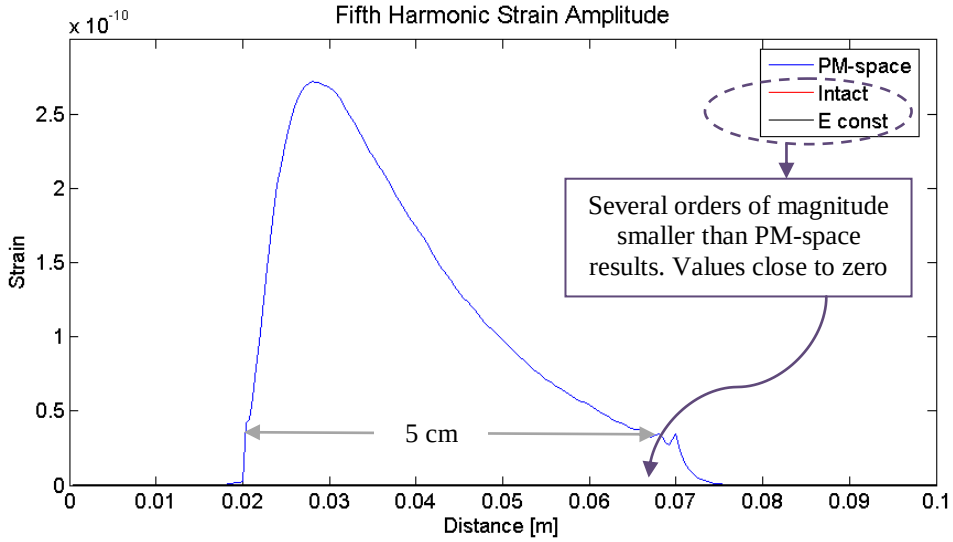

Figure 6.7 Fifth Harmonic Strain Amplitude against the distance. The damage is located at 2 cm from the right end, and the dimension of damage is of 5 cm. The amplitude of intact (red) and damaged beam, modelled with constant value of E=9.6GPA (black), are several orders of magnitude smaller than beam modelled with PM-space.

In contrast the Figure 6.8 shows that the amplitude of second harmonic due to PM-space is quite similar to the values calculated for the other two cases. This effect has been observed for all even harmonic. This behaviour is in very good agreement with experimental data [41]

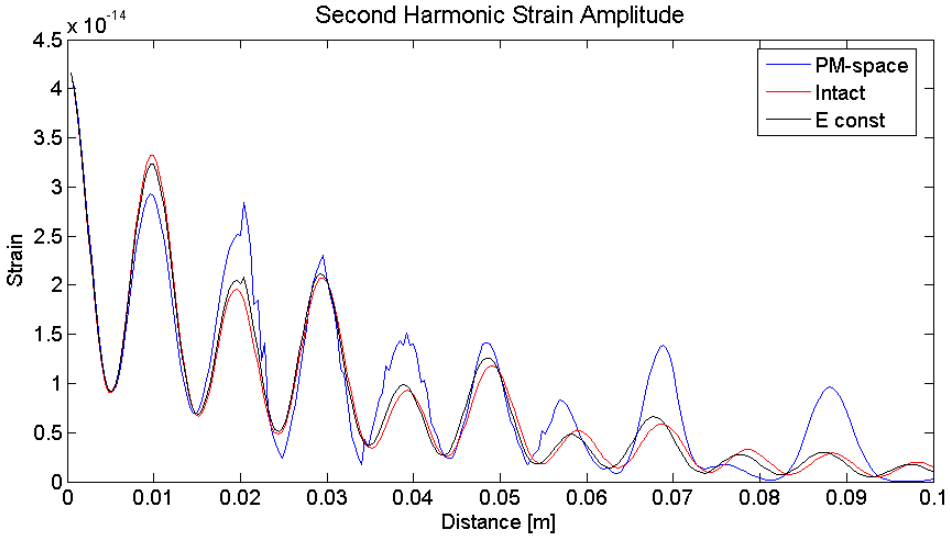

Figure 6.8: Second Harmonic Strain Amplitude against the distance. The damage is located at 2 cm from the right end, and the dimension of damage is of 5 cm. The behaviour due to the PM-space is very closed to the linear elastic behaviour.

The test carried out with the second configuration damage gives the same results as shown from Figure 6.9 to Figure 6.11.

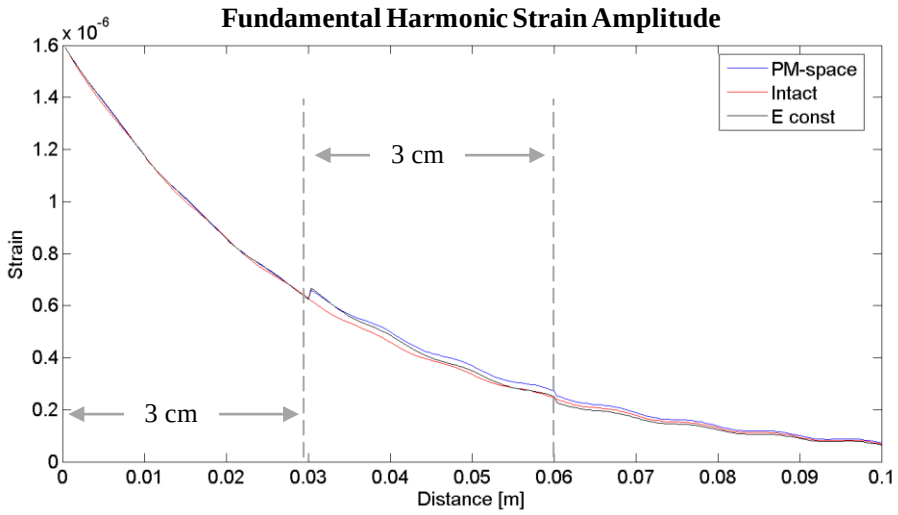

Figure 6.9 Fundamental strain amplitude for the second configuration damage. The damage zone starts at 3 cm from the right hand side 3 cm.

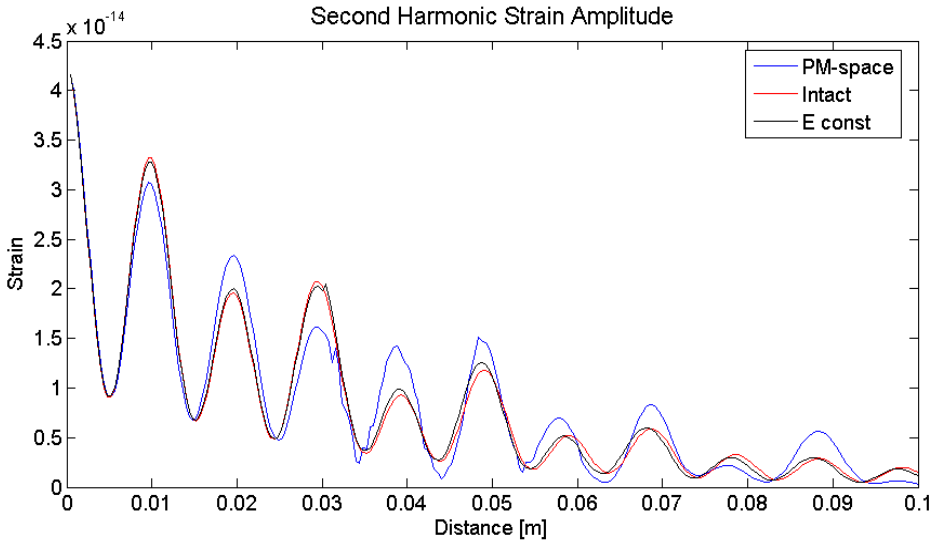

Figure 6.10 Second (A) harmonic strain amplitude for the second configuration damage. The damage zone starts at 3 cm from the right hand side 3 cm.

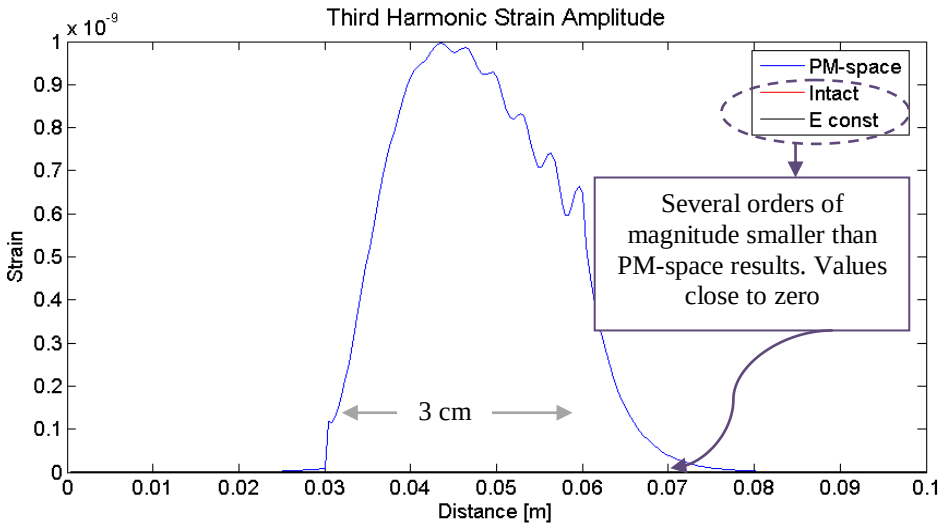

Figure 6.11: Third harmonic strain amplitude for the second configuration damage. The damage zone starts at 3 cm from the right hand side 3 cm. The amplitude of intact (red) and damaged beam, modelled with constant value of E=9.6GPA (black), are several orders of magnitude smaller than beam modelled with PM-space.

In order to understand the different behaviour of the PM-space as a function of the location and dimension of damages, the third and fifth harmonics are shown in Figure 6.12. The results show that the amplitude of these harmonics are extremely sensitive to the variation of position and dimension of the damage. However, further studies are needed to correlate damage type, location and magnitude with the non-linear elastic behaviour of damaged materials.

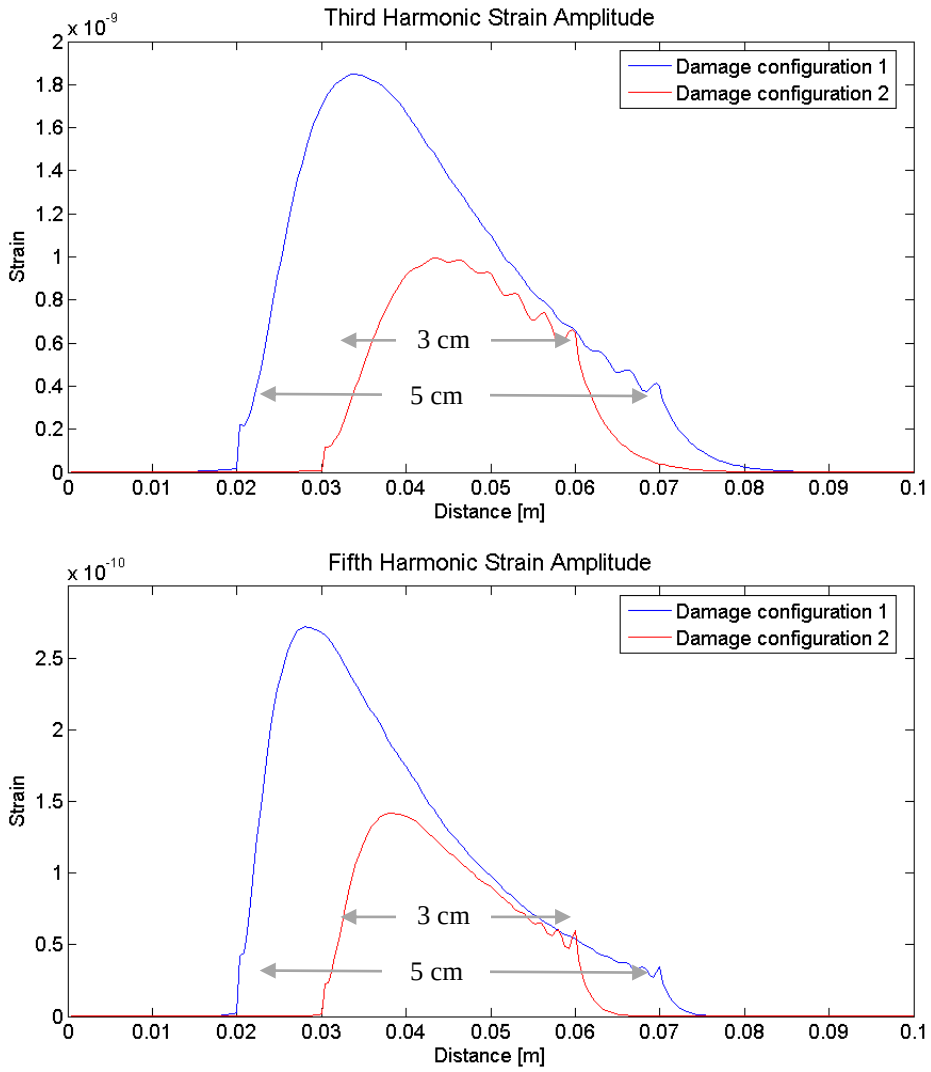

Figure 6.12 The third (A) and fifth (B) harmonics for both damage configuration. In the configuration 1 the damage is between 2cm and 7 cm from the right end, in the second configuration the damage is between 3cm and 6 cm.

Another effect caused by PM-space is the non linear behaviour of the harmonic amplitude as a function of load amplitude. Choosing one reference point along the beam for the linear elastic beam, the behaviour of the harmonic amplitude is linear, but the PM-space does not follow the linear behaviour as shown in Figure 6.13(B) and predicted by non classical non linear theory described in the paragraph 5.3.

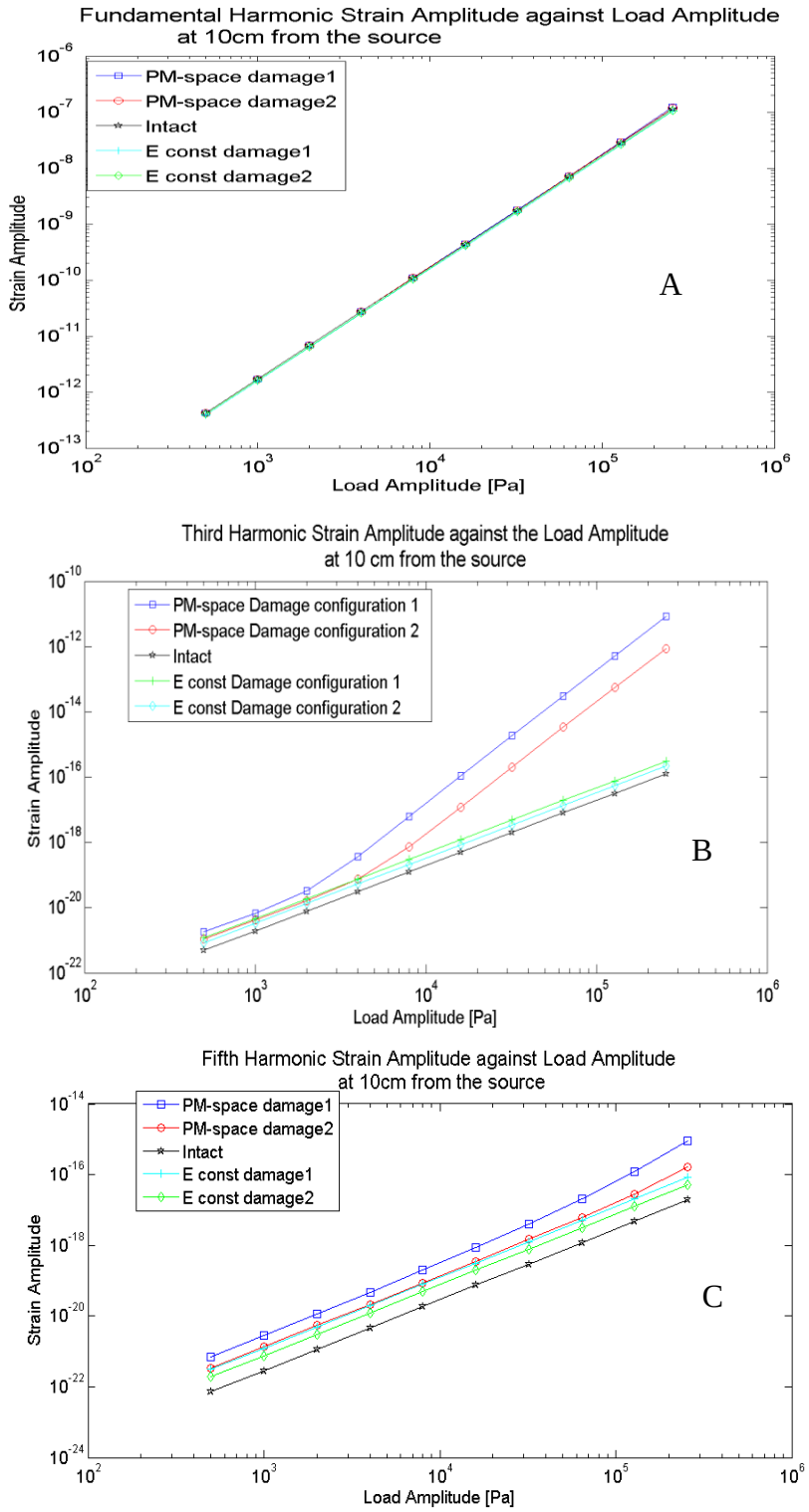

Figure 6.13: Fundamental(A), Third(B) and Fifth(C) Harmonic Strain Amplitude at 10 cm from the source against the load amplitude in logarithmic scale.

The non linear effects are more evident especially for the odd harmonics. In addition, comparing the amplitudes of the intact and linearly damaged case, the PM-space shows greater sensitivity to the damage size.

These results are in good agreement with existing experimental evidences in literature.

6.9 Numerical analysis: nonlinear 2D model

For the 2D finite element analysis the isoparametric four nodes plate has been implemented in the FE code. Gaussian points and Gaussian quadrature have been coded in order compute stiffness matrix for plane stress element (see paragraph 3.3). A full description of the method can be found in literature [59] to-[62].

The following table summarize some of the FE model and 2D properties used in the numerical test.

Plate dimension	0.5x0.3x0.003 m
Linear Material properties	• E1=140GPa • E2=30GPa • G=4GPa • ν_{12}=0.2 • ρ=1700 Kg/m^3
Nonlinear Material properties	P-M space [-5PMa,5PMa]
Excitation	bi-harmonic excitation • frequency: f1= 10 kHz, f2=200kHz • amplitude: A1=[0.5-3.5] MPa A2=0.05MPa

Table 6-1. Summary of 2D FE model

The Figure 6.14 is a representation of the FE model used to perform the non linear transient analysis. The red point represents the location of nodes where displacement has been measured. Black point indicates the location of nodes where external forces have been applied. The whole rectangle is the area where non P-M space is used to compute the non linear material response.

The total number of element used for this simulation is greater than 100,000, whereas the damaged area corresponds to 24 elements.

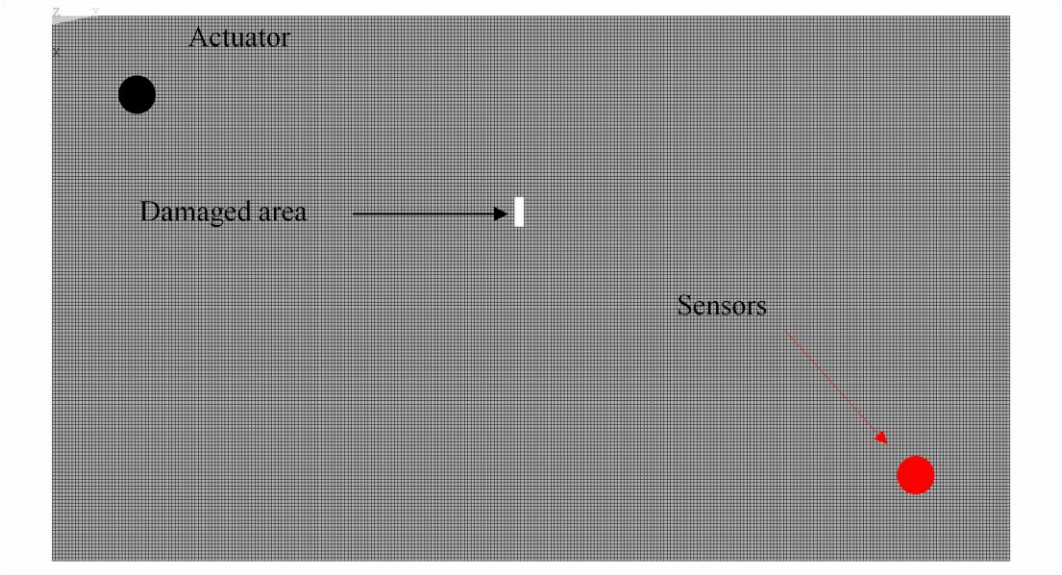

Figure 6.14 Schematic representation of 2D model.

According to the formulation provided in the equation (6.46) the correction terms is computed for each time step to take into account the non linear material characterization.

6.9.1 Numerical Results

The damaged area has been modelled with 3 different material types: undamaged, PM-space model and with 80% of undamaged properties.

The results of transient analysis have been processed using the Short Time Fourier Transformation [65] as reported in Figure 6.15, where the presence of sidebands around the high frequency component is evident in the PM-space results.

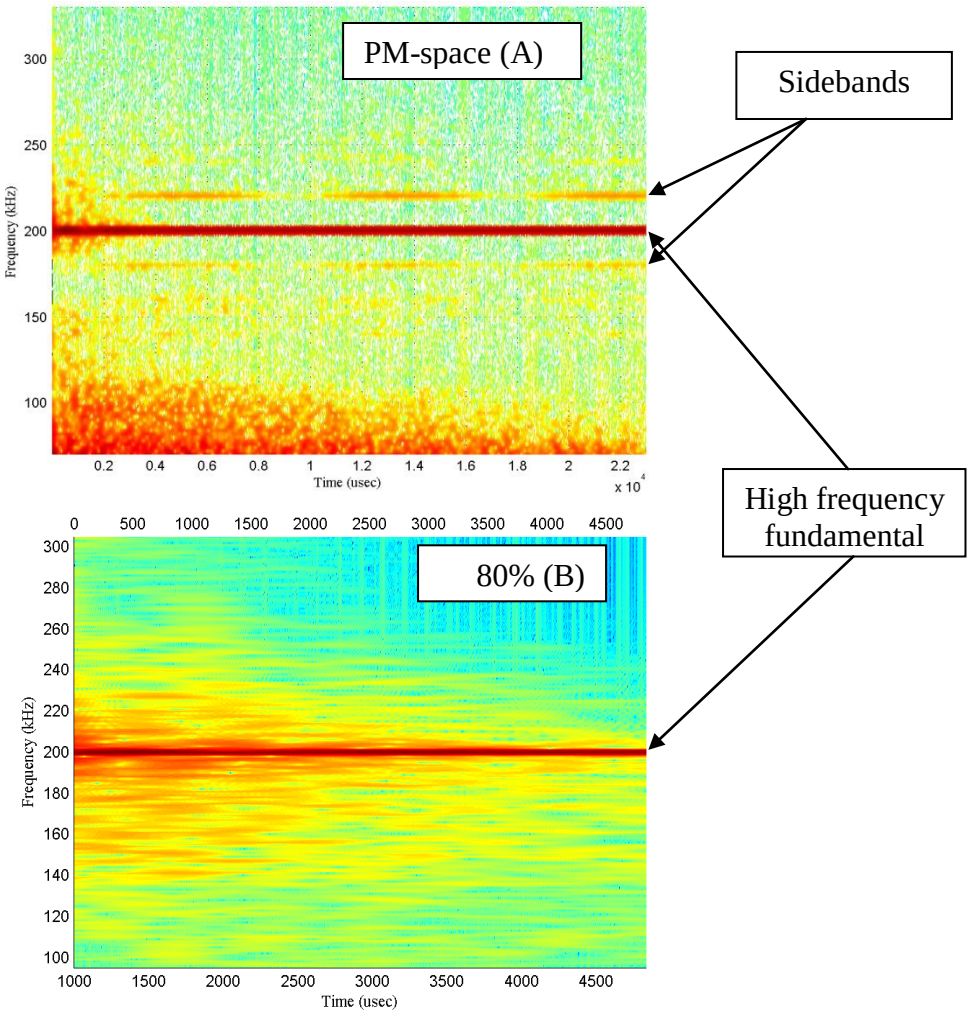

Figure 6.15 STFT of plate during the excitation period with PM-space (A) response and material properties at 80% of undamaged properties (B).

These sidebands are the effect of non linear modulation introduced by the PM-space model. Indeed the damaged area modelled with material properties at 80% of undamaged properties does not produce a clear modulation effect between the fundamental components of excitation and the spectrum of structural response (red line in Figure 6.16) is almost identical to the undamaged case (green line in Figure 6.16). The spectrum analysis of the three material responses is also reported in Figure 6.16 where both undamaged material and damaged at 80% of intact properties do not generate any of the inter modulation observable in the PM-space case.

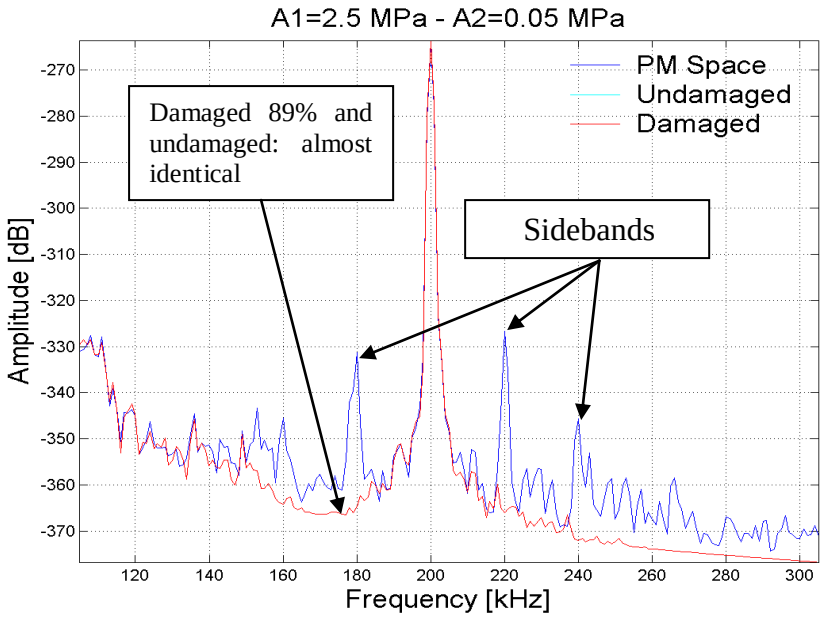

Figure 6.16 Spectrum of plate response in the vicinity of high frequency excitation fundamental.

Sideband amplitudes are also dependent on the low frequency amplitude. This dependency is observable in the Figure 6.16 and pictures (a)-(b) of Figure 6.17 that represent the amplitude of fundamental and sidebands for different values of the low frequency excitation component.

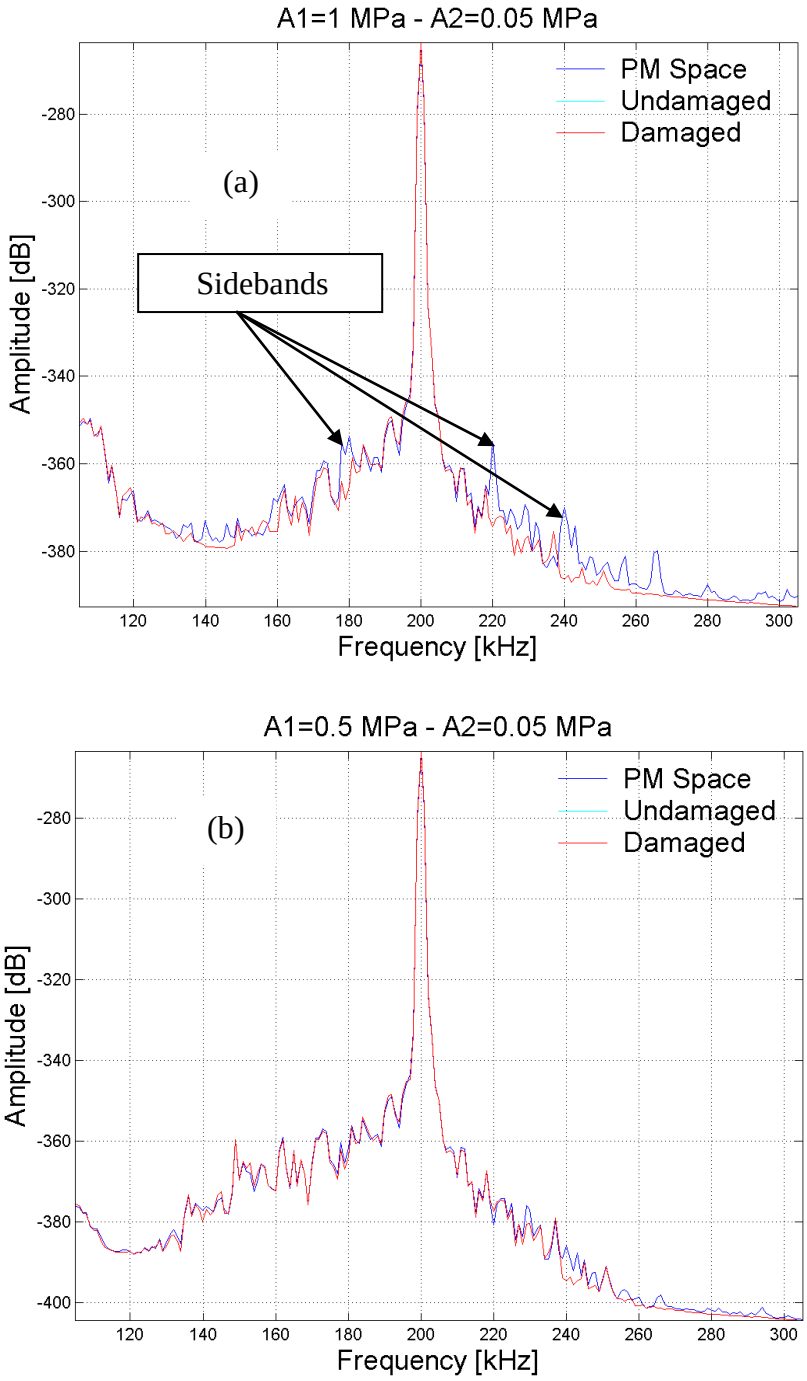

Figure 6.17 Spectrum of plate response in the vicinity of high frequency excitation fundamental at A2=0.05MPa and A1=1MPa (a) and A1=0.5MPa (b).

A closer look around the low excitation frequency component is presented in Figure 6.18. In this case the spectrum in the vicinity of the lowest component does not highlight any of non linear effects as odd or even harmonic components and the results of the three model (undamaged, 80% of undamaged properties and PM-space) are almost identical.

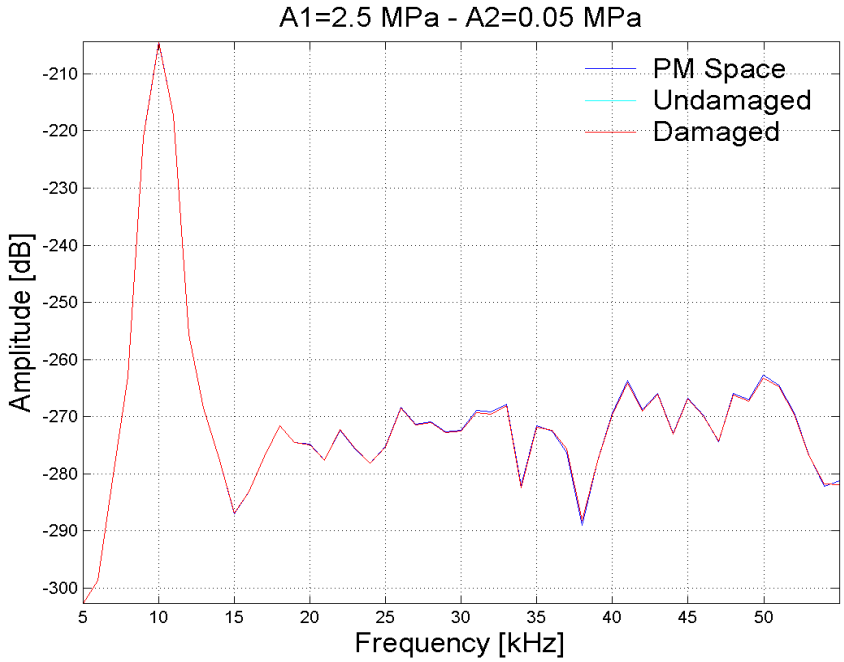

Figure 6.18 Spectrum of plate response in the vicinity of low frequency excitation fundamental

However even harmonics of high frequency components are observable plus the relative sidebands that, even in this case, represent the signature of the non linear hysteretic model (see Figure 6.19). Indeed the presence of odd harmonics has been predicted by the CAN approach (see paragraph 4.3.1) for non bonded rough surfaces.

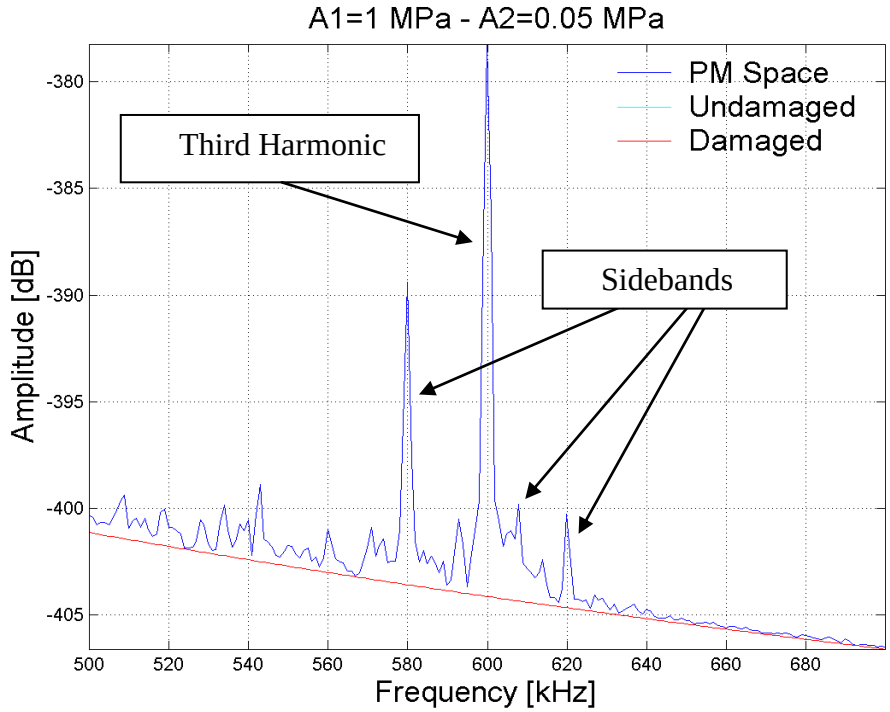

Figure 6.19 Third harmonic of the high frequency fundamental plus sidebands.

6.10 Conclusion

The approach proposed in this chapter is based on the implementation of PM-space as a non linear material model in FE code developed in house for the dynamic analysis of 1D and 2D model.

Results presented have demonstrated the ability to reproduce non linear effect induced by discontinuity interfaces, characterized by a hysteretic stress-strain relationship. According to the experimental evidence and mathematical model found in literature, and presented previously, numerical simulation has highlighted the presence of harmonics and modulation effects which can be used to estimate the presence of imperfections in homogeneous medium. These

imperfections behave as a local source of nonlinearities that propagate in the medium.

The experimental campaign described in the next chapters is based on the evidence just presented even if the approach selected does not allow direct comparison with experimental results due to the lack information and complexity of defect morphology and properties. However, the information collected in this chapter is a quantitative estimation of non linear properties induced by damage and defects such as delamination and weak bonds and these data have been used to organize the laboratory testing campaign.

CHAPTER 7 EXPERIMENTAL MEASUREMENT OF NONLINEARITIES

7.1 Introduction

Experimental tests in the literature have shown how geomaterials can be well described by nonlinear material models which include hysteretic phenomena due mainly to the presence of voids (as discussed in chapter 3). Numerical analyses presented in the previous chapter have shown how a small portion of nonlinear hysteretic material in a homogeneous medium is a not insignificant nonlinear source which affects the waves that propagate through the medium.

In this chapter the attention is focused on laminated composite materials and on experimental tests carried out to understand if the phenomena observed in the previous chapters are measurable in the laboratory on material of aerospace interest, and if these phenomena can be used for non destructive evaluation (NDE) of sample integrity.

Several samples have been used for lab testing, unfortunately of unknown material properties. The samples provided by the Mechanical Engineering Department of the University of Bath are carbon fibre laminate and they have been damaged with a low velocity impact.

Most of the samples provided have barely visible damage consequent to the impact, and an estimation of damage size has been provided using the active thermography method or C-scan.

Due to the low energy level used during the impact test the specimens under investigation present delamination of internal layers with barely visible indentation on the impacted surface. Thus after the impact the morphology of the area in proximity of impact is complex and it includes voids, discontinuity surfaces and broken fibres.

The reader is referred to chapter 7 for more details about the typology of damage that can occur after a low velocity impact.

The scope of these experiments is to verify if defects caused by impact are able to trigger nonlinearities in material behaviour, to define an experiment procedure that can highlight the nonlinearities and finally to correlate the magnitude of nonlinearities with the damage severity.

7.2 Non linear Wave Modulation Spectroscopy (NWMS)

Non destructive techniques (NDT), as seen in the first chapter, are usually based on physical phenomena to be used as defect signatures in materials. Under the assumption that barely visible damage induced by impact are characterized by discontinuities and voids in composite materials, thus the phenomena to be observed in order to detect those defects are mainly due to the interaction of damaged part with the linear structural response.

Geophysics scientists are extremely interested in the mechanical behaviour of materials that presents a large number of discontinuities and defects due to the

nature of geophysical material. Much effort have has expended in order to characterize, model and measure the nonlinear effects for this class of material and details of experimental tests can be found in references from [41] to [49] and from [51] to [70]. The inspiration for this work came especially from the work of P. A Johnson ([50] and [68]) and K. Van Den Abeele ([41] and [46]) where the effort is focused on the classification of nonlinear effects induced by voids during a continuous periodic excitation. Recently [71] this methodology has also been successfully applied to damage detection in glass specimen.

Similar to numerical test presented in the fourth chapter, the two authors carried out experimental test on geomaterials to detect the effect of wave modulation. The technique is also called NWMS (nonlinear wave modulation spectroscopy).

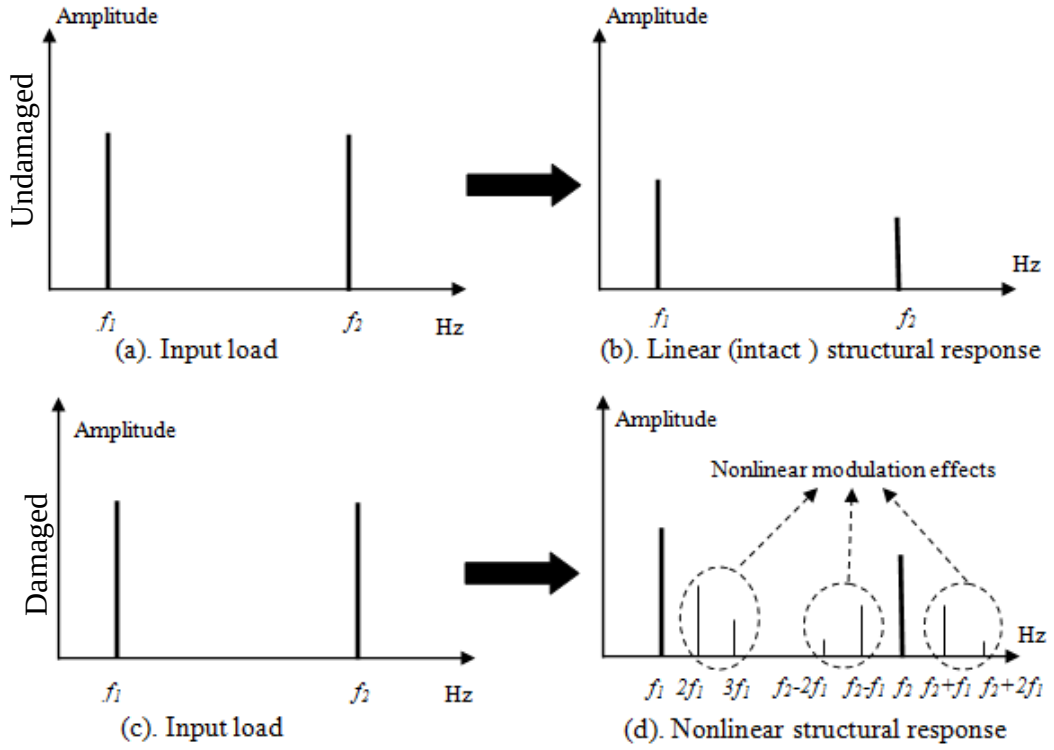

Figure 7.1. (a) and (c) represent the excitation frequencies spectrum. (b) is the response of a linear undamaged material (d) Nonlinear response of a damaged material : harmonics (nf1 ; n=1,2,3…) and sidebands (f2±nf1 ; n=1,2,3…).

Figure 7.1 summarizes the effects induced by damage in a sample under a bi-harmonic excitation, one low frequency excitation and one high frequency component that generates harmonics and sidebands thanks to modulation induced by the nonlinear behaviour of voids, interstices and damage.

7.3 Nonlinear Resonance Ultrasound Spectroscopy (NRUS)

A second approach can be used to identify nonlinear signature induced by damages. This methodology is based on the observation of structural response in correspondence of resonance frequency to different excitation amplitudes.

Linear elastic material have well know behaviour [72]; for simplicity taking into account a one degree of freedom system under a periodic force the response of a structure is :

$$X(\omega) = \frac{A}{\sqrt{\left[1 - \left(\frac{\omega}{\omega_n}\right)^2\right]^2 + \left(\frac{2\zeta\omega}{\omega_n}\right)^2}} \tag{7.1}$$

ζ = viscous damping factor

ω_n = natural frequency of undamped oscillation

ω = excitation frequency

$X(\omega)$ = harmonic response

Equation (7.1) highlights the dependency of structural response in terms of material properties through natural frequency and damping and external excitation in terms of frequency and amplitude. Thus the structural response varying the amplitude in an interval around a resonance frequency can be represented as in Figure 7.2.

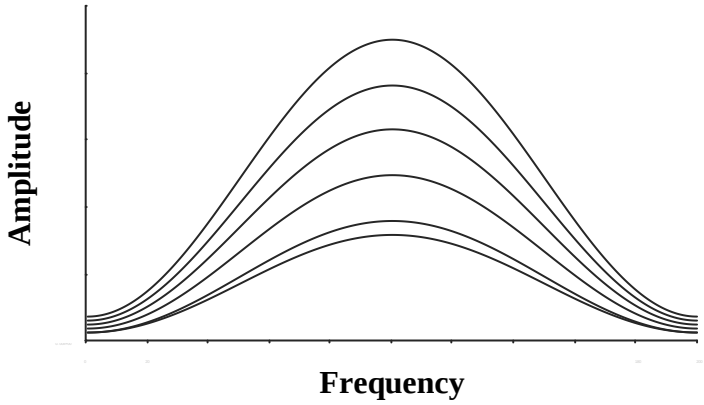

Figure 7.2. Forced harmonic response of linear system in proximity of natural mode

The system natural frequency is also constant how as shown in Figure 7.2 and for single degree of freedom is:

$$\omega = \omega_n\sqrt{1-2\zeta^2} \tag{7.2}$$

Moreover equation (7.2) links the system natural frequency only with material properties: undamped natural frequency and viscosity damping.

Although equation (7.2) and the relative extension to a multi-degree of freedom is a valid approach for large applications in engineering for damaged materials nonlinear effects must be taken into account. According with experimental evidence [46]-[67] there is a connection between the resonance frequency and excitation amplitude

The dependency of external amplitude can be explain as a consequence of nonlinear stress strain curve where elastic properties now depend on the strain level reached in the material as shown in equation (5.6). Thus the shift of natural frequency for different amplitude levels can also be considered as a signature of nonlinearity.

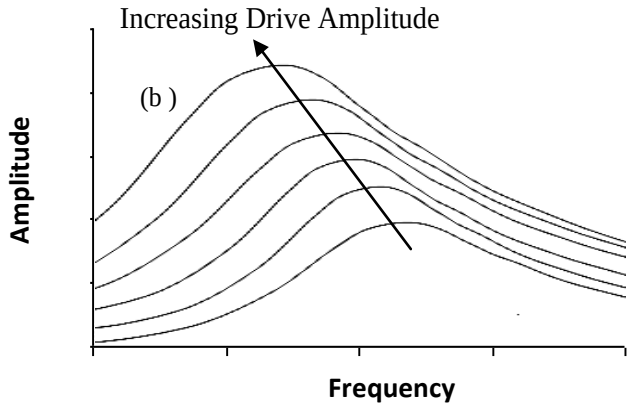

Figure 7.3. Forced harmonic response of nonlinear system in proximity of the natural vibration mode

7.4 Experimental SET-UP

The test pieces investigated were carbon fibre composite plates. The plate's dimensions are 150x100x4mm. The specimens under investigation were damaged by a low velocity impact. The impacts were made with different energy levels by changing the impact velocity. The damage introduced was a barely visible impact damage characterised by a small indentation on the front face, and by the back-plate delamination.

In Table 7-1 a selection of three samples is presented with some of the impact characteristic as energy of impact and damaged area resulting after impact estimated using C-scan equipment.

Specimen	Thickness [mm]	Impactor diameter [mm]	Impactor Mass [Kg]	Impact Energy [J]	Damaged area [cm^2]. C-scan
1	4	16	6.22	10.24	3.90
2	4	20	6.22	10.34	3.60
3	4	6	6.22	9.85	2.90

Table 7-1. Summary of sample under investigation with impact properties and damaged area estimated with C-scan Equipment.

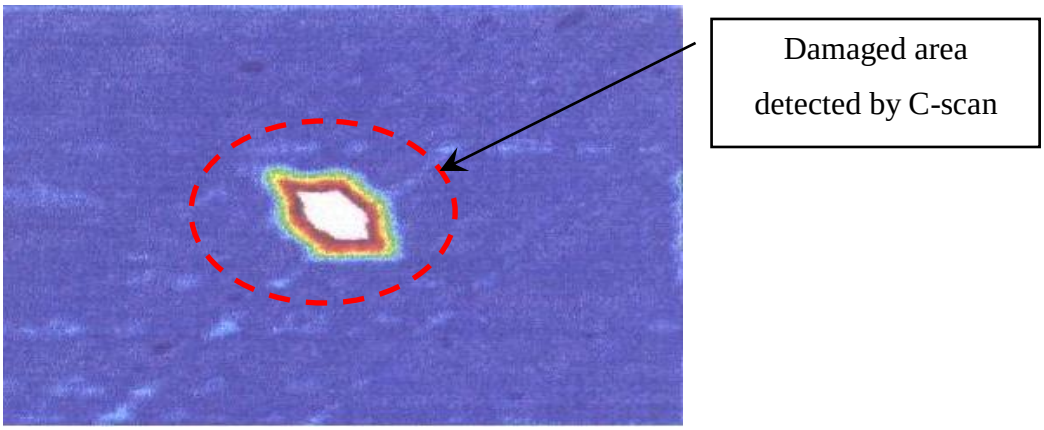

Figure 7.4. C-scan image of impact face on sample 2

An example of a C-scan image of sample 2 is shown in Figure 7.4 where the damage induced by impact is clearly visible. The delamination following a low velocity impact test is a discontinuity area in the medium that reflects ultrasonic waves. The difference in amplitude between the back face of the sample (which is the natural reflecting surface for intact samples) and the delamination is the basic feature driving image processing in C-scan methodology, which can achieve high contrast image for intact and damaged area as showed in Figure 7.4.

Also flash thermography inspection has been carried out on the sample under investigation. This methodology is based on the different cooling properties between the intact materials and voids usually present inside the delamination area. Inspection of the impacted face does not reveal a clear evidence of impact area, however on the back face, where the delamination is more critical, the active thermography shows a hot area in contrast with the background. This is the indication of damage presence which cools itself much slower than the rest of intact sample.

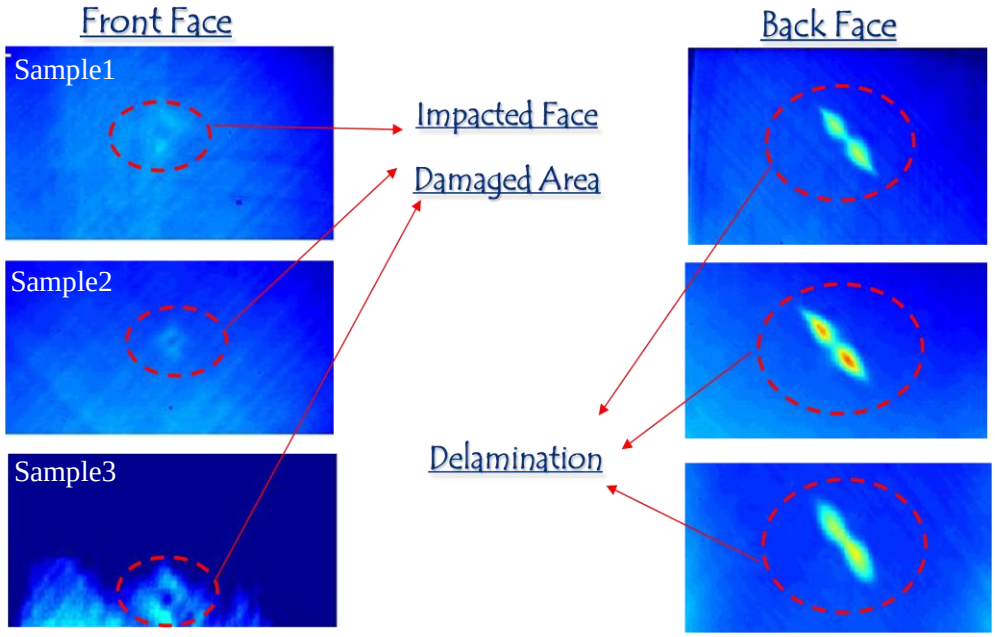

Figure 7.5. Flash Themography results: infrared images of impacted and back face samples

7.4.1 Equipments

The choice of equipment and protocols for experiments has been very carefully considered; the main issues are the necessity to not alter the specimens and the definition of a repeatable procedure. For these reasons piezoelectric transducer which needed to be glued on the sample to ensure the sensor-sample coupling could not be used for the experimental campaign even if piezoelectric transducers are particularly reliable from a repeatability point of view.

Another necessity is to use transducers and sensors able to induce the smallest possible interference on the structural response. Thus a low frequency speaker (50-3000 Hz) has been chosen as exciter to avoid the contact between the actuator and sample. A small and light accelerometer with its bandwidth in acoustic range has been used as sensor for these experiments.

The experiment setup, shown in Figure 7.6, consisted in a fibre composite plate with one fixed end. The acoustic speaker is driven by a signal generator through the power amplifier, and the acquisition equipment is the Brüel & Kjær Pulse system [73] with the Endevco 27A12 accelerometer. The accelerometer was located in the middle of plate at 2 cm from the free edge, on the front face of the plate.

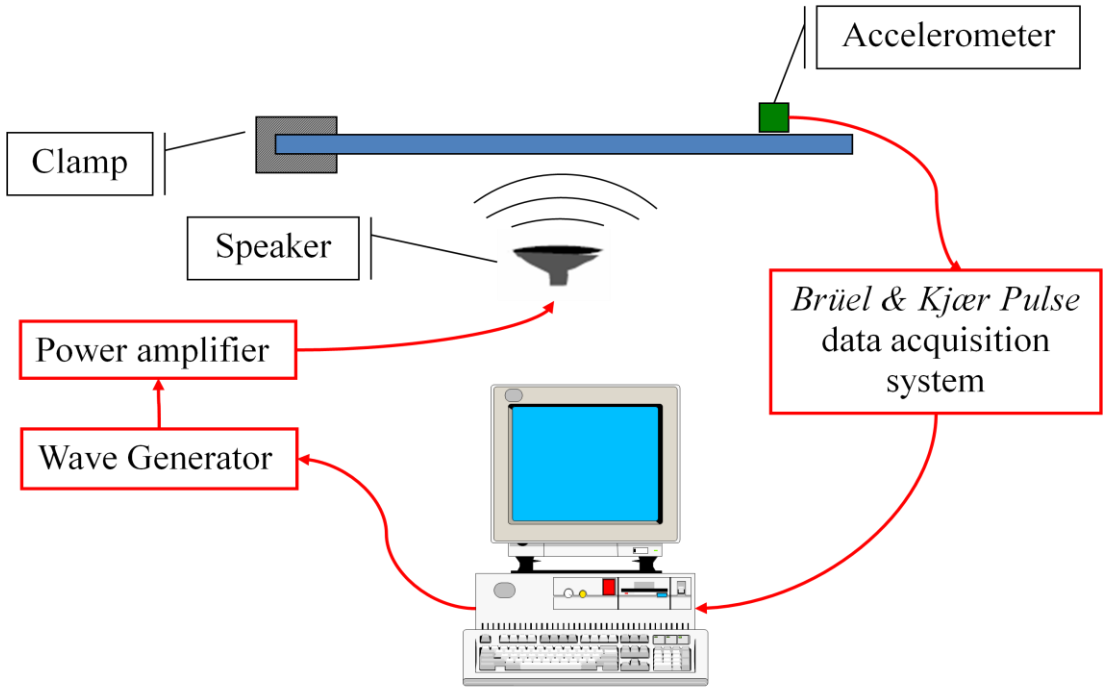

Figure 7.6. Experimental set-up. Lines in red indicate the cabling.

The Brüel & Kjær Pulse system hardware allows the user to digitalise process and store the signal on a common computer. Particularly interesting are the processing capabilities that allow the user to perform Fast Fourier Transform (FFT) with a choice of signal window and filters. For this experimental campaign all the acquisition has been done performing FFT with Hamming window in the time domain and applying a low pass-filter to reduce high frequency noise. For further details on FFT and signal windowing the reader is remanded to the signal processing books presented in the references from [74] to [77] .

7.5 Non Linear Resonance Ultrasound Spectroscopy test case

In order to highlight the nonlinear behaviour of the damaged plate, three different samples with different damage size were investigated (see Table 7-1).

The resonant frequency of an object is studied as a function of the excitation level; as the excitation level increased, the elastic nonlinearity manifests itself as a shift in the resonance frequency. The frequency shift is a manifestation of nonlinearity due to the presence of the cracks, in this case back-plate delamination. As the damage increases, the NRUS test reveals a corresponding increase in the nonlinear response. The measured change in nonlinear response is much more sensitive than the change in linear modulus.

A sine sweep was used to drive the speaker with constant amplitude, with its frequency range around the first resonance mode of the plate. The first resonance frequency for the tested plates was between 160 Hz and 200 Hz. In order to measure the resonance shift as a function of external amplitude the experiments were performed using different signal generator output voltages: 10Vpp, 8Vpp, 6Vpp, and 4Vpp respectively.

The NRUS test showed a significant shift of resonance frequency with an increase of the external drive amplitude as shown in Figure 7.7, Figure 7.8 and Figure 7.9.

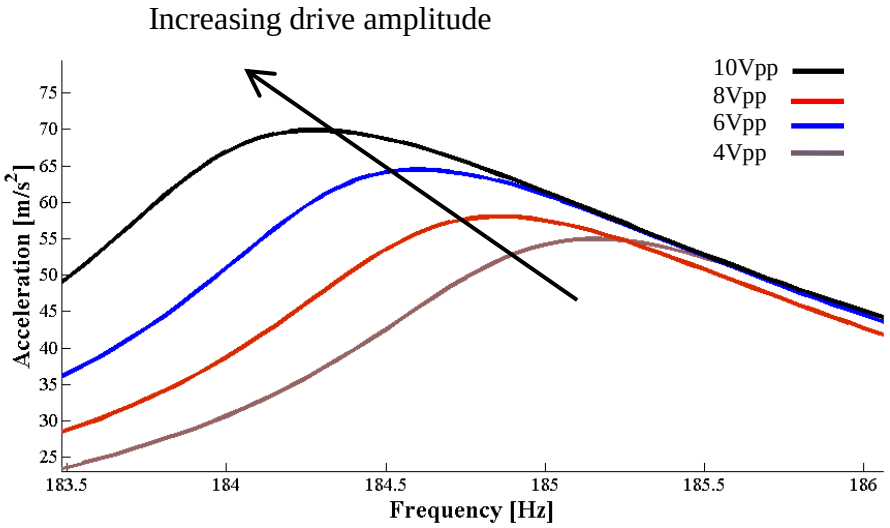

Figure 7.7. Resonance mode curves of sample 1 (Table 7-1) for different sweep excitation amplitude

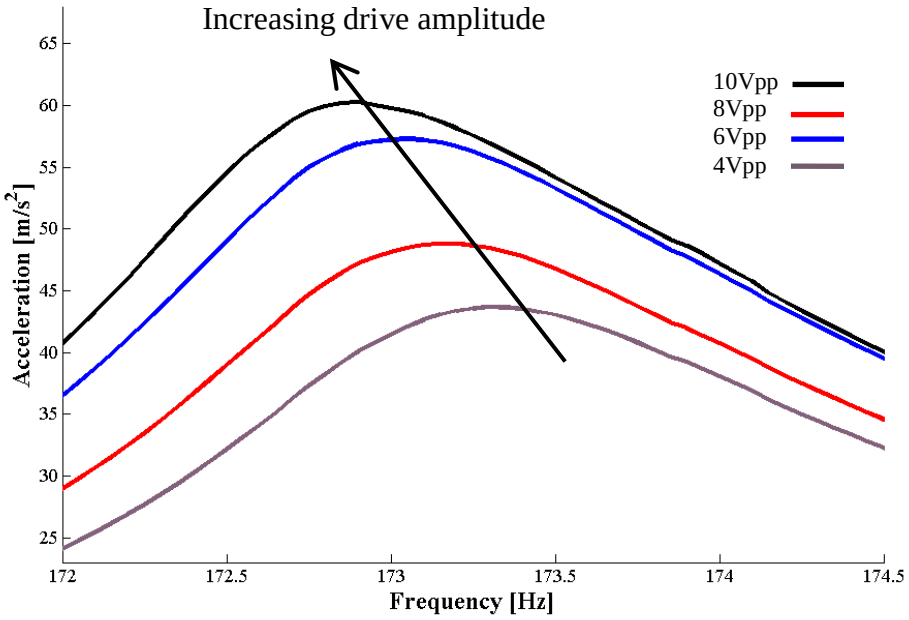

Figure 7.8. Resonance mode curves of sample 2 (Table 7-1) for different sweep excitation amplitude

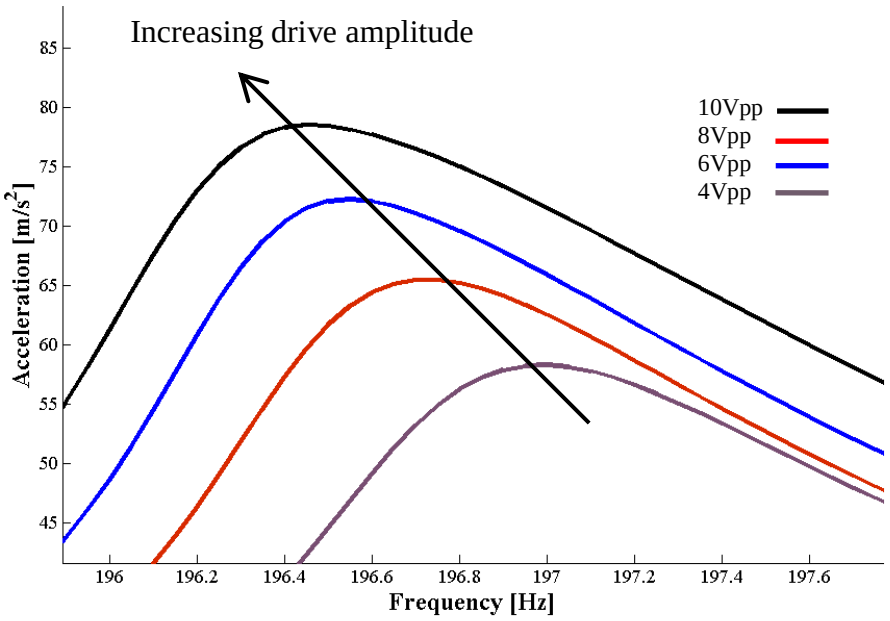

Figure 7.9. Resonance mode curves of sample 3 (Table 7-1) for different sweep excitation amplitude`

A measure of the damage was evaluated by measuring the nonlinear parameter α, which was calculated from the resonance frequency as follows:

$$\alpha = \frac{f_0 - f_{max}}{f_0} \tag{7.3}$$

where f_0 is the resonance frequency of undamaged plate or the lower resonance frequency, and f_{max} is the maximum resonance frequency measured increasing the drive amplitude. Comparing the nonlinear parameter α against the corresponding damage size it is possible correlate the nonlinear signature with the severity of damage as shown in Figure 7.10.

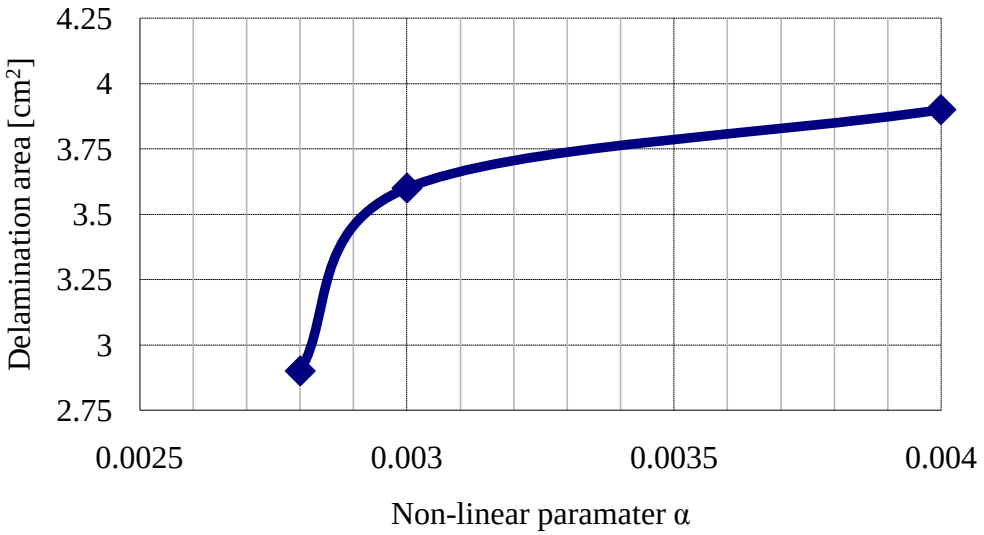

Figure 7.10. Non linear parameter α for each samples of Table 7-1 against damaged area.

7.6 Non linear Wave modulation spectroscopy test case

In the second class of experiment the input signal chosen was a double frequency sine wave, where the fundamental frequencies (*F1 ,F2*) are the first and the third resonance mode of the samples (*160<F1<200 Hz, 2260<F2<2320 Hz*). Figure 7.11 shows the time domain and frequency domain of excitation used for this experiment.

Even in this case amplitude of one of the two driving signals was increased in order to correlate the non linear phenomena with the external amplitudes.

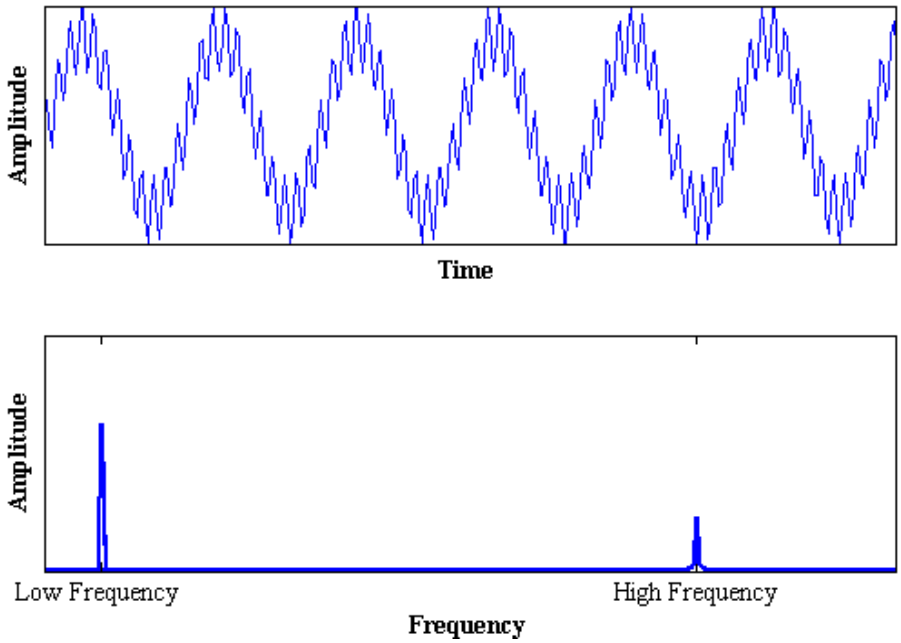

Figure 7.11. Double harmonic excitation. The top figure shows a signal portion in the time domain, the bottom figure is the relative FFT indicating the signal harmonic content

The first two samples of Table 7-1 were the object of the experimental investigation. For both samples different drive amplitudes were chosen in order to understand the behaviour of nonlinear effects. Adjustment of signal generator output between 0.3 V and 0.7 V peak to peak (Vpp) for the first (*F1*) and third (*F2*) mode was done in order to vary the fundamental amplitude of the signal. In Figure 7.12 an example of Fast Fourier Transformation (FFT) of the acceleration measured on the first sample is displayed. In each chart five FFT are presents for different values of drive amplitude obtained varying the signal generator output voltage from 0.3Vpp to 0.7Vpp. In Figure 7.12 – A the FFT are plotted with the F2 drive amplitude kept constant using the signal generator output at 0.5Vpp. In Figure 7.12 - B the amplitude of high frequency (*F2*) is varied and low drive amplitude is kept constant at 0.5Vpp. Nonlinear effects are clearly observed; the first noticeable effect is the presence of harmonics of low structural frequency response: *2F1, 3F1, 4F1*…etc. The second phenomenon is the modulation effects

between the two excitation frequencies; indeed, some sidebands (n *sb=F2* ± n *F1*) are observable in Figure 7.12 – A and B.

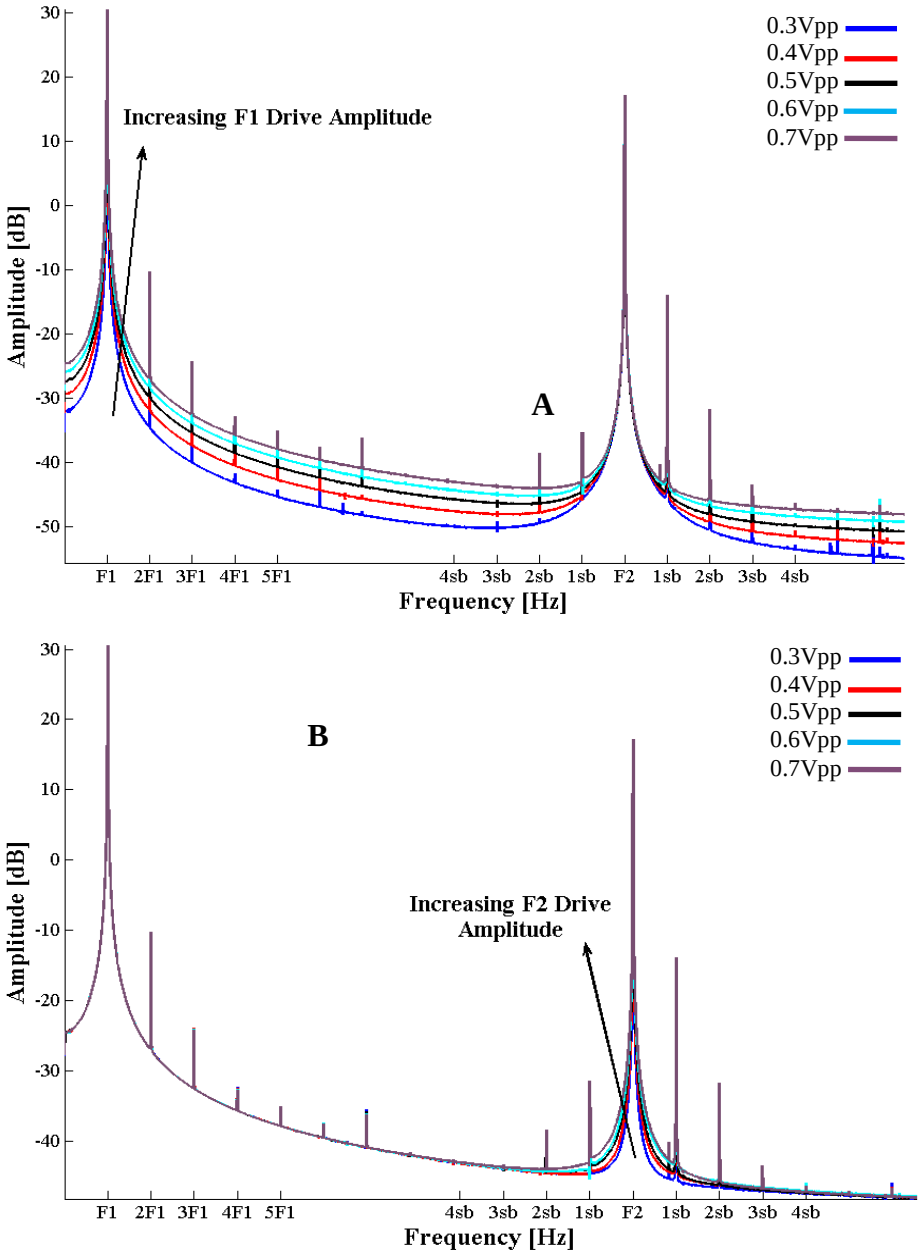

Figure 7.12. Harmonic response of Sample 1 in Table 7-1. In Section A harmonics response displayed for 5 levels of low frequency *F1* drive amplitude In Section B high frequency *F1* drive amplitude is varied.

Peak values of fundamental, harmoncis and sidebands have been extracted from the harmonic response using ad hoc Matlab code. The same process described up

to here has been applied to the second sample in Table 7-1, and harmonic and sideband peak values of the first two samples have been compared against F1 and F2 amplitudes as showed in

Figure **7.13** and Figure **7.14**.

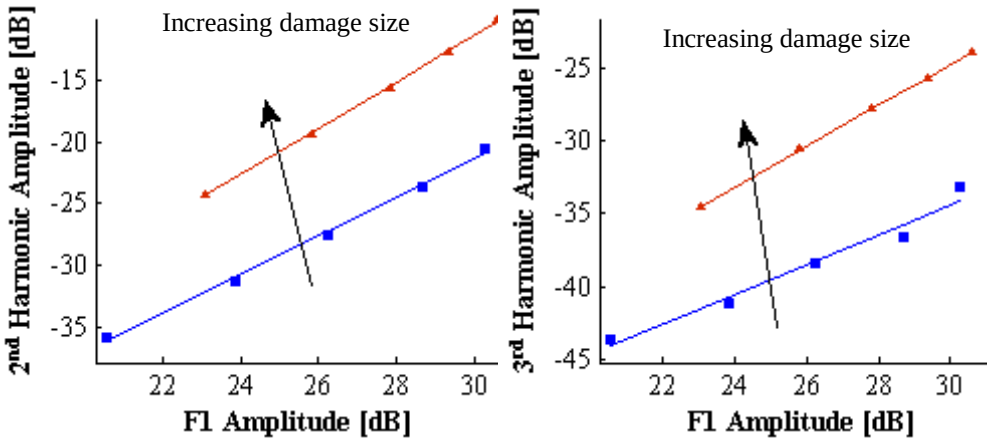

Figure 7.13. Harmonic amplitudes of first two samples in Table 7-1 against the fundamental low frequency amplitude *F1*. Line marked indicates the peak values, continuous lines are linear interpolation across the experimental measurements. Red line corresponds to the sample 1 and blue line to sample 2.

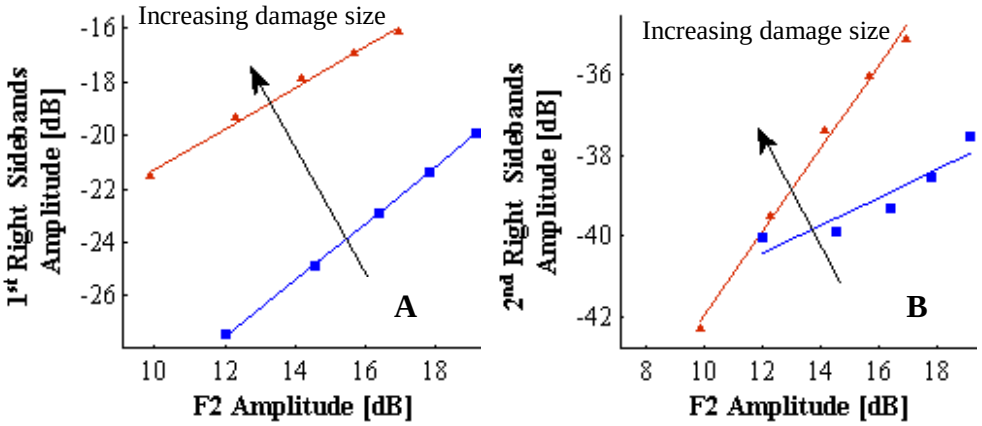

Figure 7.14. Sidebands amplitudes of the first two samples in Table 7-1 against *F2*. . Line marked indicates the peak values, continuous lines are linear interpolation across the experimental measurements. Red line corresponds to the sample 1 and blue line to sample 2.

Amplitude values of sidebands and harmonics displayed in

Figure **7.13** and Figure **7.14** show a clear dependency from damage size and fundamental amplitude.

The order of magnitude of non linear components is coherent with the damage area measured by C-scan and with the increase of the drive amplitude of the two fundamental.

7.7 Non linear acoustic measurement for a weak bond

As discussed in paragraph 4.3.2 nonlinear hysteretic behaviour also characterizes the acoustic contact between bonded surfaces. Thus the quality estimation of clamping condition is another potential filed of application for NRUS and NWMS methodology.

A feasibility study is here presented where the main target is to understand the validity of methodologies applied to damage monitoring previously described are also applied to the estimation of bonding condition.

The test pieces investigated were carbon fibre epoxy composite plates with unknown material properties. The size of the plate size was 210 × 100 ×4mm3 and it was inspected with a C-scan to assess the presence of damage or defects. During this preliminary inspection, no damage was found and the specimens appeared in pristine condition. The experimental set-up used is shown in Figure 7.15 The composite plate was fixed on one side and left free to move on the other end. Two different values of torque were applied on the bolts (measured with a torquemeter), T1 and T2, in order to analyse the effect of the clamp pressure difference on the materials non-linear elastic behaviour. The torque T1 corresponds to a firmly fixed sample edge, and T2 was 20% greater than T1. The plate excitation was obtained by using a low-distortion speaker, operating in a low and medium acoustic frequency range. The speaker was driven by a signal generator through the power amplifier, and the data were acquired by using an accelerometer and a Brüel & Kjær pulse system. The accelerometer (ENDEVCO

27A12) was located at 2 cm from the free short edge and at 5 cm from the long edges, on the front face of the plate. Two different types of NEWS tests were carried out: nonlinear resonance ultrasound spectroscopy (NRUS) and nonlinear wave modulation spectroscopy (NWMS). The first resonance frequency (flexural mode) for the plates considered was around 200 Hz. The experiments were performed using different drive amplitudes in order to measure the resonance shift versus external amplitude. For the NWMS tests, the input signal was the superposition of two sine waves, where the fundamental frequencies (F1 and F2) are the first and the third resonance modes of the sample (199<f1 <201 Hz, 2230<f2 <2260 Hz). Different external load amplitudes were tested in order to correlate the non-linear phenomena with the external amplitudes.

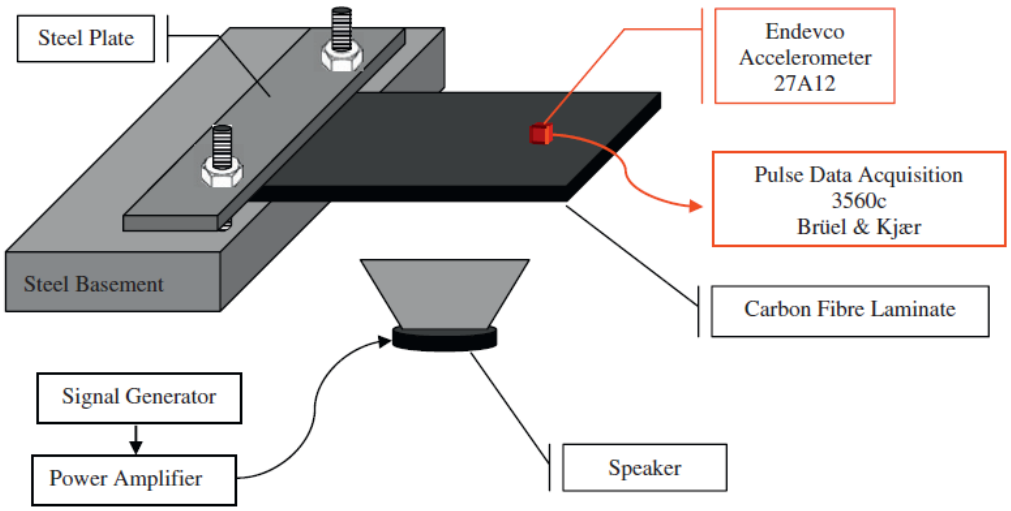

Figure 7.15 Schematic representation of equipment configuration.

The results show that in both cases there is a significant shift in the resonance frequency with increasing load amplitude. However, since the same external load was used for both tests, when using T2 as the clamping torque, the value of acceleration amplitude is higher than when using T1. This behaviour is caused by an increase of the stiffness due to the higher torque used. By measuring the non-linear hysteretic parameter (see equation (7.3)) an indication of the level of hysteretical non-linear effects introduced by the contact between the sample and the clamp could be obtained.

The nonlinear parameter α has been evaluated from the nonlinear resonance test. In Figure 7.16 the four different curves have been obtained varying the output voltage of the signal generator from 10Vpp to 4Vpp.

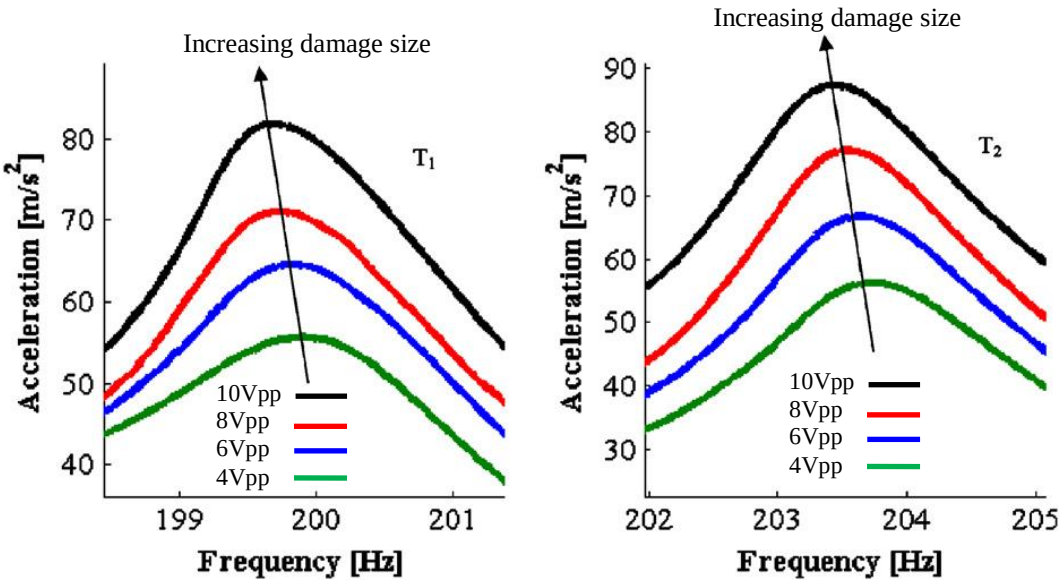

Figure 7.16 NRUS tests on one sample with two clamping torques: T1 and T2, where T2 >T1.

An increase of clamp torque has caused an increase of nonlinear parameters (see Figure 7.17). This result was not expected as according to the nonlinear theory previously presented an increase of contact force should guarantee a perfect bond and so it should cause a decrease of contact nonlinearity. Various

other amounts of clamping torque have been investigated and the same conclusion was drawn.

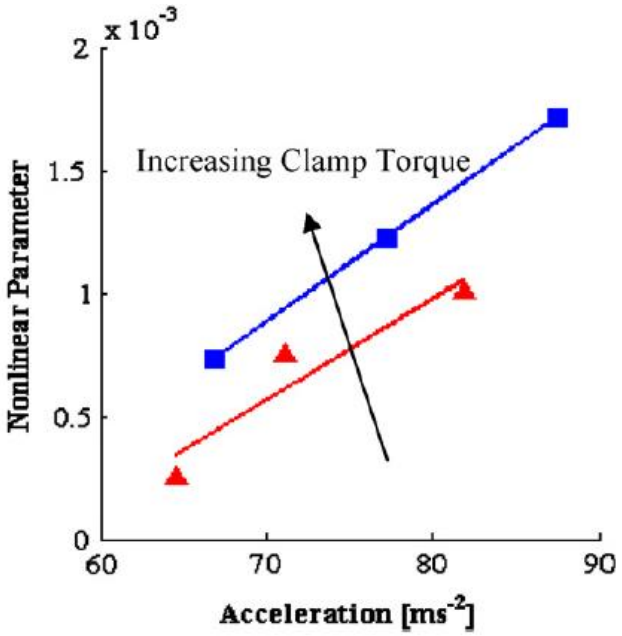

Figure 7.17 Non-linear parameter versus acceleration. The marker "▲" indicates data for torque level T_1 and the marker "■"indicates data for torque levelT_2, where $T_1 < T_2$.

In Figure 7.18 and Figure 7.19 the spectra of the accelerations measured with the NWMS test are shown for both clamp conditions. Different amplitudes of external loads were used in order to correlate the amplitude of non-linear features versus the structure linear response, represented by fundamental amplitude. The generation of non-classical non-linear hysteretical features is clearly observable as highlighted by the presence of harmonics and sidebands. The increase of low frequency amplitude in Figure 7.18Figure 7.19 has been obtained varying the signal generator output voltage from 0.3Vpp to 0.7Vpp and keeping constant the amplitude of high frequency amplitude at 0.5Vpp. The variation of high frequency component has been obtained inverting the voltage output used for the low component and keeping constant the low frequency drive voltage at 0.5Vpp.

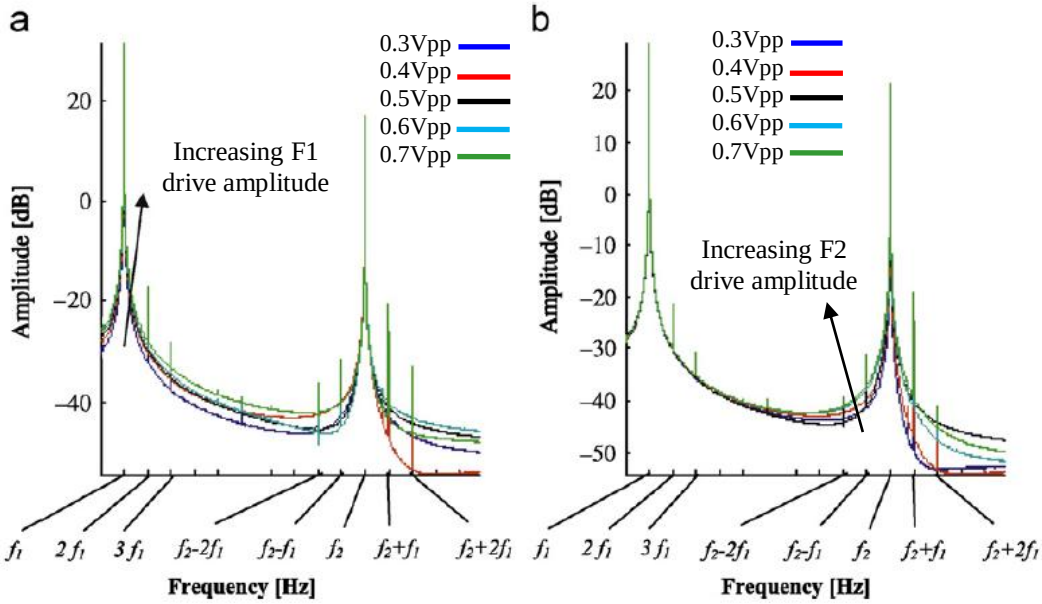

Figure 7.18 Fourier spectra of accelerations measured with NWMS approach relative to the clamp condition T_1. (a) Increasing f_1 amplitude. (b) Increasing f_2 amplitude.

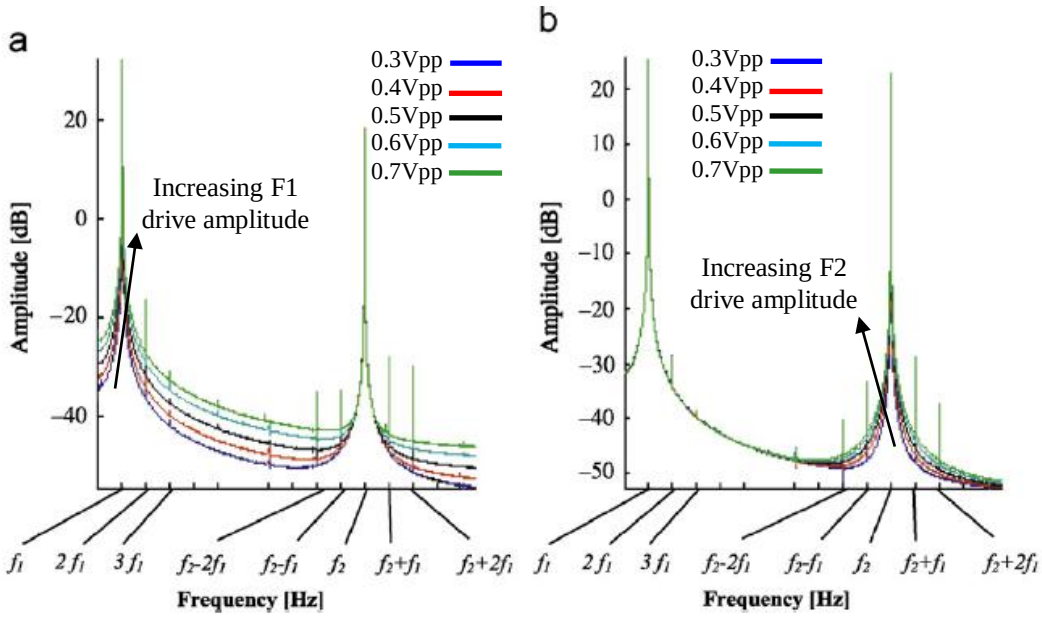

Figure 7.19 Fourier spectra of accelerations measured with NWMS approach relative to the clamp condition T_2. (a) Increasing f_1 amplitude. (b) Increasing f_2 amplitude.

The results show that by varying the boundary conditions (torque value); a variation of the structural non-linear effects was observed. In particular, a decrease of the second and third harmonic and the first right and left sidebands was observed as shown in Figure 7.20 and Figure 7.21

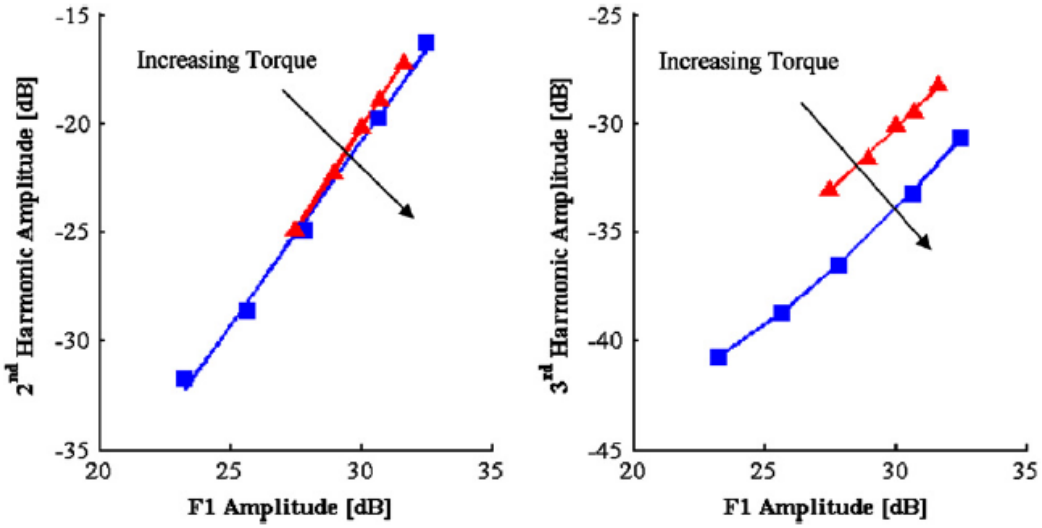

Figure 7.20 Effect of the clamping torque on the observed second and third harmonics. The marker "▲"indicates data for torque level T_1 and the marker "■" indicates data for torque level T_2, where $T_1 < T_2$.

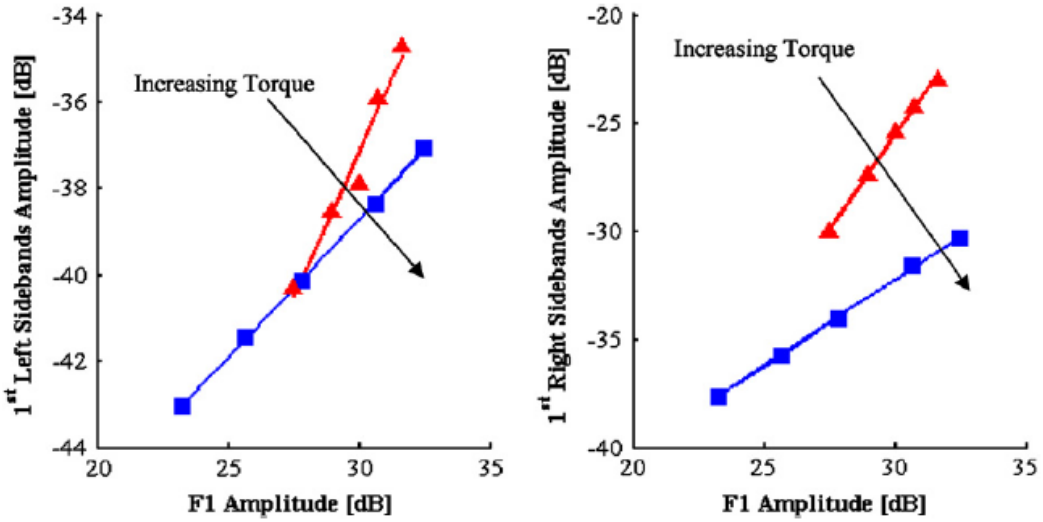

Figure 7.21 Effect of the clamping torque on the observed sidebands against F_1 amplitude. The marker "▲"indicates data for torque level T_1 and the marker "■" indicates data for torque level T_2, where $T_1 < T_2$.

In Figure 7.22 sidebands amplitude are displayed against amplitude of f_2. Tests were conducted by varying the amplitude of frequency f_2 and keeping constant the amplitude of frequency f_1. In this case, the effect of increasing clamp torque is a decrease of the amplitudes of non-linear properties.

The results of these tests show some of the limitations of the NDT based on the monitoring of the non-linear elastic effects.

Non-classical non-linear effects can also be generated by the presence of contact regions, i.e. boundary conditions. There is, therefore, the need to optimize the NEWS methods and to further study these effects with other geometrical configurations, for example, structures in pure contact (kissing bonds, joints, etc.), and to develop methods to discern the non-classical non-linear effects caused by geometrical configurations from that generated by the presence of impact damage.

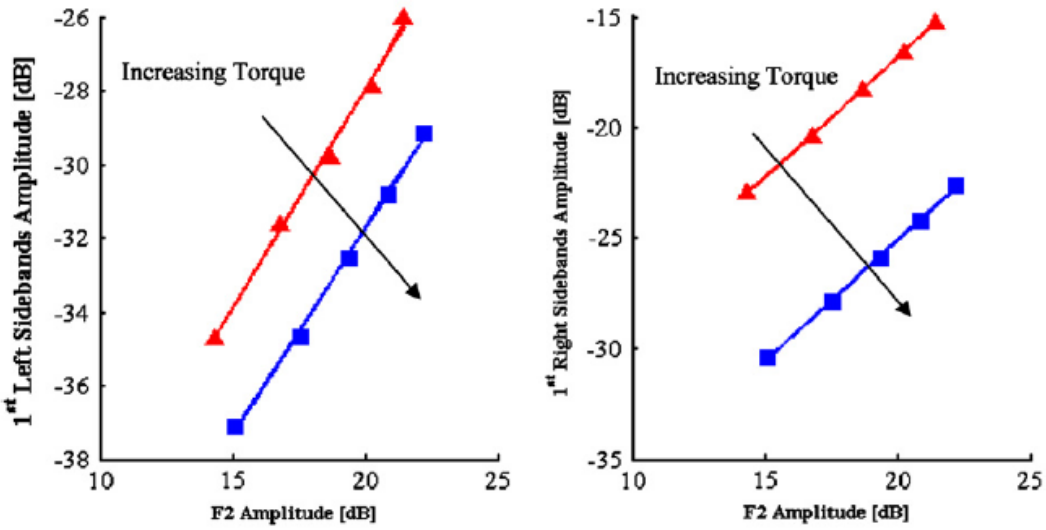

Figure 7.22 Effect of the clamping torque on the observed sidebands against F_2 amplitude. The marker "▲"indicates data for torque level T_1 and the marker "■" indicates data for torque level T_2, where $T_1 < T_2$.

7.8 Conclusion

Following the experimental evidence found in the literature on nonlinear behaviour of materials that contains present large number of voids and discontinuities (such as geomaterials) an experimental campaign has been carried out in order to understand the feasibility of the NWMS and NRUS approaches for non destructive technique in the aerospace field.

Non linear evaluation of the shift resonance frequency and harmonics and sideband amplitudes has been performed on a set of damaged samples. The samples had different damage severity and the magnitude of nonlinear manifestation was correlated with damage size.

The results presented in the previous paragraphs have demonstrated the connection between the damaged area with non linear phenomena such as shift of resonance frequency and harmonics and sideband amplitudes. These results might open up a new scenario for the future development of NDT in aerospace for composite structures where the ability to detect damage due to low velocity impact (an example of this class of damages could be tools dropped down during operator servicing) in their early stages has become critical as the amount of composite parts for aircraft primary structures is constantly increasing.

Using the same approach a bonded joint has been investigated using NRUS and NWMS methods highlighting the presence of non classical non linear features in the spectrum responses. In the first case a considerable shift of the first natural mode was clearly observed in the undamaged sample. Using NWMS, the intermodulation effects were evident, highlighted by the presence of sidebands and harmonics, induced by the boundary conditions. However, the non-linear properties showed a decrease in amplitude when the clamp torque was increased. The results of these tests demonstrate that boundary condition can cause linear material to behave in a non-linear elastic manner, therefore providing false-positive indications of damage.

The data presented in this chapter are only a selection of all measurement performed during the experimental campaign. In particular different attempts have been done in order to establish the configuration that allows the measure to be repeatable. Clamping condition might introduce variation in the results, however, in order to estimate the repeatability of the proposed configuration (clamping condition and measurement devices) the measures presented have been repeated several times using the same setting and no significant variation (less than 2%) was found in the results.

The results show that more work is needed to demonstrate the effectiveness of the non linear elastic wave spectroscopy (NEWS) methods and further research studies and methodology development are needed to discern non-linear effects generated by contacts between mating parts from those generated by the presence of damage.

However, the harmonics and sidebands observed in the spectrum analysis have consistent behaviour with the literature of CAN and NEWS methods, which make this methodology promising.

CHAPTER 8 NONLINEAR WAVE SPECTROSCOPY FOR DAMAGE LOCALIZATION AND COMPARISON WITH THERMAL BASED TECHNIQUES

8.1 Introduction

Barely visible impact damage may occur for many reasons: tools dropping down, impact with debris and etc. All of this class of impacts have in common the low energy level correlated with the low velocity impact. In order to reproduce this kind of impact condition a drop test was chosen to cause damage on the composite sample.

8.2 Low velocity impact test

The drop tower used for these tests (see Figure 8.1) consists of a pipe that works as a guide for the impactor running inside it. On the impactor, made in steel, one strain gauge is built in, in order to measure the axial strain in the impact direction. Moreover a reflective object sensor is mounted at the end of the pipe; this is useful to detect the velocity before and after the impact. The impactor is covered by black and with stripes of fixed width (0.5cm), and the reflective sensor gives a different output for the white and black, in this way it is possible to evaluate the time needed by the impactor to cover a distance equal to the stripes width. The data from strain gauge and reflective objector sensor was collected with Tektronix digital oscilloscope (see Figure 8.2).

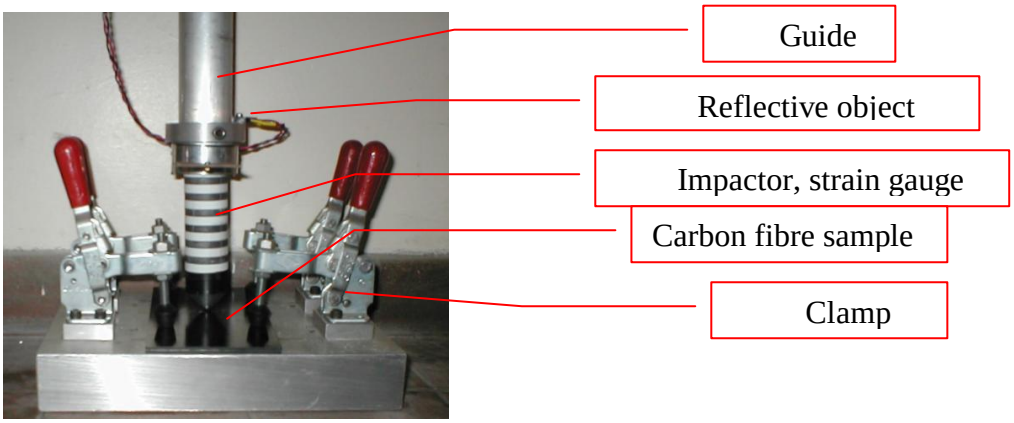

Figure 8.1 Drop Tower and clamp system

Two samples were under investigation and they were impacted with different energies. In Figure 8.2 section A and C strain time history and output of the reflective object sensor are displayed for the sample1, the black circle in section C highlights the instant when the impactor rebound from the sample, and comparing with section A this point correspond the maximum strain measure on the impactor. Comparing the two plot of strain time history and reflective sensor

response it is possible evaluate the time needed to the impactor to cover a distance equal to the width of white or black stripe just before and after the impact. The velocity has been measured to estimate the impact energy (Ei) and of the energy after rebound (Er). The same process has been done for sample 2 displayed in section B and D of Figure 8.2.

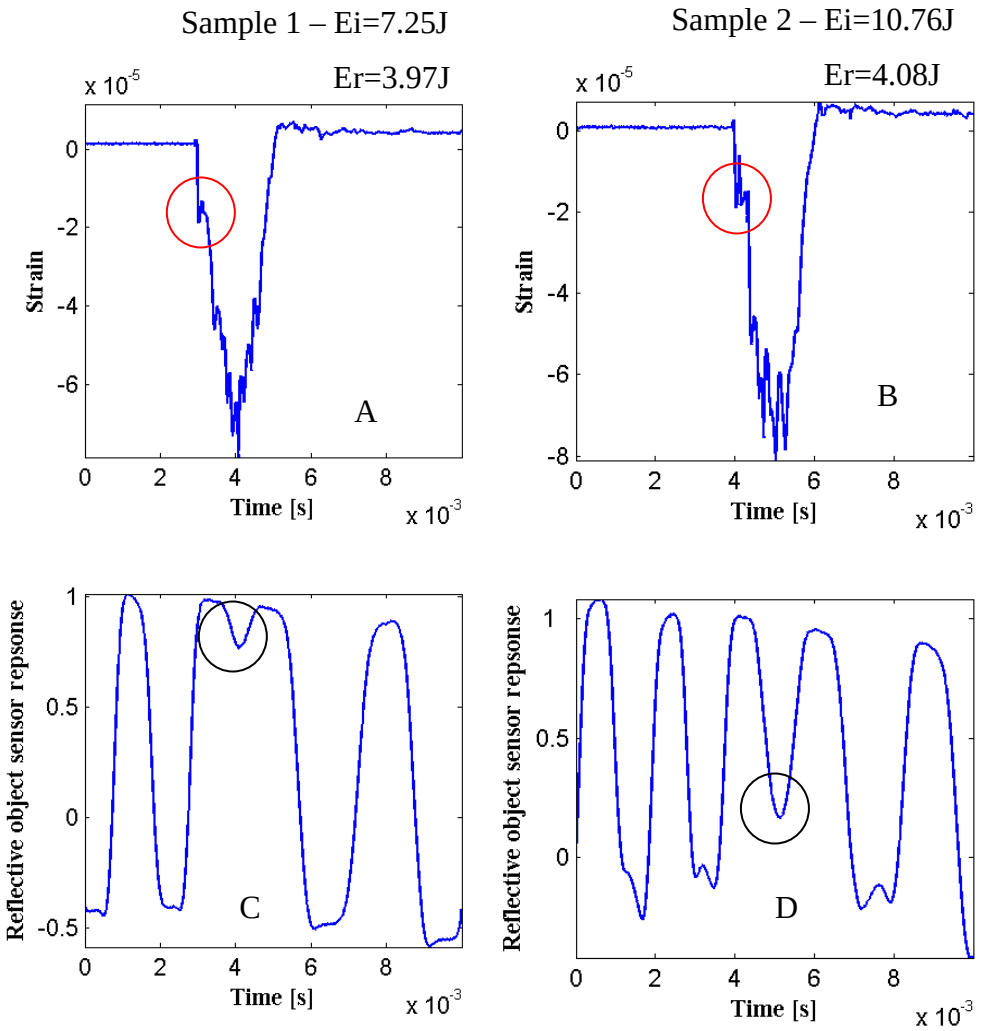

Figure 8.2 Test results of impact on two samples. Section A: sample 1 strain time history. Section B: sample 2 strain time history. Section C: output of reflective object sensor for sample 1. Section D: output of reflective object sensor for sample 2. The red circle in section A and B indicate the first material damage. In section C and D the black circle highlights the time interval around the maximum strain and consequently the rebound of impactor.

During the contact between impactor and sample large oscillations of strain indicate that the impact is damaging the sample. According with the literature [29]-[33] the first large oscillation (see red circle area in Figure 8.2 section A and B) denotes the first material damage, in low velocity impact this kind of damage is usually correlated to the matrix failure. The measured strain increases in amplitude during contact up to the point when first failure occurs, when the capability of the sample to absorb energy in elastic form decreases due to the presence of damage and some energy is dissipated in the damage generation process. At this stage fibre failure and delamination may occur. For these reasons large oscillation are observed not only at the first material failure but also at the maximum strain reached in correspondence of maximum displacement of the impactor (see Figure 8.2 section C and D).

The output of reflective object sensor depends on the reflective characteristics of surfaces observed by the sensor. In these tests the white and black stripes on the impactor generate, respectively, an output between 1 and -0.5 volts, the voltage remains nearly constant when the footprint of the sensor on the surface covers an area of uniform properties that for these experiments means the surface of the same colour. From the Figure 8.2 the calculation of impact velocity and rebound velocity was done taking into account that each stripe, both black and white, is 0.5cm wide. Moreover the impact energy and rebound energy has been calculated and reported in Figure 8.2.

8.3 Imaging method

The test pieces investigated were carbon fibre composite plates. The plate's dimensions were 210x100x4mm. The specimens under investigation were damaged by a low velocity impact. The impacts were realized with different

energy levels by changing the impact velocity. The damage introduced was a barely visible impact damage characterised by a small indentation on the front face, and by the back-plate delamination.

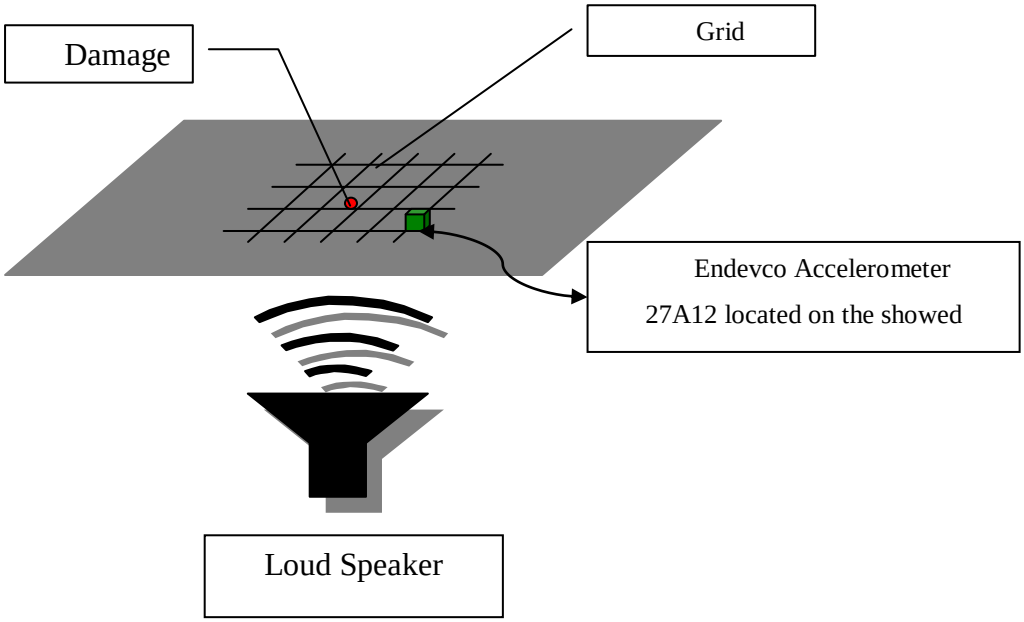

Figure 8.3 Equipment configuration

The experiment setup, shown in Figure 8.3 consisted of a fibre composite plate with two fixed edges, an acoustic speaker driven by a signal generator through the power amplifier, and the acquisition equipment was a the Brüel & Kjær Pulse system with Endevco accelerometer. The accelerations were measured at points representing the acquisition grid that surrounds the damage location.

The external load used was a periodic signal with the same amplitudes for each grid point and the frequency was one of the first resonance modes of the plate, typically between 1.75 and 1.9 KHz.

In order to highlight the nonlinear behaviour of the damaged plate, two different samples (S1 and S2) with different damage position and severity were investigated. Mechanical properties of the sample and the extent of the damage were unknown. For the two samples two different energy level of impact E_1 and

E_2 were used with $E_1<E_2$. In Figure 8.4 the FFT of the signal acquired in one of the grid point for both sample are displayed. The sample in box (a) was impacted with E_1 energy level, and the sample in box (b) with E_2 energy level. The amplitudes of harmonics in the second case, box (b), are much higher than the first case, box (a), and where the energy used during the impact was lower (see Figure 8.4),

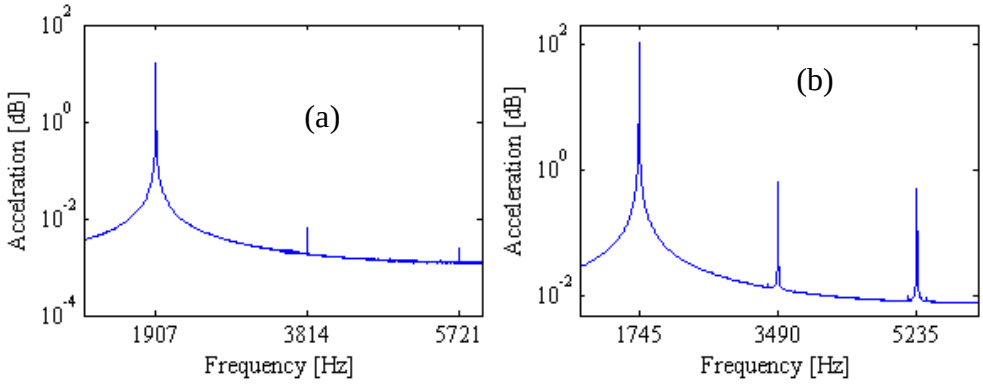

Figure 8.4 . FFT in the same grid point for both samples. Box (a): first sample impacted with E_1 impact energy. Box (b): second sample impacted with E_2 impact energy. $E_1<E_2$.

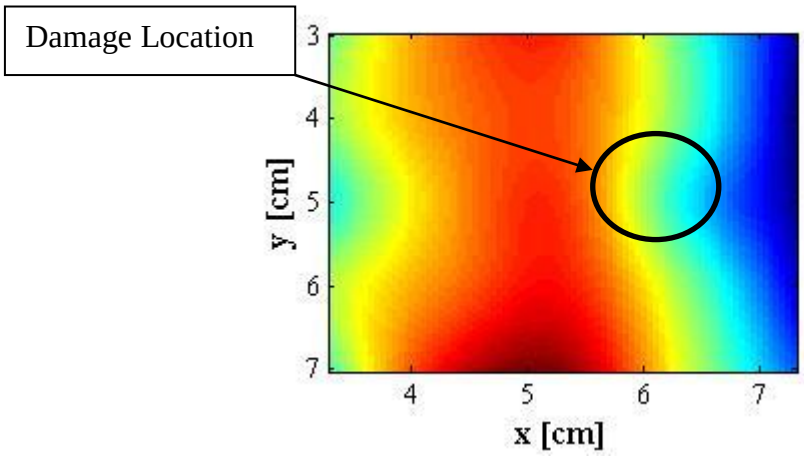

Figure 8.5 Fundamental amplitude distribution across the sample S1 surface under investigation.

The imaging system for damage position estimation required an evaluation of those properties that are strictly dependent on the damage position.

In this work attention is focused on the second harmonic of structural response and its distribution in the sample itself.

The boundary condition used induces a non constant response structure in the plate as showed in Figure 8.5. Thus in this case the accelerations acquired in each grid point are correlated not only with the damage position but also by geometry position on the plate too. Indeed the fundamental amplitude A_1^i (amplitude at excitation frequency measure at the grid point *i*) appears to be driven by geometrical and modal shape condition more than damage position. (Figure 8.5).

A_2^i is the second harmonic response amplitude at the grid point *i* and the ratio between the harmonic amplitude and the fundamental amplitude A_2^i / A_1^i may be computed. This approach consists in scaling that allows the estimation of the nonlinear contribution due by the damage without taking into account the linear contribution which is driven by geometry and boundary condition. Figure 8.6 shows the spatial distribution of the ration A_2^i / A_1^i for both test samples.

Even if the material properties are unknown, the ratio A_2^i / A_1^i is able to identify the damage position by just imposing the symmetry of boundary condition and exciting one of the first resonance modes.

An additional benefit of evaluating the ratio A_2^i / A_1^i is the correlation between its amplitude and the energy of impact, and then to the damage severity, as shown in Figure 8.4 and Figure 8.6.

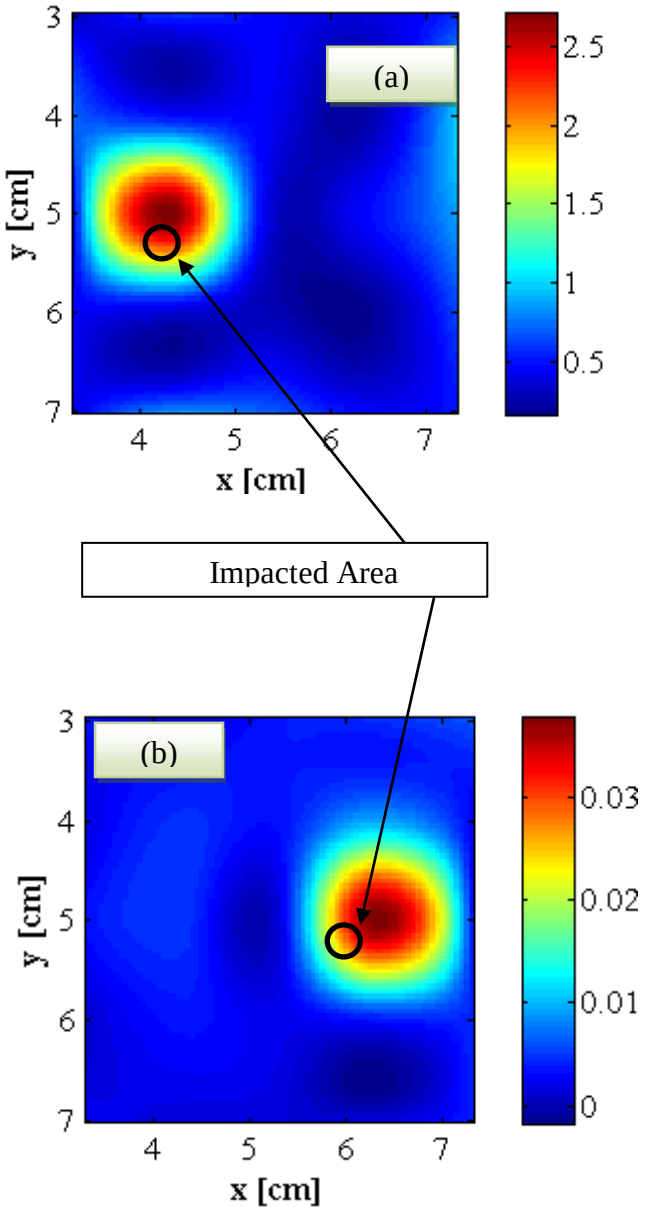

Figure 8.6 . Colour map of ratio A_2^i / A_1^i for each grid points, with marked position indicating the impacted area and consequently the damage localisation. In picture (a) the sample impacted with energy E_1 and in picture (b) the specimen with energy E_2. $E_1<E_2$.

8.4 Comparison with thermal based NDT techniques

The pulse thermography [18] technique was used to investigate the damage position in the sample. The methodology is based on the assumption that cracks affect material thermal properties, so after exciting the structure with a heat pulse, typically provided by flash lamps, natural cooling is observed with an infrared camera (see Figure 8.7). The monitored surface infrared emissions are affected by the presence of surface and subsurface discontinuities; for example a delamination usually causes a slower cooling, therefore after the heat pulse a difference in the temperature of the sample surface is observable at the area corresponding to the damage. The infrared image can provide a good contrast image with a hot spot corresponding to the damage as shown in Figure 8.8 where the back face of samples have been inspected. Unfortunately in this occasion due to the small size of impact damage the pulse thermography failed to detect BVID damage on the front face as shown in Figure 8.9.

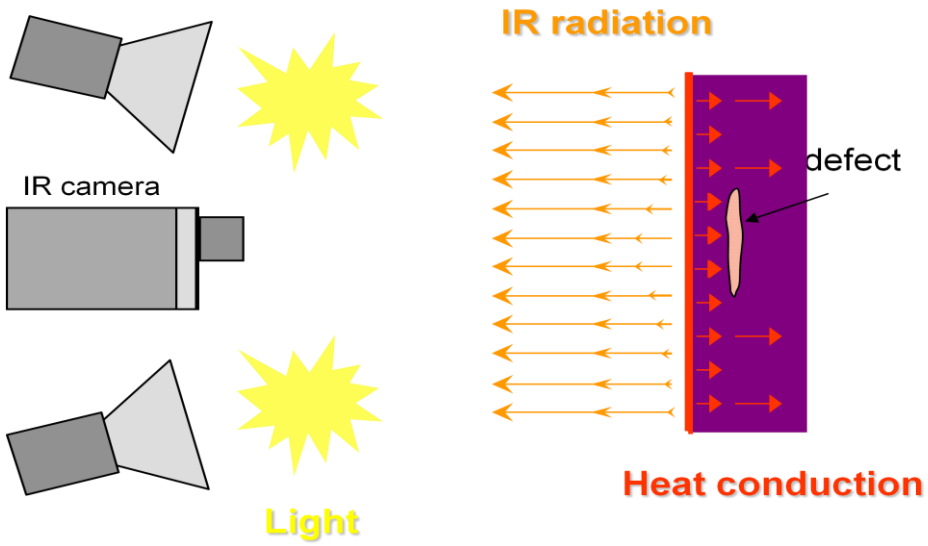

Figure 8.7 Pulse thermography experiment set-up

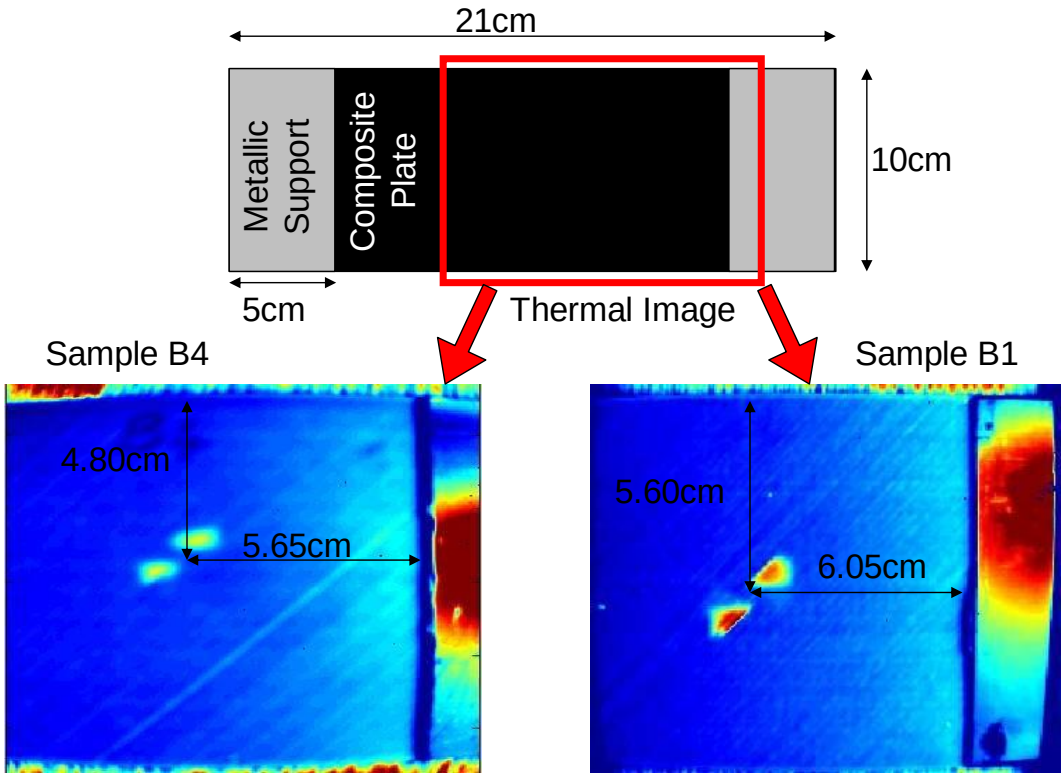

Figure 8.8 Pulse thermography image of back sample surfaces under investigation

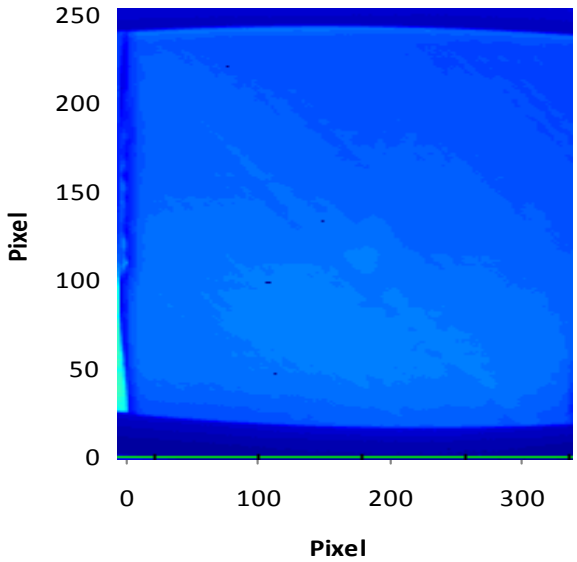

Figure 8.9 Pulse thermography image of front sample surface under investigation

Results showed in Figure 8.8 have also allowed the location of delamination, as reported in the pictures. The position of the damage has been computed using a measurement tool provided with the Pulse Thermography equipment and the reference edges chosen correspond to the x and y axis of Figure 8.6. Pulse thermography test performed on the back surface and nonlinear spectroscopy imaging results are in good agreement on the localization of delamination

An alternative and recent technique called Thermosonics (or Sonic IR) [19] was also used to identify and locate impact damage. In contrast to pulse thermography, this method is based on the observation of defects while the material is heating up.

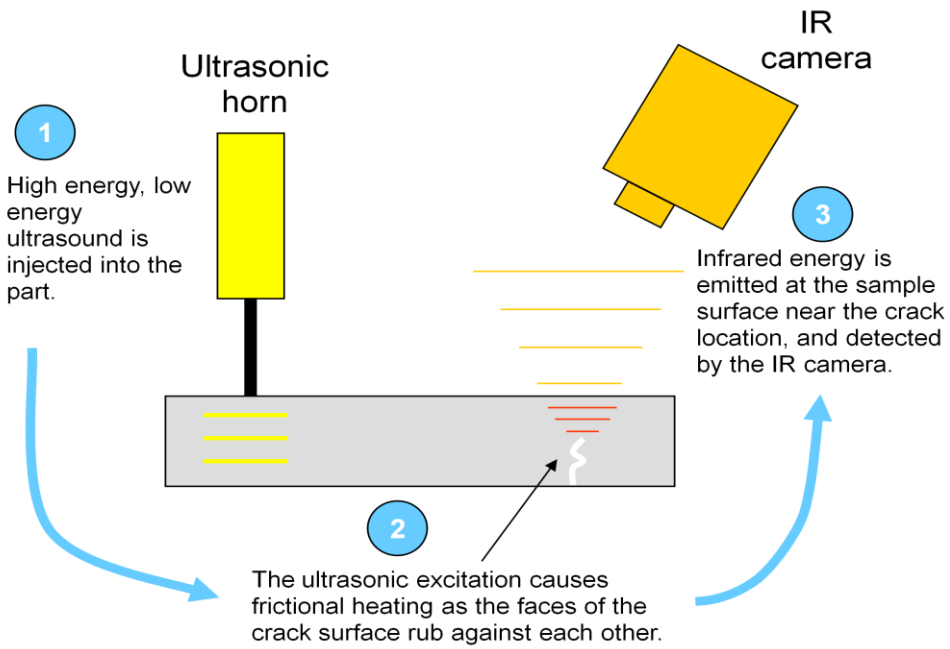

Figure 8.10 Thermosonics set-up

This is accomplished by exciting the sample with a short pulse of high energy ultrasound while an IR camera is monitoring the sample. Burst excitation typically is provided by an ultrasonic horn and the coupling between the horn and the

specimen is accomplished by duct tape. In Figure 8.10 a schematic representation of the Thermosonics techniques is presented. With this setting the excitation generated is chaotic and contains many frequency components, typically harmonics and sidebands of the horn fundamental frequency (35 kHz).

Chaotic excitation is the key factor for the damage identification in Thermosonics; the presence of many frequency components is able to excite discontinuity surfaces and make them rub together, whatever is their position or orientation in the specimen. This rubbing mechanism generates a local friction or hysteresis which turns a dynamically loaded defect into a heat source which can be identified by an infrared camera. The friction induced by ultrasonic waves makes cracks or delamination lips warm up within few milliseconds after the beginning of excitation.

In the case of composite materials, due to their low conductivity the heat waves do not "travel far" and therefore the surrounding areas of defect (intact parts perhaps) are slightly affected by heat waves. On the other hand, it is necessary to provide enough energy in a proper time window to make visible not just surface defect but also subsurface faults, thus the probability of defect detection through thickness is heavily affected by time excitation and the IR acquisition time window. For the tested samples, in order to preserve the sample from surface damages caused by the horn itself low power amplitude, ~20W, has been used to drive the horn for 2s.

To magnify the effects of defects, the tests were carried out using a background subtraction technique. This image processing technique consists of the acquisition of a set of IR images before the excitation, and using this set of images it is possible to statistically evaluate background temperature and noise that will be subtracted from the set of images during excitation.

In Figure 8.11 the temperature field recorded with the infrared camera after the ultrasonic excitation is illustrated showing that a local temperature rise was located at the damage location, in particular the image was selected by evaluating the best contrast between the hot spot and background.

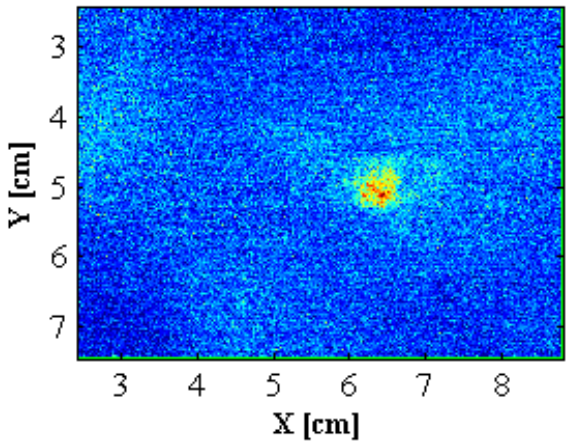

Figure 8.11 Temperature field recorded during the thermosonic test

8.5 Conclusion

The objective of this work was to image low velocity impact damage on a composite sample by observing the nonlinear phenomena generated when the specimen is periodically excited at one of its natural frequencies. In particular, harmonics of the fundamental excitations are the non linear phenomena detected in the area close to the damage, and mapping the spatial distribution of harmonic amplitudes scaled by the fundamental amplitude it was clearly possible to localize the damage. Others non destructive techniques were used in order to estimate damage position and compare results with the nonlinear image method. While the well-established pulse thermography technique failed to detect the BVID damage on the impacted surfaces the new promising alternative techniques called Thermosonics succeeded in localizing the damage.

The results presented in this section show that Pulse Thermography performed on the back surface, Thermosonics data and nonlinear spectroscopy imaging are in good agreement on the identification of low velocity impact damage.

CHAPTER 9 CONCLUSION

During the last few decades the research community and many industrial sectors have been more and more involved in the research no new material types and possible applications.

Laminated composite materials, such as CFRP or GFRP, are one of these new classes of material and recently their use is constantly growing in a wide range of applications in many industrial sectors; aerospace and energy are just an example of possible fields of use.

Although laminated composites offer an important improvement in terms of material performances, some of their characteristics are still a matter of concern, such as the ability to absorb impact energy without compromising the structural integrity. Certainly safety operative conditions are a critical issue for many applications and aerospace is one of them.

One of the research fields that might help, in the future, improving reliability and safety for composite material is the one related to the non destructive monitoring health condition of structures and assess damage severity and location.

This main scope of this work was to explore a novel technique for non destructive damage evaluation on composite material.

The research activity has been inspired by previous publications that have demonstrated the ability to measure nonlinear material properties for the identification of damages at an early stage.

Thus the first part of the work is focused on the analysis of current studies on the characterization of material defects and imperfections through the understanding of non linear wave propagation phenomena which are often induced by material imperfections or damage.

Low velocity impact damage is of particular interest for this work. Indeed this class of defects is critical for laminated composite material, dropping tools or debris during aircrafts take off can seriously damage composite components and drastically affect the structural integrity.

Low velocity impact damage has complex morphology in laminated composites where delamination, matrix and fibre cracks are commonly observed after a low velocity impact, even if the energy involved is low (1 Joule).

All these defects includes discontinuous surfaces and opened/closed interfaces, which are also observable on a large scale in non homogeneous material such as rock or sandstone.

The literature provides interesting approaches based on nonlinear wave interaction with discontinuities from different fields of application including geomaterials characterization and nonlinear contact acoustic phenomena. This study shows that the contact interfaces are an important source of nonlinearities that can affect waves travelling in to the medium.

Inspired by the published literature, hysteresis properties of interfaces have been investigated. Geomaterial science has been involved in this field for many years as this class of material is particularly rich in discontinuity and internal cracks.

The most promising results regard methodology able to measure nonlinear phenomena as shift resonance frequency (Nonlinear Resonance Ultrasound

spectroscopy-NRUS) or modulate periodic wave propagating in the medium, (Nonlinear Wave modulation Spectroscopy- NWMS).

Experimental evidences have demonstrated that nonlinear hysteretic elastic material model (PM-space) well represents nonlinear properties in geomaterials; and no previous attempts have been done for materials such as laminated composite.

For this reason the first task was to establish a relationship between non linear hysteretic properties of defects in homogeneous material, and verify if the defects so represented act like source of nonlinearity features. A numerical analysis was performed in order to study wave propagating through isotropic beams and orthotropic plate. Finite Element in house code was developed and PM-space has been used to characterize the damaged area.

Numerical results have predicted the presence of harmonics and sidebands caused by nonlinear material properties, these features are also connected to the position, damage size and on the excitation amplitude.

Unfortunately, due to the complexity of defect morphology and the lack of sensible data, it was not possible to establish a quantitative correlation between the nonlinear hysteretic elastic material properties model (PM-space) and the damage severity and size. However, qualitative results on nonlinearities were extremely important to define the experimental campaign on laminated composite.

A collection of CFRP samples have been provided by the Department of Mechanical Engineering department of the University of Bath. Those specimens have been used during a previous research activity which was focused on the evaluation of delamination area with C-scan after and a low velocity impact test.

Using bi-tone excitation or sweep in proximity of sample resonance frequency, harmonics, sidebands and resonance dependency from excitation amplitude have been observed. Overall the results obtained agree with mathematical and previous experimental evidences moreover nonlinear features correlate quite well with damage severity. In addition qualitative behaviour of nonlinearities has been predicted by nonlinear FE analysis.

The same approach has also been used also to investigate clamping condition on composite samples. NWMS methodologies provided promising results as the sideband amplitudes are consistent with the clamping force applied: weak bonds generate higher nonlinearity.

Once the correlation between damage severity and nonlinear properties, such as the harmonic amplitudes in homogeneous material, has been established the last point to prove was the link between nonlinear features and damage position. In other word if defects in a linear medium act as a unique non linear source, then damage localization should be possible.

Prior to performing this investigation, two CFRP samples were inspected (Pulse Thermography) to verity the intact condition of the sample. Later the samples were impacted using the drop tower available at the University of Bath. Pulse thermography on the sample back face and thermosonic inspection of the impacted side revealed the presence of damage corresponding to the impact location.

Using a single tone excitation at the sample resonance frequency harmonic amplitudes were measured at different locations across the impacted sample face. The nonlinear part of the structural response was highlighted, normalizing the second harmonic amplitude respect to the fundamental component for each measurement location. Using this approach the normalized harmonic amplitude contour map showed significant increase of nonlinear component in the proximity of impact location.

Numerical and experimental evidence presented in this work have demonstrated the ability of non linear methodology, inspired by geological materials using NRUS and NWMS for damage detection and localization in laminated composite materials.

9.1 Future work

The methodologies here proposed are not yet mature enough for industrial application.

More effort is required to characterize damage using nonlinear mechanisms. Numerical quantitative simulation of nonlinear hysteretic features can be extremely helpful in the prediction and understanding of modulation and resonance shift phenomena.

In this work two different methodologies have been presented, nonlinear spectroscopy and Thermosonics, which are based on the interaction between discontinuities and waves. Correlating these two methodologies with the phenomena observed (heat, harmonics and sidebands) is advisable for a better understanding of damage.

Further development could be achieved using different measurement and excitation devices. Contactless probes might be an extremely interesting development.

9.2 Publications

During the PhD programme the following publications have been proposed to the research community:

- U. Polimeno, M. Meo, D. P. Almond. **Smart nonlinear acoustic based structural health monitoring system.** Advances in Science and Technology, Vol.56 (2008) pp. 426-434.

- E. Barbieri, M. Meo, U. Polimeno. **Nonlinear wave propagation in damaged hysteretic materials using a frequency domain-based PM-space formulation"**. International Journal of Solids and Structures. Volume 46, Issue 2009, Pages 165-180

- U. Polimeno, M. Meo. **Understanding the effect of boundary conditions on damage identification process when using non-linear elastic wave spectroscopy methods.** International Journal of Non-Linear Mechanics. Volume 43, Issue 3, April 2008, pages 187-193.

- M. Meo and U Polimeno. **Barely visible impact damage detection in aircraft composites plates**. 6th ICCST, 22-24 JANUARY 2007, DURBAN, SOUTH AFRICA

- M. Meo, G. Zumpano, U Polimeno. **Nonlinear Time Reversal Acoustics to detect stress corrosion cracking in a welded plated**. 11th International Workshop on Nonlinear Elasticity in Materials.

- Meo M., Zumpano G., and Polimeno U. **Finite element simulation of wave propagation phenomena in a damaged plate to support development of Non-linear elastic wave spectroscopy (NEWS) techniques**. NDT Prague, October 10-12 2005.

- M. Meo, G. Zumpano, U. Polimeno. **Corrosion identification on an aluminium plate-like structure by monitoring wave propagation phenomena**. First World Congress on Corrosion in the Military, Sorrento, Italy, June 6–8, 2005.

References

[1] http://en.wikipedia.org/wiki/Nondestructive_testing. Date accessed: March 2011

[2] S. Low**. Jane's all the World's Aircrafts**. Janes information Group, 2001.

[3] R. Halmshaw. **Non-destructive testing,** second edition. Butterworth-Heinemann, 1991

[4] T. E. Munns, R. E. Beard, A. M. Culp, D. A. Murphy, R. M. Kent. **Analysis of regulatory guidance for health monitoring.** NASA/CR-2000-210643, 2000.

[5] W.J. Staszewski, C. Boller and G.R. Tomlinson. **Health monitoring of aerospace structures.** Wiley, 2004.

[6] Peter B. Nagy. **Fatigue damage assessment by nonlinear ultrasonic materials characterization.** Ultrasonics 36 (1998) p. 375-381.

[7] O. Buck, W. L. Morris and J. M. Richardson. **Acoustic harmonic generation at unbounded interfaces and fatigue cracks.** Applied Physics Letters 33 (1978) p.371-373.

[8] W. L. Morrison, O. Buck and R. V. Inman. **Acoustic harmonic generation due to the fatigue damage in high-strength aluminium.** Journal of Applied Physics, 50 (1979) p. 6737-6741

[9] Holroyd, H. Meisuria, D. Lin, N. Randall. **Development of a practical acoustic emission based structural monitoring system.** T., Proceedings of the First European Workshop – Structural Health Monitoring. Paris, France 2002.

[10] G. T. Zheng. **Non destructive structural health monitoring with acoustic emission signal processing.** Proceedings of the First European Workshop – Structural Health Monitoring. Paris, France 2002.

[11] Lester W. Schmerr, Jr. **Fundamentals of ultrasonic nondestructive evaluation.** Plenum Press, New York 1998.

[12] J. David, N. Cheeke. **Fundamentals and applications of ultrasonic waves.** CRC PRESS, 2002.

[13] W. Liu, R. Hunsperger, M. Chajes, E. Kunz. **An overview of corrosion damage detection in steel bridge strands using TDR**. Proc. of the 2nd International Symposium on TDR for Innovative Applications, Evanston, Illinois, 2001.

[14] N. Khemiri, N. Angelidis, P. E. Irvin. **Experimental and finite element study of the electrical potential technique for damage detection in CFRP laminates**. Conference of Smart Structures & Demonstrators, December 2001.

[15] Todoroki, Y. Tanaka, Y. Shimamura. **Electric resistance change method for monitoring of embedded delaminations of quasi-isotropic CFRP laminated plate.** Proceedings of the First European Workshop – Structural Health Monitoring. Paris, France 2002.

[16] Peter J. Shull, **Non destructive evaluation**. Marcel Dekker, 2002

[17] Charles J. Hellier. **Handbook of non-destructive evaluation.** Mc Graw-Hill, 2003

[18] X. P. V. Maldague. **Theory and practice of infrared technology for nondestructive testing.** John Wiley & Sons, 2001

[19] Barden, T. J., Almond, D. P., Cawley, P., Morbidini, M., 2006. **Advances in thermosonics for detecting impact damage in CFRP composites**. *INSIGHT*, 48 (2), p. 90-93.

[20] S. Timonshenko and J. N. Gooder. **Theory of elasticity.** Mc Graw-Hill, 1951

[21] G. H. Staab. **Laminar composite.** Butterworth-Heinemann, 1999

[22] M. H. Sadd. **Elasticity. Theory, applications and numerics.** Elsevier, 2005.

[23] J.N Reddy. **Mechanics of laminated composite plates and shells. Theory and analysis.** CRC PRESS,2004

[24] Yu. A. Amenzade. **Theory of elasticity.** Mir Publisher Moscow, 1979

[25] K. F. GraFF. **Wave motion in elastic solids**. Clarendon Press, Oxford 1975

[26] L.D. Landau and E. M. Liifshitz. **Theory of elasticity.** Pergamon Press 1959

[27] Z. A. Goldberg. **Interaction of plane longitudinal and transverse elastic wave.** Soviet Physic: Acoustic, 6, p. 306-310.

[28] Xingzhou Liu. **Non linear elastic, seismic anisotropy, and petrophysical properties of reservoir rocks.** Ph.D Thesis. Stantford University 1994.

[29] Serge Abrate. **Impact on composite structure.** Cambridge University Press. 1998.

[30] J. Bayandor, R. S. Thomson, M. L. Scott, M. Q. Nguyen and D. J. Elder. **Investigation of impact and damage tolerance in advanced aerospace composite structures.** IJCrash 2003 Vol. 8 No. 3 p. 297-306.

[31] S. Takeda, S. Minakuchi, Y. Okabe, N. Takeda. **Delamination monitoring of laminated composites subjected to low-velocity impact using small-diameter FBG sensors.** Composites: Part A 36 (2005) 903-908

[32] G. Belingardi and R. Vadori. **Low velocity impact test of laminate glass-fibre-epoxy matrix composite materials plates.** International Journal of Impact Engineering. 27 (2002) p. 213-229.

[33] G. Belingardi and R. Vadori. **Influence of the laminate thickness in low velocity impact behaviour of composite material plate.** Composite Structure 61 (2003) p. 27-38.

[34] Tien-Wei Shyr and You-Hao Pan. **Impact and damage characteristics of composite laminates.** Composite Structure 62 (2003) p. 192-203.

[35] G. A. Shoeppner and S. Abrate. **Delamination threshold loads for low velocity impact on composite laminate.** Composites Part A 31 (2000) 903-915.

[36] Tien-Wei Shyr and You-Hao Pan. **Low velocity impact responses of hollow core sandwich laminate and interply hybrid laminate.** Composite Structure 64 (2004) p. 189-198.

[37] Ik Heyon Choi and Cheol Ho Lim. **Low-velocity impact analysis of composite laminates using linearized contact law.** Composite Structure 66 (2004) p. 125-132.

[38] E. J. Herup and A. Palazotto. **Low-velocity impact damage initiation in graphite/epoxy/nomex honeycomb-sandwich plates.** Composite Science and Technology 57 (1997) p. 1581-1598.

[39] Y. Shui and I. Yu Solodov. **Nonlinear properties of Rayleigh and Stonely waves in solids.** J. App. Phys, 64(11), p. 6155-6165. 1988

[40] I. Yu Solodov. **Ultrasonics of nonlinear contacts: propagation, reflection and NDE application.** Ultrasonic 36 (1998) p. 383-390.

[41] I. Yu. Solodov. **Ultrasonics of nonlinear interfaces in solids: new physical aspects and NDE applications.** WTC 2003, Paris, September 7-10, 2003.

[42] http://en.wikipedia.org/wiki/Heaviside_step_function. Date accessed: March 2011

[43] I. Yu Solodov, N. Krohm and G. Busse. **CAN: an example of nonclassical acoustic nonlinearity in solids.** Ultrasonics 40 (2002) p. 621-625

[44] A. Moussatov, V. Gusev and B. Castagned. **Self-induced hysteresis for nonlinear acoustic waves in cracked material.** Physical Review Letters V 90, No 12

[45] K. E. A. Van Den Abeele, P. A. Johnson and A. Sutin, **Non linear elastic wave spectroscopy (News) techniques to discern material damage.**

Part I: non linear spectroscopy (NWMS). Res Nondestr Eval (2000) 12:17-30

[46] K. E. A. Van Den Abeele, P. A. Johnson and A. Sutin, **Non linear elastic wave spectroscopy (NEWS) techniques to discern material damage. Part II: single-mode nonlinear resonance acoustic spectroscopy.** Res Nondestr Eval (2000) 12:31-42

[47] R. A. Guyer, P. A. Johnson. **Nonlinear mesoscopic elasticity: evidence for a new class of materials.** Physics Today, April 1999, p. 30-36.

[48] K. Van Den Abeele, K. Van De Velde, J. Carmeliet**. Inferring the degradation of pultruted composites from dynamic nonlinear resonance measurements.** Polymer Composites, Aug 2001, Vol. 22: 555-567.

[49] Marco Scalerandi, Valentina Agostini, Pier Paolo Delsanto, K. E. A. Van Den Abeele, Paul Allen Johnson. **Local interaction simulation approach to modelling nonclassical, nonlinear elastic behaviour in solid.** J. Acoust. Soc. Am. 113(6) p. 3049-3059, June 2003

[50] L. A. Ostrovsky and P. A. Johnson. **Dynamic nonlinear elasticity in geomaterials.** Rivista del nuovo cimento. Vol.24, N. 7, p. 1-47. 2001

[51] P. A. Johnson, P. N. J. Rassolofosson. **Manifestation of nonlinear elasticity in rock: convincing evidence over large frequency and strain intervals from laboratory studies.** Nonlinear Process in Geophysics (1996) 3:77-88

[52] R.A. Guyer, K. R. McCall, P. A. Johnson, P. N. J. Rasolofosaon and B. Zinszner. **Equation of state hysteresis and resonant bar measurement on rock.** Proceeding of the 35th U.S. symposium on rock mechanics. University of Nevada, Reno 5-7 June 1995, p. 177-181

[53] K. R. McCall and R. A. Guyer. **Equation of state and wave propagation in hysteretic nonlinear materials.** Journal of geophysical research. vol. 99 p. 23,887-23,897. December 10, 1994.

[54] K. R. McCall and R. A. Guyer. **A new theoretical paradigm to describe hysteresis, discrete memory and nonlinear elastic wave propagation in rock.** Nonlinear Processes in Geophysics (1996) 3: 89-101.

[55] R. A. Guyer, K. R. McCall, G. N. Boitnott, L. B. Hilbert Jr. and T. J. Plone. **Quantitative implementation of Preisach-Mayergoyz space to find static and dynamic elastic moduli in rock.** Journal of Geophysical Research, vol. 102 p. 5281-5293, March 10, 1997.

[56] D. Mayergoyz, **Hysteresis models from the mathematical and control theory point of view**. J. App. Phys. 57 (1) p. 3803-3805, April 1985.

[57] D. Mayergoyz and G. Friedman, **Generalized Preisach Model of Hysteresis, IEEE Transaction on Magnetic.** vol. 24, No. 1 p212-217, January 1988.

[58] D. Mayergoyz, Dynamic Preisach Model of Hysteresis. **IEEE transactions on magnetic.** Vol. 24, No. 6, November 1988.

[59] Klaus-Jürgen Bathe. **Finite element procedures.** PRENTICE HALL. 1996

[60] R. Cook, D. S Malkus, M. E. Plesha. **Concepts and applications of Finite Element Analysis.** John Wiley and Sons, 1989

[61] O. C. Zienkiewic, R. L. Taylor. **The finite element method. Volume 1: the basis.** Fifth edition**,** Butterworth-Heinemann, 2000.

[62] Ansys: Theory reference Guide. Ansys V8 Documentation. 2007

[63] W.H. Press, S.A.Teukolsky, W. T. Vetterling, B. P. Flannery, M. MEcalf. **Numerical recipes in Fortran 90.** Cambridge University Press 1992

[64] G. H. Golub and C. F. Van Loan. **Matrix Computation, second edition**. The John Hopkins University Press, 1996

[65] V. C. Chen and H. Ling. **Time Frequency Transformation for Radar Imaging and Signal Analysis.** Artech House, Boston, London 2002.

[66] K. Van Den Abeele, J. De Visscher. **Damage assessment in reinforced concrete using spectral and temporal nonlinear vibration techniques.** Cement and Concrete Research 30 (2000) p. 1453-1464.

[67] K. Van Den Abeele, A. Sutin, J. Carmeliet, P. A Johnson. **Micro-damage diagnostic using nonlinear elastic wave spectroscopy (NEWS).** NDT&E International 34 (2001) 239-248.

[68] P. A. Johnson, B. Zinszner, P. Rasolofosaon. **Dynamic measurement of the nonlinear elastic parameter α in rock under varying condition.** Journal of geophysics research, Vol.109, B02202, p. 1-12. 2004

[69] I. Solodov, J. Wackerl. K. Pfleider, G. Busse. **Nonlinear self-modulation and subharmonic acoustic spectroscopy for damage detection location.** Applied Physics Letters. Volume 84, Number 26 p. 5386-5388. 2004

[70] J. A. Ten Cate, T. J. Shankland. **Slow dynamics in the nonlinear elastic response of Berea sandstone.** Geophysical Research Letteres, Vol 23, No 21, p. 3019-3022. 1996

[71] V. Zaitsev, V. Nazarov, V Gusev, B. Castagnede. **Novel nonlinear-modulation acoustic technique for crack detection.** NDT&E International Volume 39, Issue 3 April 2006, p. 184-194

[72] Leornard Meirovitch. **Element of Vibration Analysis.** Mc Graw Hill 1986

[73] http://www.bksv.com/Products/PULSEAnalyzerPlatform/DataAcquisitionandAnalysis-PULSEsystem.aspxhttp://www.endevco.com/product/Product.aspx?product_id=93. Date accessed: March 2011

[74] S. W. Smith. **Digital Signal processing.** Newnes 2003

[75] K. V. Rangaro, R. K. Mallik. **Digital signal processing – A practitioner's approach.** John Wiley & Sons 2005

[76] Lai, Edmund. **Practical digital signal processing.** Elsevier Newnes 2004

[77] Elliot, Douglas. **Handbook of digital signal processing: engineering applications.** Elsevier Academic Press 1987

[78] http://www.mathworks.com/help/toolbox/signal/bqie2vw.html. Date accessed: March 2011

APPENDIX - A EXPERIMENTAL ANALYSIS OF LOW VELOCITY IMPACT

Contact Force versus displacement (a) and time history (b) in low velocity impact on laminated plate with no rebound [32].

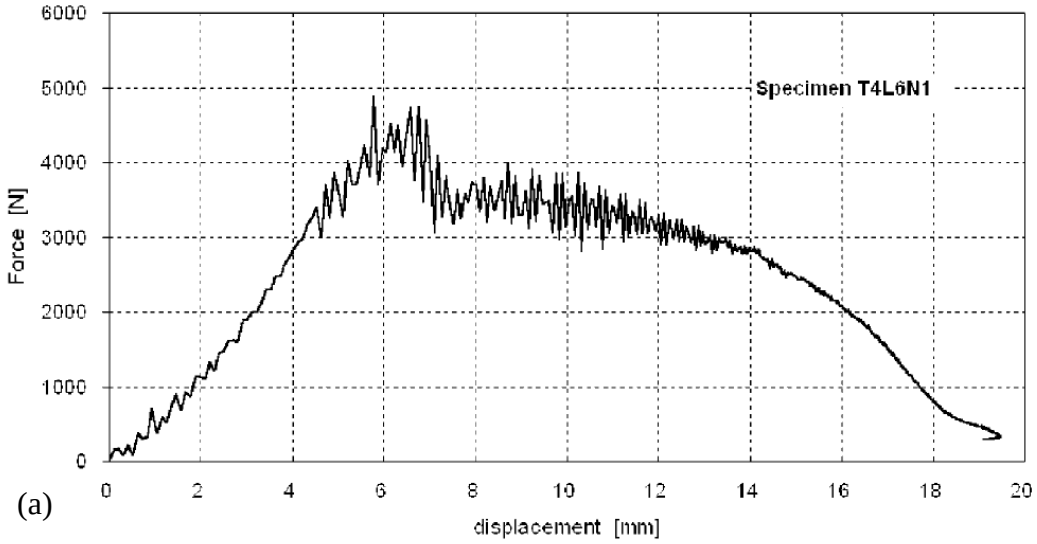

(a)

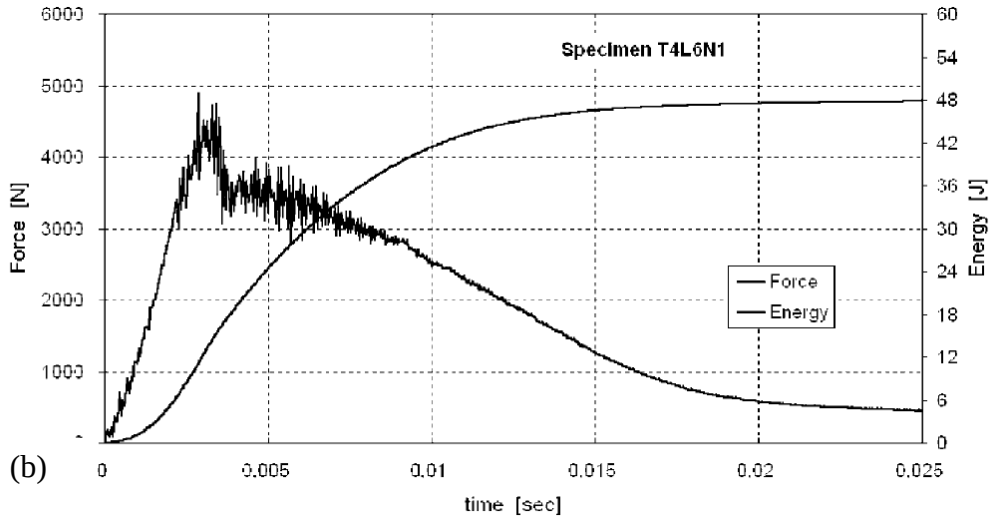

(b)

Contact force versus displacement (a) and time history (b) in low velocity impact on laminated plate with perforation [32].

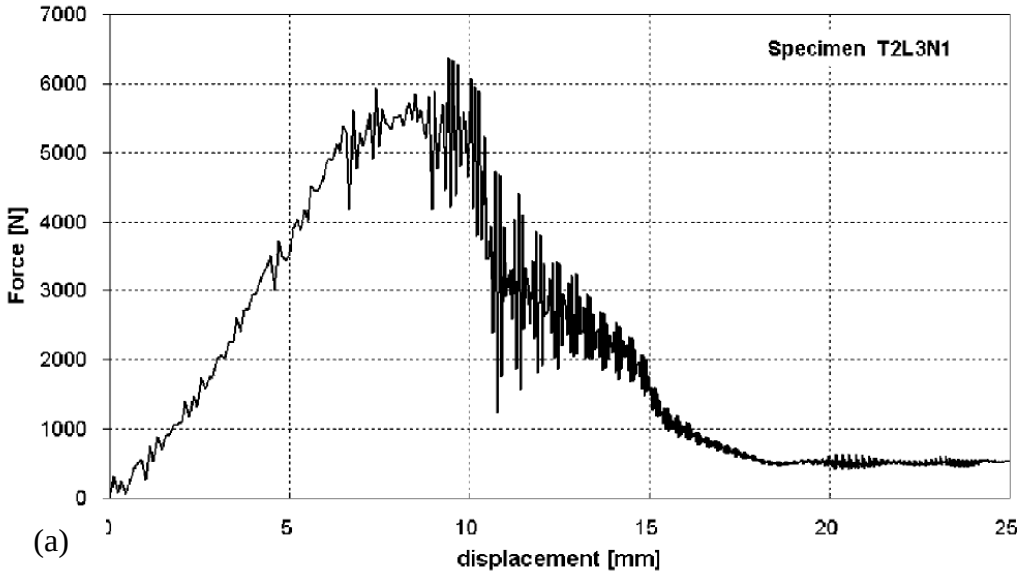

(a)

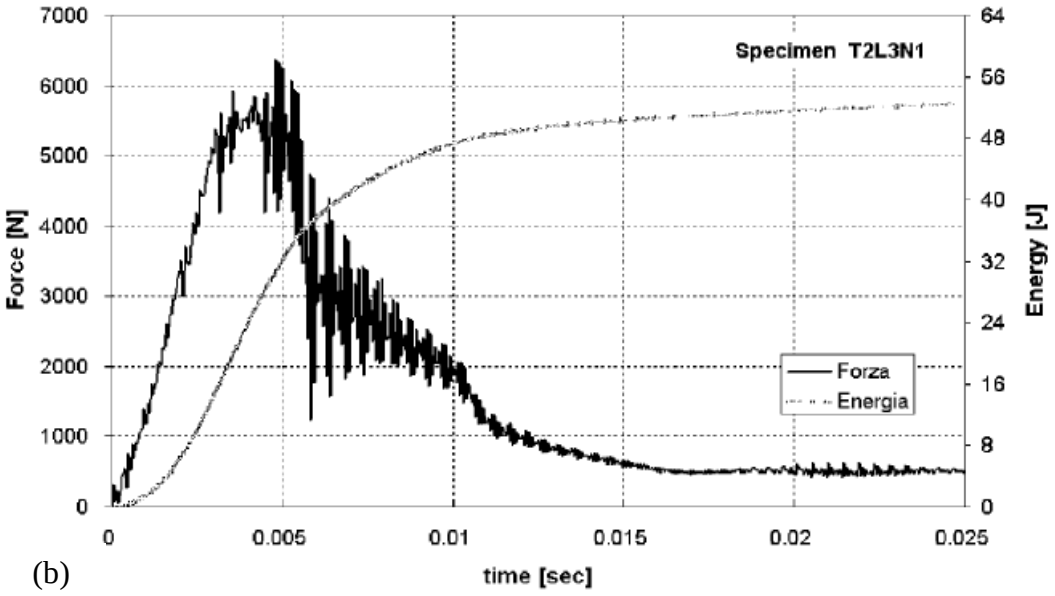

(b)

APPENDIX - B NEWMARK FLOW CHART FOR FINITE ELEMENT SOLVER